Medizinische Fakultät der Technischen Universität München

Comparing electric-field-navigated and line-navigated TMS for cortical motor mapping in patients with brain tumors

Moritz Fabian Klug

Vollständiger Abdruck der von der Fakultät für Medizin der Technischen Universität München zur Erlangung des akademischen Grades eines Doktors der Medizin genehmigten Dissertation.

Vorsitzender: Prof. Dr. Jürgen Schlegel

Prüfende/-r der Dissertation:

1. apl. Prof. Dr. Sandro M. Krieg

2. 2. Prof. Dr. Simon N. Jacob

Die Dissertation wurde am 20.12.2019 bei der Technischen Universität München eingereicht und durch die Fakultät für Medizin am 16.06.2020 angenommen.

Mit Genehmigung der Medizinischen Fakultät
der Technischen Universität München

Berichterstatter:	Prof. Dr. med. Sandro M. Krieg, MBA
Mitbetreuung durch den promovierten Mitarbeiter:	Dr. med. Nico Sollmann, Ph.D., B.A.
Dekan:	Univ.-Prof. Dr. med. Peter Henningsen
Tag der mündlichen Prüfung:	15.07.2020

Für Daniela,

Max, Mary und Holger.

TABLE OF CONTENTS

1. INTRODUCTION

1.1. Navigated transcranial magnetic stimulation-based motor mapping

Transcranial magnetic stimulation (TMS) is a non-invasive method of electrically stimulating the human cortex (Barker, Jalinous, & Freeston, 1985; Hugues Duffau, 2012). Aside other appliances, the addition of neuronavigation to TMS has allowed for the diagnostic and therapeutic usage of navigated TMS (nTMS) for different neurophysiological and neurosurgical purposes (Krings et al., 2001). Through nTMS, the cortex can be safely stimulated while stimulus-response observations can be used to identify the functional activity of certain cortical areas (Ettinger et al., 1996; Ruohonen, Ravazzani, & Grandori, 1998). An important appliance that follows this principle is nTMS based mapping of the motor cortex, also called motor mapping in the presurgical context for patients suffering from intracranial tumors (Krieg et al., 2012; Krieg et al., 2015).

Intracranial tumors can be subdivided into gliomas, metastasis and non-glial primary brain tumors (Gupta & Dwivedi, 2017). Aside of general symptoms due to increased intracranial pressure, intracranial tumors often lead to focal deficits depending on their location. Specifically, tumors close to the motor cortex in the prefrontal cortical area can lead to varying degrees of motor function deficits. For most CNS tumors, primary resection is the therapy of choice (Lacroix et al., 2001; Smith et al., 2008).

Safely maximizing the extent of resection (EOR) is regarded as the most influential factor for optimal patient outcome and survival rate in CNS tumor surgery (Capelle et al., 2013; Khan et al., 2016; Lacroix et al., 2001; Marko et al., 2014; Roelz et al., 2016; Sanai et al., 2011; Smith et al., 2008). Resection safety is mainly determined by the avoidance of iatrogenic neurologic deficits due to intraoperative damage to so-called eloquent regions of the brain (Martino et al., 2011). As tumors were found to be bordering or involving eloquent cortical areas in up to 92% of cases, balancing the maximization of the EOR and resection safety is a challenge (Capelle et al., 2013; Lacroix et al., 2001; Leroy et al., 2019; Sagberg et al., 2019). This challenge is further increased by the significant inter-individual variance in the cortical distribution of neurological function (Buonomano & Merzenich, 1998; Raffin & Siebner, 2019).

In this context, nTMS based motor mapping allows for preoperative mapping of the motor cortex to identify the spatial extent of motor eloquent cortical areas that need to be spared during surgery (Krieg et al., 2013; Krieg et al., 2015). The accuracy and sensitivity of this method are on par with the current gold standard of intraoperative direct cortical stimulation (DCS) (Barbosa et al., 2015; Picht et al., 2011). Further, as nTMS unlike DCS is performed preoperatively, this information can be included in the planning of the procedure (Krieg et al., 2015; Picht et al., 2016). Thanks to these assets, nTMS based motor mapping is increasingly used in the preoperative setting (J. Jung et al., 2019; Krieg et al., 2015). Yet, the application of nTMS existentially relies on neuronavigation (Frey et al., 2014; Julkunen et al., 2009; Krings et al., 2001).

Currently, there are two technical approaches towards neuronavigation in nTMS, line navigated TMS (LnTMS) and electric field navigated TMS (EnTMS)(Hugues Duffau, 2012; Saisanen, 2011). These two approaches considerably deviate from another regarding their underlying assumptions of the E-field and approaches to neuronavigation. Yet, nTMS has so far to be discerned for the underlying technical approach to neuronavigation. As distinct as the influence of neuronavigation on nTMS based motor mapping has been found, a comparison of the differences between LnTMS and EnTMS based motor mapping has yet to be conducted. This study therefore marks the first comparison of the clinical differences between EnTMS and LnTMS based preoperative motor mapping for patients suffering from intracranial tumors.

1.2. Functional human anatomy – motor function

1.2.1. Motor cortex

1.2.1.1.Macro- and micro-anatomic properties

Unlike reflexes and involuntary motor function, which at least partially stem from lower parts of the CNS, voluntary motor function mainly originates from a cortical region referred to as the motor cortex. Surrounded by the three meninges (pia mater, arachnoid mater and dura mater), as well as cerebrospinal fluid (CSF), the motor cortex is located in the precentral gyrus of the frontal lobe, branching into further rostral gyri (Figure 1) (Gray & Lewis, 1918; Schünke et al., 2009).

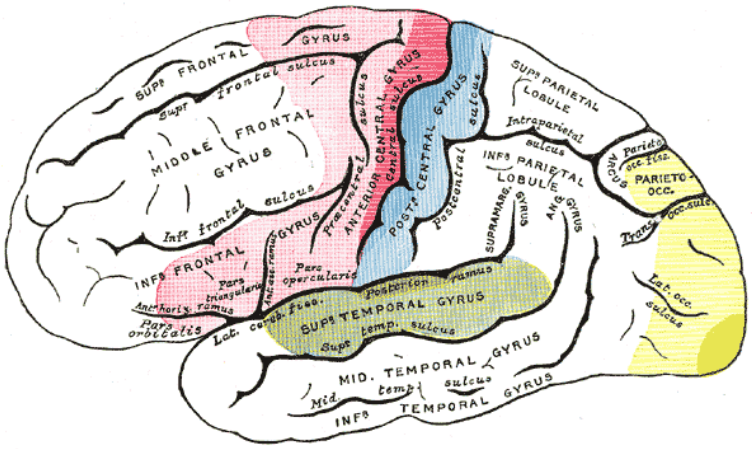

Figure 1 Location of the motor cortex (marked in red, M1 marked in dark red) based on structural parameters. (Gray & Lewis, 1918)

The motor cortex is further divided into the primary motor cortex, also referred to as M1 and supplementary areas that will be described in detail below. M1 has several relevant macro-anatomical characteristics. To identify M1 and the precentral gyrus on a patient's MRI or X-ray computed tomography (CT) scan, one can identify the central sulcus between the frontal and temporal lobe and proceed in the rostral direction where the precentral gyrus borders the sulcus (Gray & Lewis, 1918; Schünke et al., 2009).

Another typical landmark of M1 is the hand knob where the cortical representation for the muscles controlling hand and finger movement can usually be found (Yousry et al., 1997). It can be identified by its typical shape resembling an inverted Greek "Ω" or "ω" with the convexity directed towards the central sulcus. This is also referred to as the Omega Sign (M. C. Park et al., 2007; Schünke et al., 2009). Aside of the hand knob, hand motor function in M1 can also

be located by identifying the "*pli de passage fronto-pariétal de moyen"* (PPFM) that was first described by the French anatomist Paul Broca (Boling et al., 1999). The PPFM is a small gyral bridge that is present in most individuals. It lies in the depth of the central sulcus and connects the pre- and postcentral gyrus. Both sensory and motor representation of the hand and fingers are usually located at either side of the PPFM (Boling et al., 1999; Boling & Olivier, 2004; White, 1997).

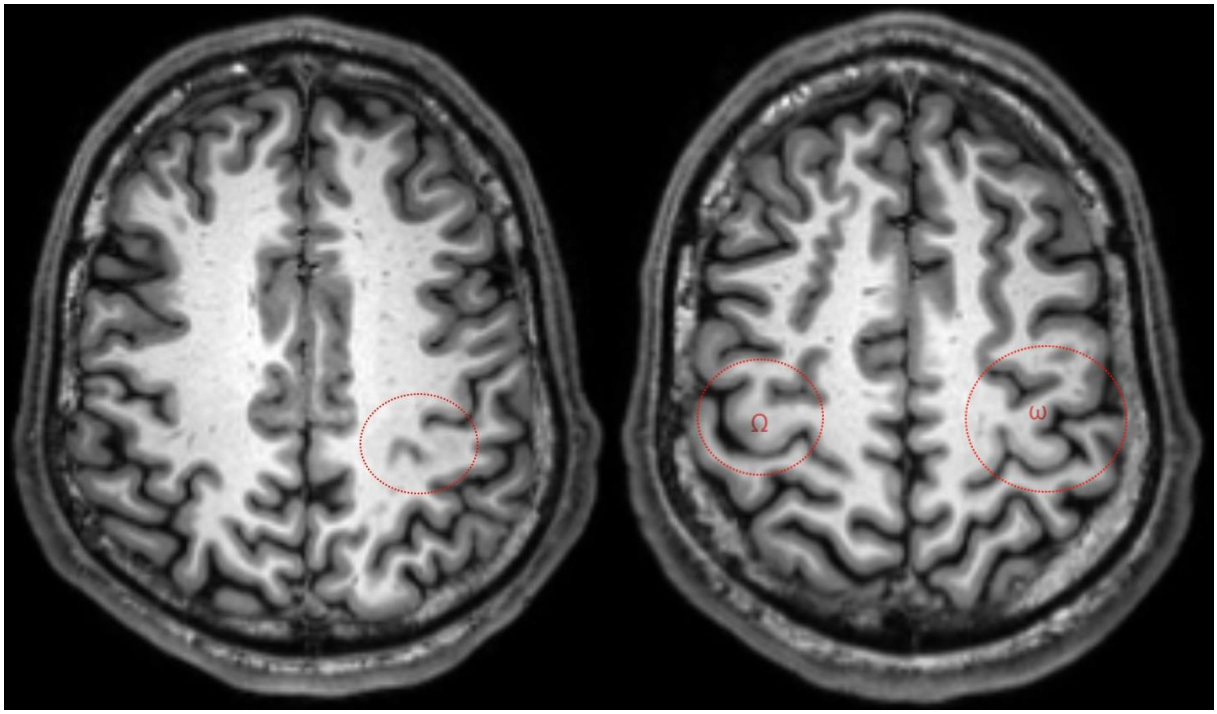

Figure 2 Axial magnetic resonance imaging (MRI) scan of a healthy subject's brain. Left: pli-de-passage fronto-pariétal de moyen marked in red. Right: Both hemispheres' omega-shaped hand knobs marked in red. Note that the hand knob can resemble both an uppercase "Ω" or a lowercase "ω"

As seen in *Figure 1*, macroscopic structures do not serve well at clearly identifying the exact borders of either the motor cortex or its subdivisions. Another way of anatomically classifying brain regions aside of macroscopic structures is the Brodmann cyto-architectonic map based on the different striation of different cortical regions. (Brodmann, 1909).

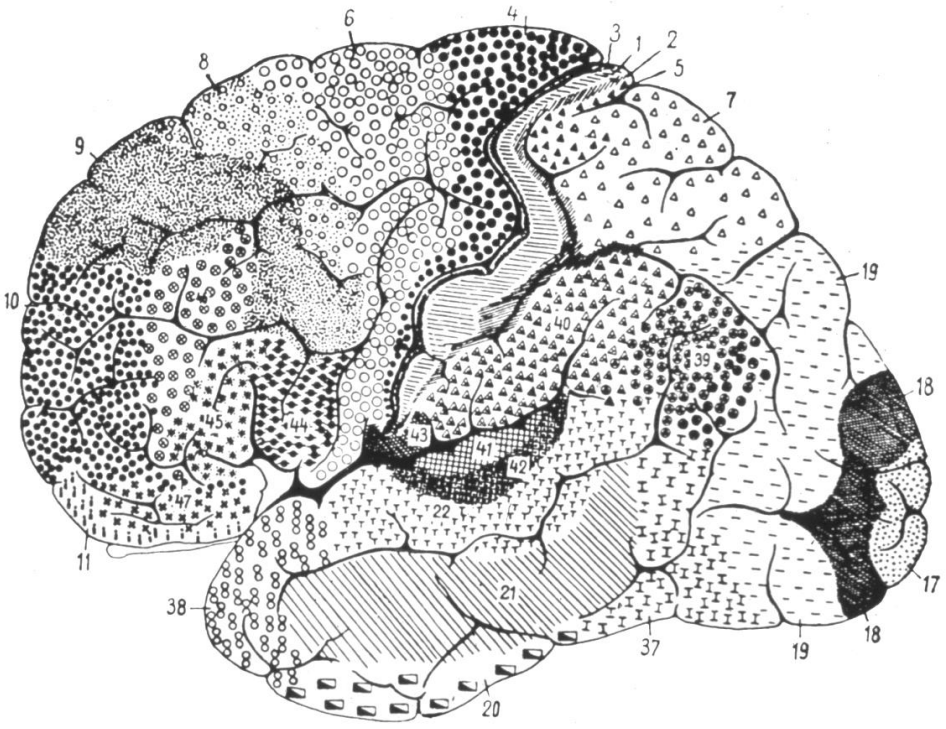

Figure 3 Brodmann areas as originally described. (Brodmann, 1909)

M1 is identical to the Brodmann area 4 (BA4). BA4 is identified by its typical cyto-architecture with almost no distinguishable Layer IV and very large neurons present in Layer V. These neurons are called Betz cells and project directly onto the corticospinal tract (CST). Betz cells are typical for BA4 and characterize it. Yet, they only contribute for about 5% of the efferent fibers of BA4. The remaining 95% stem from smaller pyramid cells (Lüllmann-Rauch, 2009; Schünke et al., 2009; Welsch et al., 2014). Neighboring rostral cortical areas also contribute to the motor cortex. These areas are found mostly within Brodmann area 6 (BA6, no distinguishable Layer IV, no Betz cells in Layer V) (Lüllmann-Rauch, 2009).

BA6 includes the premotor cortex (PMC) and the supplementary motor area (SMA). Both PMC and SMA are believed to mainly be involved in higher planning and preparation of motor function while M1 is believed to be the main origin of executive motor function (Penfield & Boldrey, 1937; Saisanen, 2011). Nevertheless, CST fibers have been shown to stem not only from M1: at least 50% of fibers have been shown to stem from areas in BA6 (including the PMC and SMA) as well as somatosensory areas in the postcentral gyrus (Aksu et al., 2011; Lassek, 1941; Lüllmann-Rauch, 2009; Schünke et al., 2009).

1.2.1.2. Functional distribution and somatotopy

An important characteristic of M1 is somatotopy, first described by Penfield and Boldrey in 1937 after experiments based on direct cortical stimulation (DCS)(Penfield & Boldrey, 1937). Somatotopy describes the principle that neighboring cortical areas innervate neighboring muscle groups. Yet, the size of the cortical representation area does not correlate with the size of the corresponding muscle group. Instead, it is thought to correlate with the degree of precision of said muscle group's movements. The principle of somatotopy can also be observed in other cortical areas such as the primary somatosensory cortex and is seen as an example of higher brain differentiation (Penfield et al., 1950; Penfield & Boldrey, 1937).
Somatotopy can be visually depicted using so-called Homunculi in which a cortical representation area is depicted by the corresponding muscle group or sensory area drawn over it. Using this method, the disproportion between size of cortical representation area and real muscle size becomes clearly visible (Kocak et al., 2009; Penfield et al., 1950).

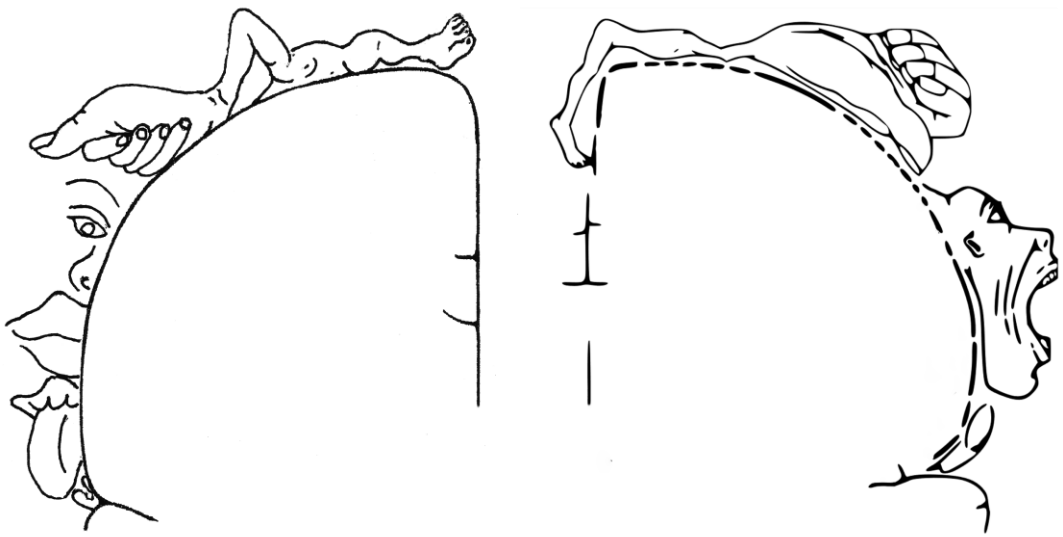

Figure 4 Somatotopy represented by Penfield's Homunculus of S1 (left) and M1 (right). (Penfield et al., 1950)

Recent studies found cortical representations to vary inter-individually by several centimeters from their position as described by the Homunculus. Yet, the basic principles of somatotopy - the vicinity of neighboring areas' cortical representation sites as well as the gross localization of a certain representation area on the cortex - remain unchallenged (Farrell et al., 2007).

Due to somatotopy neighboring muscles' cortical representation areas can be assumed to be neighboring as well and cortical representation sites of e.g. one extremity can hence be

assumed to be spatially cohesive. In this study, this principle is used to generate continuous maps of the cortical motor function representation sites for both the upper extremity (UE) and lower extremity (LE). As visible in *Figure 4*, the cortical representation site for the UE motor function is grossly located on the outside surface of the cortex. This makes it easily accessible for stimulation. The lower extremity representation site, one the other hand, reaches into the interhemispheric fissure, thus hindering direct effective stimulation.

1.2.2. Corticospinal tract

The CST mainly composes of efferent cortical fibers descending from the motor cortex as well as S1 (Gray & Lewis, 1918). It passes through the brainstem where most fibers cross to the contralateral side and form the pyramidal decussation at the height of the medulla oblongata. Fibers that have crossed side continue to form the lateral CST while running through the spinal cord. Ipsilateral fibers that did not cross sides form the anterior corticospinal tract and cross sides at the segment height of their target α-motoneuron. The α-motoneuron is innervated both monosynaptically by CST fibers as well as polysynaptically by interneurons. These interneurons are influenced by CST fibers as well. Axons of the α-motoneuron leave the spinal cord through each segment's anterior root and then form spinal and peripheral nerves to reach their target muscles (Welsch et al., 2014). Each muscle activation is achieved via synaptic activation of the muscle at the neuromuscular plate (Lüllmann-Rauch, 2009). Muscle activation can be observed via electromyography (EMG) in the form of motor evoked potentials (MEPs) (Wassermann et al., 1992).

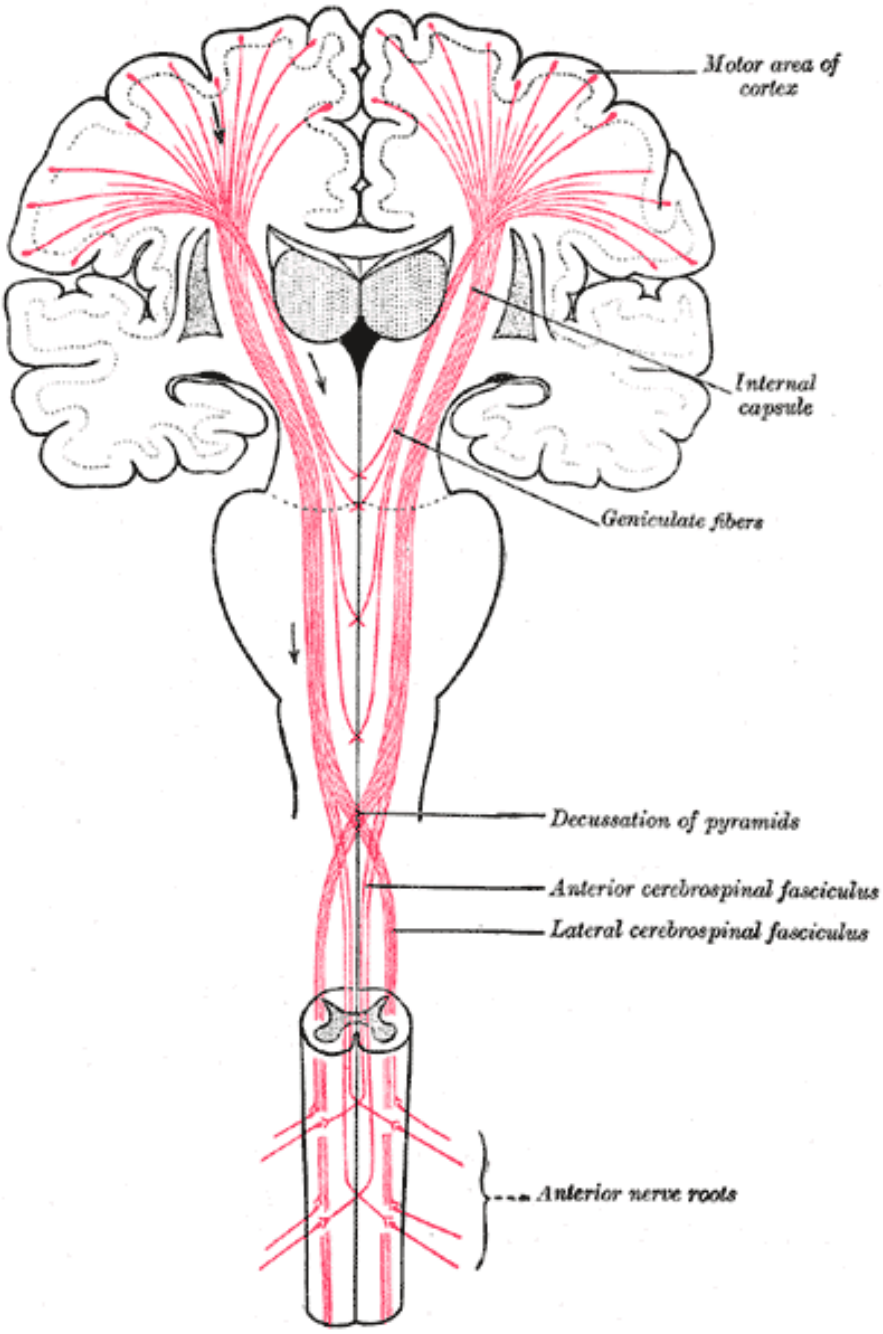

Figure 5 Pathway of the corticospinal tract (CST). (Gray & Lewis, 1918)

1.2.3. Neuroplasticity

An important factor to consider when describing functional distribution of the human (motor) cortex is neuroplasticity (Buonomano & Merzenich, 1998). Neuroplasticity describes the flexibility of cortical area-function relations, meaning that areas of the human cortex can undergo a certain degree of fluent changes in their function over time. This variability is thought to be mostly based on the micro-anatomical process of synaptic plasticity. In this process, neural cell synapses either increase (long-term potentiation, LTP) or decrease (long-term depression, LTD) their connectivity and excitability depending on their activation frequency (Buonomano & Merzenich, 1998; R. F. Schmidt et al., 2011). Adapted to a macro-anatomical level, cell connectivity of certain regions varies through both LTP and LTD when the utilization of said regions' functions changes over time. In the end, this leads to these regions' neurons being connected to other cortical areas than before and thus executing different functions than before. Due to these individual processes, the static allocation of certain cortical areas to certain neurological functions based on anatomic structures can only be used for gross functional relationships (Buonomano & Merzenich, 1998; Chen et al., 2002; H. Duffau, 2008).

While neural plasticity is mostly seen in the context of general learning processes, it has also repeatedly been shown to play an important role for the cortical distribution of motor function. Motor function sites were found to demonstrate neuroplasticity both functionally as well as compensatory. Functional neuroplasticity is based on different degrees of activity of certain muscle groups e.g. due to periods of bedrest, changes in lifestyle or occupational factors and was found to be observable even within a timeframe of 48 h (Ngomo et al., 2012; Raffin & Siebner, 2019). Compensatory plasticity on the other hand follows damage to the original representation site due to bleeding, trauma or tumor growth (Chen et al., 2002; Conway et al., 2016; Dai et al., 2016; Langlet et al., 2012; Penhune & Steele, 2012). Regarding compensatory plasticity, especially tumors with a low rate of progression such as LGG have been shown to provoke an extensive degree of plasticity of the surrounding cortical areas. (H. Duffau, 2005, 2008).

1.3. Assessment of the motor system

1.3.1. Rationale in a preoperative setting

The aim in the resection of intracranial tumors is the maximization of the EOR whilst avoiding iatrogenous neurological deficits. This basic principle especially holds true for tumors that grow close to or within parts of the motor system: general mobility, independency from assistance and the ability to carry out work largely determine the quality of life (QOL) of tumor patients. These motor based factors hence account for large parts of common measurements of a patient's functional status such as the Karnofsky-Index (KI), or the Eastern Cooperative Oncology Group (ECOG)/World Health Organization (WHO) performance status (ECOG-PS) (Blagden et al., 2003; Karnofsky et al., 1948; Oken et al., 1982; Péus et al., 2013). Both the KI and the ECOG-PS have repeatedly been found to be not only a valid parameter for patient quality of life but also reliable predictors for mortality in tumor patients (Marko et al., 2014; Patel et al., 2018).

The importance of preserving motor function leads to extensive preoperative diagnostic procedures when patients present with intracranial tumors in cortical regions associated to motor function such as the precentral cortex. As the motor cortex cannot be sufficiently identified by mere macroscopic structural measures alone and the cortical representation sites of motor function vary interindividually due to neuroplasticity, diagnostics must include functional measures to identify the exact spatial extent of the motor cortex, particularly in patients with space-occupying lesions. Further, high-resolution structural diagnostic tools are required to assess the spatial properties of the tumor and its infiltration of the surrounding tissue, as well as the shape and structure of the surrounding tissue itself. This holds true especially as the gyral pattern is often distorted and/or unrecognizable due to local pressure caused by the tumor itself as well as extensive peritumoral edema, which is common in patients with CNS tumors (Blystad et al., 2017; Capelle et al., 2013; Wu et al., 2015).

1.3.2. Structural diagnostics

Structural preoperative examinations include MRI, CT and positron emission tomography (PET). Additionally, diffusion tensor imaging (DTI) fiber tracking (DTI FT) allows for the identification of cortical fiber tracts running in proximity to the tumor. All these techniques are used to precisely locate the tumor in its full extent and are therefore an integral part of preoperative diagnostics (Krivosheya et al., 2016). As only MRI and DTI FT are part of this study, the following short depiction will be restricted to these two techniques.

1.3.2.1.Magnetic resonance imaging

Based on electromagnetic fields and especially suitable for soft tissue structures, MRI has been established as one of the elementary three-dimensional structural diagnostic techniques next to CT scans (Brown, 2014; Reiser et al., 2017). Underlying MRI is the difference in magnetic signal alteration of volumetric units – referred to as voxels – depending on the composition of molecules inside of said voxel. The underlying physical principles leading to these signal alterations will shortly be described in the following (Brown, 2014; Demtröder, 2013; Fließbach, 2012).

The atomic nucleus consists of nucleons (neutrons and protons) which themselves are made up of elementary particles. Elementary particles exhibit an intrinsic angular momentum – called spin. Due to their spin, these particles exhibit a magnetic moment. Consisting of such particles, nucleons also exhibit a specific spin and magnetic moment. Finally, each atomic nucleus exhibits a cumulative nuclear spin which – among other factors – depends on the spin of its nucleons (Fließbach, 2012). The nuclear spin as well as its magnetic moment is the basis of MRI (Brown, 2014).

In MRI, a subject is placed in a static magnetic field. This magnetic field affects the atomic nuclei by inducing a torque that is directed towards aligning the axis of the nuclei's magnetic moment with the magnetic field direction. Due to momentum conservation, this leads to a precession of the nuclear cores' magnetic momentum around the magnetic field axis – the so-called Larmor precession. The rate at which the momentum revolves around the magnetic field axis is called Larmor frequency and depends – among other factors – on the external magnetic field strength (Ruh et al., 2018). In the state of thermodynamic equilibrium, a slight excess of the otherwise diffusely spread nuclear spins are directly aligned to the magnetic field axis. This leads to a longitudinal magnetic field induced by the excess magnetic momentum of these atomic cores (Reiser et al., 2017).

To conduct an MRI sequence, a second electromagnetic field – directed perpendicular to the static field – is repeatedly applied at a frequency that is identical to the Larmor frequency of the atomic (for medical purposes usually hydrogen) nuclei. As for hydrogen, this frequency is in the range of radio waves. This resonant field leads to the alignment of the nuclear precession movements. When all nuclei move synchronically and aligned, this results in a measurable so-called transversal rotating magnetic field (Reiser et al., 2017). Due to the principle of electromagnetic induction, which will be described in detail further below, varying magnetic fields cause the generation of secondary electric fields when applied to conductive materials

(Demtröder, 2013). This is used to measure the magnetic field strength in the MR devices receiving coils. After the secondary magnetic field is turned off, the atomic nuclei over time revert to their original, non-aligned asynchronous precession. This process is called spin relaxation and can be observed in several ways (Reiser et al., 2017).

On the one hand, one can observe spin-lattice relaxation. In short, this term describes the process of the return of the overall vector of the atomic nuclei's magnetic moments to the original state – meaning thermodynamic equilibrium with the vector aligned to the static magnetic field axis. The time it takes for the vector to return to 63% of that state is referred to as spin-lattice relaxation time, or T1 time (Behe et al., 2013; Reiser et al., 2017).

Further, the spin-spin relaxation depicts the decomposition of the aligned and synchronous precession movement. As the atomic nuclei return to their original – asynchronous - precession movements, their common momentum dissolves and the transversal magnetic field decays. The time it takes for the field to lose 63% of its initial field strength is referred to as spin-spin relaxation time, or T2 time. In common practice, the transversal field strength was found to be decaying faster than predicted by theoretical models. This is thought to – among other factors – stem from inhomogeneities in the static magnetic field. The resultant observed time is referred to as T2* time whereas T2 describes the expected time of desynchronization based on theoretical models (Behe et al., 2013; Reiser et al., 2017). By modifying the examination procedure, a sequence can be performed to be T2*-weighted. Doing so accents differences in magnetic homogeneity and is used in techniques like fMRI (*See 1.3.3.1.*).

Both T1 and T2 are dependent on the physical properties and interactions between the atomic cores of the examined tissue. These dependencies are used in MRI to gain high-contrast and high-resolution images of especially soft tissue – such as the CNS. For reasons of clarity, this thesis will not include exact specifications of certain sequences and mechanisms of encoding of each voxel's position.

1.3.2.2.Diffusion-tensor-imaging fiber tracking

As implied be the name, DTI FT is based on the data gained from DTI. DTI is a MRI technique that depicts both the absolute degree and the direction of diffusion for each voxel using a voxel-specific three-dimensional tensor (Basser et al., 1994; Brown, 2014). In principle, this detection of diffusion is again based on the change of the magnetic properties of hydrogen nuclei following the application of an external field gradient effecting the nuclei's signal emission.

Alignment of diffusion can be calculated in several ways, one if it being fractional anisotropy (FA), used in this study. A voxel in which diffusion happens only directed in a specific direction depicts a high FA value while completely homogenous, non-directional diffusion or isotropy would result in a FA of 0 (Basser & Pierpaoli, 2011). As diffusion paths in the CNS follow the neural axons, large quantities of parallel fibers e.g. of the CST correlate with concordant diffusion directions and therefore high FA values. Using this information, fiber tracts can be depicted through systematic analysis of diffusion tensors for unidirectional tensor accumulation (Basser et al., 2000; Sollmann et al., 2015). The calculation can be further refined to only include tensors with an FA above of a certain threshold as well as to only depict fibers of a given minimal length (Reiser et al., 2017).

The varying magnetic fields induce secondary electric fields in conductive materials such as the MRI device's magnets (Brown, 2014; Demtröder, 2013). These electric fields then lead to eddy currents in the affected conductive materials. In the case of DTI, the varying external gradient field induces varying eddy currents in parts of the MRI device's magnets. These eddy currents themselves induce varying magnetic fields which distort the original magnetic field and therefore lead to signal alterations. These signal alterations interfere with the actual signal alteration generated through diffusion inside each voxel. Additional, involuntary head movement during image generation also leads to erroneous signal alteration. To balance said interferences, so-called eddy current correction utilizing the structural information from other MRI scans recorded in the same session can be applied on all DTI images. Using this correction prior to tractography allows for filtering of interfering signal alterations due to both eddy currents and movement. (Mohammadi et al., 2010)

To track specific parts or tracts of the CNS, certain regions of interest (ROI) can be put into the software to modulate the fiber tracking process (Sollmann et al., 2015). ROIs can be set to be included meaning that the system explicitly analyses the DTI only for diffusion patterns that run through all included ROIs. Alternatively, ROIs can also be excluded meaning that all diffusion paths that run through the ROI are excluded from the results.

1.3.3. Functional diagnostics

Functional diagnostic measures include fMRI, magnetoencephalography (MEG) and navigated transcranial magnetic stimulation (nTMS) (Hugues Duffau, 2012). As this thesis is solely based on nTMS, the prior two techniques will be shortly described below. For reasons of clarity, the extensive description of nTMS and its characteristics will then follow as a new section.

1.3.3.1.Functional MRI

fMRI uses the blood oxygenation level as an indicator for the degree of cell metabolism. Blood flow has been shown to correlate with neuronal activity. An increase of neural activity induces an increased blood flow to said cortical area through so-called neurovascular coupling (R. F. Schmidt et al., 2011). As blood flow increases, the amount of oxygenated blood in the cortical area increases as well. The level of blood oxygenation has been shown to correlate with the T2* signal of an MRI. Areas with a high level of blood oxygenation emit a higher T2* signal. This effect has been called Blood Oxygenation Level Dependent (BOLD) effect and is based on the different magnetic properties of hemoglobin depending on oxygenation state (Mark et al., 2015). Deoxygenated hemoglobin shows paramagnetic properties which influences the surrounding magnetic field leading to an increase in T2* spin relaxation time (*1.3.2.1.*) and thus a decreased T2* signal. Oxygenated hemoglobin on the contrary induces a diamagnetic field with decreases T2* spin relaxation time thus increasing the T2* signal. (Logothetis et al., 2001; Logothetis & Pfeuffer, 2004; S. Ogawa et al., 1990; Seiji Ogawa et al., 1990; Thulborn et al., 1982).

Therefore, to e.g. identify the representation site of motor function, a patient would be asked to move a certain muscle with neural activity and thus metabolism increasing at the corresponding cortical representation site. The increase in neural activity would lead to an increase in blood flow through neurovascular coupling which could be observed by a rise in the T2* signal (Behe et al., 2013; Reiser et al., 2017).

This method has been proven to be of both high sensitivity and specificity. Therefore, fMRI currently is the most widely used method for preoperative functional diagnostics of motor function (Mehta & Klein, 2010; Wager et al., 2013).

1.3.3.2.Magnetoencephalography

Again based on electromagnetic induction, MEG detects subtle changes in the magnetic field induced by the brain's own electric activity (Vieth, 1984). Principally speaking, changes of electric activity of a certain cortical area lead to changes in the induced magnetic field. This magnetic field is extremely subtle. To be able to detect both the magnetic field itself as well as the induced changes, the patient therefore must be insulated from the earth's magnetic field. This is achieved using large, superconducting magnetic coils also called Helmholtz-coils (Demtröder, 2013; Vieth, 1984). Like the technically similar electroencephalography (EEG), MEG is capable of achieving high degrees of temporal resolution while lacking exact spatial resolution. (Darvas et al., 2004; Najib et al., 2011). Due to the necessity for elaborate preliminary measures such as insulation of the patient prior to the examination and the lack of spatial resolution, MEG is by far less commonly used than fMRI, or nTMS and is not usually part of a clinic's routine measures (Krivosheya et al., 2016).

1.4. Transcranial magnetic stimulation

1.4.1. Technical and physical basics

TMS was first described in 1985 and proclaimed as an alternative to non-invasive transcranial electric stimulation (TES) (Barker et al., 1985). While TES is based on the direct generation of an electric field (E-field) via electrodes placed on a patient's skull, TMS is based on the induction of a magnetic field. This magnetic field passes the patient's skull and then itself induces an E-field inside the cranium. (Barker et al., 1985; Barker, Freeston, Jabinous, & Jarratt, 1986; Karhu, Hannula, Laine, & Ruohonen, 2014; Ruohonen et al., 1998; Tofts & Branston, 1991).

The generation of both the primary magnetic and the secondary E-field are described by Faraday's law of Induction and follow Maxwell's equations of electrodynamics. Most notably, the Maxwell-Faraday equation describes the shape and size of the induced electromagnetic fields (Demtröder, 2013; Fließbach, 2012; Maxwell, 1865).

In TMS, the magnetic field or B-field is induced by the current running through a circular coil held by the operator. The current is generated by a stimulating unit also known as stimulator, a capacitor charged with high voltage which is then rapidly discharged through the coil. In the original design, the stimulator delivered a current of up to 4kA in amplitude (Barker et al., 1985). The induced B-field is solenoidal in shape and directed perpendicular to the winding plane of the coil. Therefore, the operator can steer the B-field by moving the coil. Unlike an E-field, the B-field is not affected by biological tissue. Therefore, when the coil is held with the winding plane tangential to the patient's skull, the B-field passes the scalp unhindered and reaches the patient's brain tissue. The magnetic field strength of the B-field correlates to the amplitude of the current running through the coil. Discharging the stimulator through the coil leads to a rapid peak of amplitude of the current running through the coil. This induces a rapid change of the magnetic field strength in the B-field. The change in magnetic field strength induces E-fields in all tissues affected by the B-field. When the change in the B-field strength is large enough, it induces an E-field sufficiently strong to excite grey matter neurons of different layers. (Barker et al., 1986; Esser et al., 2005; Fink & Christiansen, 1989; Mills, Boniface, & Schubert, 1992; Ruohonen et al., 1998; Tofts & Branston, 1991).

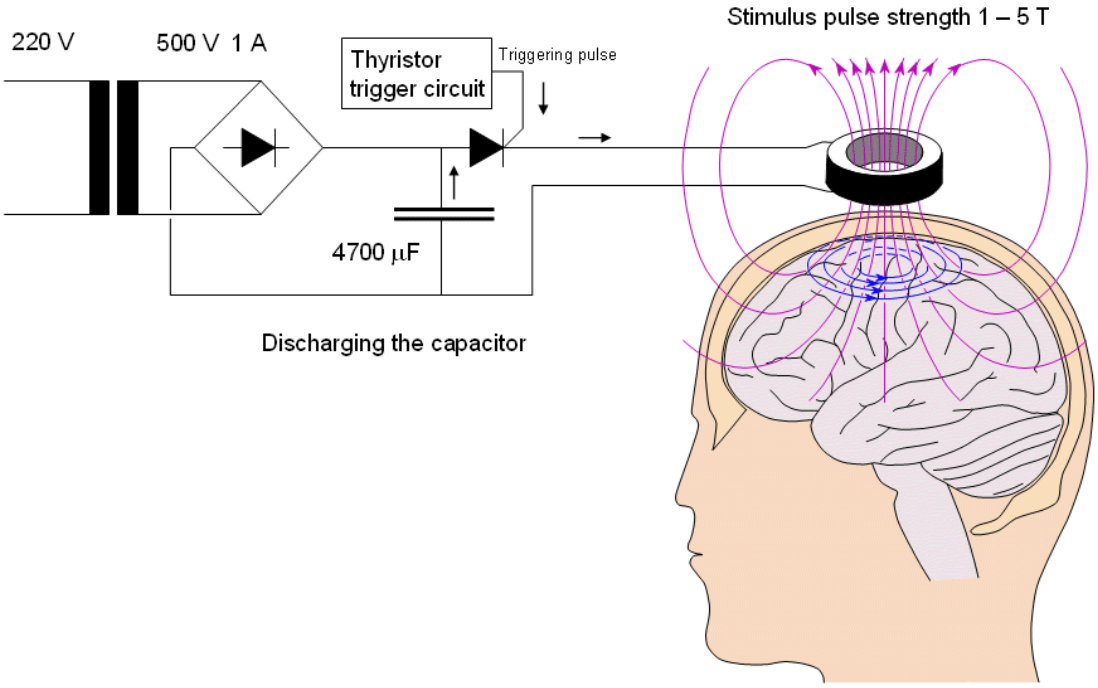

Figure 6 Schematic of the general technical principle of TMS using a round coil.
Purple: Solenoid magnetic B-field induced by the current in the coil.
Blue: Secondary induced E-field on the cortex.
Cave: Shape and location of the induced fields are merely schematic and do not depict actual field characteristics.(Malmivuo & Plonsey, 1995)

The E-field on the patient's cortex is induced by the change of the B-field. The change of the B-field again is induced by the change of the current in the coil. Consequently, E-field strength and gross E-field shape are based on the change in B-field strength and the B-field's shape which are based on the change in amplitude and the shape of the current running through the coil (Malmivuo & Plonsey, 1995).

The current's change in amplitude after discharge of the stimulator and the current's shape are dependent on the coil's material, shape and geometry. Changes in current characteristics affect the B-field which then affects the E-field. Therefore, coil characteristics such as material, shape and geometry are generally considered to be among the most important factors influencing the E-field (Danner et al., 2008; Fleming et al., 2012; Ruohonen & Ilmoniemi, 1999).

At this point it should be noted that while the shape and field strength of the magnetic field are of major importance to the shape and strength of the E-field, there are several other major

factors to consider that influence the E-field. These factors include e.g. local variances in tissue conductivity and will be addressed later on while this section focuses on the effects of different coil configurations (Nieminen et al., 2015; Opitz et al., 2011; Ruohonen & Ilmoniemi, 1999; Thielscher & Wichmann, 2009).

In general, there are two basic types of coil shape, round and figure-of-8 shape. Figure-of-8 shape or butterfly shape is basically a combination of two round coils side by side. Thus, while a round coil produces a rather homogenous magnetic field without local maxima, a figure-of-8 coil produces a magnetic field maximum at the conjunction site of the two singular round coils where either coils' B-fields overlap. Accordingly, figure-of-8 coils have been found to also produce a more tightly focused E-field than round coils. This makes them better suited for diagnostic uses such as preoperative mapping where accuracy is of vital importance, whereas round coils are rather suited for the homogenous stimulation of broader areas e.g. in therapeutic settings such as treatment-resistant major depression (Cohen et al., 1990; Johnson et al., 2013; Kennedy et al., 2009; Mills et al., 1992; Roth et al., 1991; Thielscher & Kammer, 2004).

Regarding stimulation characteristics, TMS stimuli can be applied as a single pulse, in the form of paired pulses and repetitively which is then referred to as repetitive TMS (rTMS). Depending on the site of stimulation as well as the form and frequency of the stimuli, TMS based stimuli can be used to study a multitude of cortical functions. These functions range from basic motor and somatosensory function up to complex functions such as speech or calculus (Forster et al., 2012; Ille et al., 2016; Krieg et al., 2014; Maurer et al., 2015; Ottenhausen et al., 2015; Picht et al., 2011; Tussis et al., 2016). It should be noted that these assets can only be achieved when combining the TMS unit with a neuronavigation system as described below.

Additional to the survey of explicit neurophysiological functions, TMS can be used as a tool in further diagnostics such as nerve conduction velocity as well as in therapeutic settings e.g. in the treatment of depression via rTMS or recovery of motor function or aphasia following a stroke (Du et al., 2016; Herwig et al., 2001; Kennedy et al., 2009; Kim et al., 2016; Lefaucheur et al., 2014; Mallik & Weir, 2005; Wall et al., 2016).

1.4.2. TMS-induced neural activation

An important factor in TMS is the site of neuronal innervation. In theory, the E-field induced by TMS could lead to a multitude of cellular reactions and therefore a multitude of changes in neuron activity depending on the part of neuron that has been stimulated by the E-field

(dendrite, soma, axon). Experimental studies found that the myelinated axon is the part of the neuron with the highest sensitivity to stimulation via external E-fields (Ranck, 1975; Rattay, 1999). As shown by Rushton in 1927, the degree of axonal excitability is highly dependent on geometrical factors such as the orientation of the E-field to the axon and the E-field's direction. Principally speaking, axonal excitability roughly correlates to the cosine of the angle between axon and E-field direction. As the cosine of 0° yields 1, stimulation is most effective when the angle between axonal axis and E-field direction is 0°. Therefore, an axon is easiest excited by an E-field directed exactly alongside the axon. (Rattay, 1999; Rushton, 1927; Thielscher et al., 2011).

The exact pathways of neuronal innervation by TMS that lead to functional reactions have best been described in the context of motor stimulation by analyzing MEPs (Esser et al., 2005; Ranck, 1975; Rattay, 1999; Rushton, 1927). Supramaximal electric stimulation e.g. via DCS usually results in the generation of several combined MEP in the observed muscle. As each single MEP depicts the activation of a single corticospinal pyramidal tract neuron in the motor cortex, the multitude of MEP following cortical stimulation depict multiple neural activations (Day et al., 1989). When also considering the latency between stimulation and the resultant MEP, short latency D-waves can be discriminated from delayed I-waves. D-waves stem from the direct stimulation of pyramidal neurons by the stimulus. I-waves on the other hand stem from the indirect stimulation of the pyramidal neuron via excitatory Interneurons in the grey matter (Day et al., 1989; Rattay, 1999). While MEP induced using TES or DCS consist of both D- and I-waves, TMS induced MEP do not exhibit a D-wave but only consist of several volleys of rhythmic I-waves. This suggests that TMS does not directly activate pyramidal neurons. Instead, the activation via TMS most likely results from the activation of both excitatory and inhibitory Interneurons (Esser et al., 2005). Interestingly, an increase in stimulation intensity does not ultimately lead to the generation of D-waves but only to an increased count of rhythmic I-waves with a constant inter-wave-delay. (Day et al., 1989; Esser et al., 2005; Rattay, 1999).

In a model study, Esser et al. found the elicited CST innervation to stem from the activation of both excitatory and inhibitory Interneurons in Layer II, III and VI (Esser et al., 2005). These interneurons project onto excitatory CST neurons in Layer V which were never directly innervated by the TMS E-field. Latency between each I-wave was found to originate from interneuron transmission and refractory timing. An increase in TMS intensity was again shown to lead to an increase in I-wave count. This was due to the induced E-field taking longer to decay thus keeping the interneurons innervated for longer amounts of time. Also, due to the resultant increase in E-field-strength, interneurons located at the border of the focal area where

the E-field was too weak to facilitate for innervation before were now innervated as well leading to higher I-wave amplitudes. (Epstein et al., 1990; Esser et al., 2005).

Fitting these findings, TMS to the motor system has early been shown to be most effective when the E-field is targeted perpendicular to the targeted gyrus' neighboring sulcus (Brasil-Neto et al., 1992; Karhu et al., 2014; Mills et al., 1992). In this case, the horizontally layered interneuron axons are being stimulated longitudinally and thus ideally stimulated as stated above (Fox et al., 2004). Furthermore, these findings imply that an increase in TMS intensity further above the intensity required for MEP generation leads to a less focal stimulation due to additional neural activation at the border of the E-field.

1.4.3. Navigated transcranial magnetic stimulation

1.4.3.1. Necessity of neuronavigation

As described above, the effect of TMS is highly dependent on both the position of the E-field on the cortex as well as its orientation. Ideally, the point of maximum field strength is aligned exactly to the desired cortical target. Further, the E-field must be oriented alongside the desired neurons' axis. For motor mapping, this is achieved by orienting the E-field perpendicular to the neighboring sulcus. This influence of coil position and coil orientation was already observed during the early stages of TMS, leading to the development of the first guidance systems (Mills et al., 1992; Roth et al., 1991). Further studies have since shown that even subtle differences in coil tilt or coil orientation already result in significant changes of the mapping results while remaining otherwise unchanged and controlled conditions for coil positioning (Fox et al., 2004; S. Schmidt et al., 2015).

Early TMS guidance and target description have been based on the geometrical reference to external anatomical skull landmarks such as the vertex, for instance. Stimulation sites were described based on their distance to the vertex in absolute values as well as the coil's angle to the midline. This system has further been supplemented by the 10-20 system otherwise used for electroencephalography (EEG) electrode placement (Brasil-Neto et al., 1992; Herwig et al., 2001; Herwig et al., 2003; Mills et al., 1992; Wassermann et al., 1992). While the latter at least pays respect to individual variance in head size and shape and is partially still being used e.g. in psychiatric settings (Anderson et al., 2016; Fitzgerald et al., 2009; Johnson et al., 2013), both systems have been shown to be insufficient methods for the guidance of TMS in a diagnostic setup and to lead to a significant decrease in TMS efficiency and repeatability (Ahdab et al., 2016; Julkunen et al., 2009; Saisanen, 2011).

Aside of the insufficiency regarding efficiency and repeatability especially when aiming to achieve levels comparable to modern techniques such as DCS (Barbosa et al., 2015; Danner et al., 2008; Roux et al., 2016), sole external landmark guidance has several further shortcomings. For once, macroscopic brain anatomy has been shown to vary significantly even in healthy subjects (Keller et al., 2007; Mylius et al., 2013). Hence, it cannot be estimated adequately based on clinical inspection and measurements alone and without respect to individual neuroimaging. This holds true especially in a clinical setting where patients often present with additional pathologic brain anomalies (tumors, atrophy, edema, scar tissue etc.). Also, aside of macroscopic anatomic differences, brain function spread exhibits significant variability in both healthy subjects and patients. For example, the motor representation area of the hand muscles may deviate significantly from its typical location inside the hand knob area of the precentral gyrus. In the case of hand motor function, spread was mainly but not always in the anterolateral direction (Ahdab et al., 2016; Branco et al., 2003; Niskanen et al., 2010; M. C. Park et al., 2007; Teitti et al., 2008). Finally, even if the target area could sufficiently be identified via external landmarks, the above-mentioned high sensitivity of TMS to subtle shifts in coil positioning and orientation cannot be compensated without permanent supervision (S. Schmidt et al., 2015).

For these reasons, TMS devices have been combined with neuronavigation systems to facilitate for nTMS. In nTMS, the neuronavigation unit serves two purposes. On the one hand, it tracks and supervises the coil's position and orientation in relation to the patient's skull. On the other hand, it uses this information to project the shape and orientation of the E-field on the patient's MRI (Gugino et al., 2001; Karhu et al., 2014).

When comparing nTMS to non-navigated TMS, Julkunen et al. found the usage of nTMS to lead to significantly shorter MEP latencies as well as significantly higher amplitudes. When repeating stimuli, MEP variation was significantly lower using nTMS. Non-navigated TMS lead to target deviations of 9.9 ± 1.9 mm when compared to the navigated target during hotspot location and inter-target distances of 7.1 ± 2.5 mm during target repetition (Julkunen et al., 2009).

Using the assets of neuronavigation, modern nTMS systems have been shown to be comparable to the gold standard of intraoperative DCS concerning their levels of accuracy and repeatability (Casarotto et al., 2010) as well as sensitivity and specificity (H. Duffau et al., 2005; Forster et al., 2011; Krieg et al., 2012; Ottenhausen et al., 2015; Tarapore et al., 2012; Tarapore et al., 2016).

1.4.3.2.Co-registration

An essential part of neuronavigation is the co-registration of the patient's MRI with the navigation system's spatial information. By aligning the spatial information derived from a camera system with certain markers on the MRI, the location of e.g. the coil can be projected onto the MRI. Modern neuronavigation systems include additional surface-based fiducial techniques to further increase registration accuracy and minimize systematic errors (Fitzpatrick et al., 2000; Karhu et al., 2014; Noirhomme et al., 2004; Potts et al., 1998).

Initially, spatial coordinates were derived off stereotactic systems with the coil permanently attached to a stereotactic arm. In this setting, both coil and patient head had to be firmly fixed to ensure stable navigation conditions. This tracking system has since been developed using optical tracking via infrared cameras and optical reflectors attached to both the patient's head and the instruments used in the process. Through the implementation of optical tracking, both the patient's head and the coil could be freely moved as long as the optical reflectors remained fixed on them (Danner et al., 2008; Ettinger et al., 1996; Krings et al., 1997). The exact tracking of the coil position and orientation in relation to the patient's head allows for the high repeatability of nTMS stimulations: each stimulation's referring coil position and orientation can be saved by the neuronavigation system and used as guidance for repeated stimulation (Karhu et al., 2014).

1.4.3.3.Line-navigated TMS

To ensure for accuracy aside of repeatability, spatial information needs to be implemented by the system to calculate the characteristics of the induced E-field on the cortex. Early model studies analyzed the characteristics of the induced E-field using homogenous models. These studies have come to the conclusion that the maximum field strength of the E-field induced by a figure-of-8 coil can be found directly under the conjunction of the two single coils by following the axis of the coil windings (Cohen et al., 1990; Mills et al., 1992; Ruohonen et al., 1998). This spot of maximal field strength was deemed equivalent to the focal point of stimulation.

Based on this, early nTMS neuronavigation systems have calculated the stimulation's focal point using geometric measures (Hugues Duffau, 2012). Starting from the center of the figure-of-8 coil, a perpendicular to the winding plane of the coil was calculated. In a next step, the intersection of said line with the patient's cortex was calculated based on the coil's position and orientation to the skull. The stimulation focal point was then presumed to be located at that intersection and marked on the MRI. The E-field was thought to be layered parallel to the winding plane of the coil. The direction of the E-field at the focal point was determined to be directed alongside the figure-of-8's midline (Ettinger et al., 1996; Gugino et al., 2001; Krings et al., 1997; Krings et al., 1997).

With the upcoming of alternative navigation techniques, this original technique has recently been referred to as LnTMS (Hugues Duffau, 2012; Saisanen, 2011). Early LnTMS systems solely projected the focal point without visual information of the E-field's direction. The LnTMS system used in this study additionally projects the expected E-field onto the cortex while still using line navigation for the determination of the focal spot and the E-field's characteristics.

1.4.3.4.Electric-field-navigated TMS

With rising evidence for the influence of additional physical factors on the E-field as well as rising technical capacities, EnTMS has been developed as an alternative method for E-field projection and focal point determination (Danner et al., 2008; Karhu et al., 2014; Saisanen, 2011; Teitti et al., 2008; Thielscher et al., 2011).

One example for additional influences onto the E-field is tissue conductivity, which varies significantly between different tissues in the human skull (CSF, cortex, dura mater, cranial bone). Depending on the angle in which the E-field passes the transition zone between two tissues, the resultant E-field strength either increases or decreases significantly (Opitz et al., 2011). Another factor greatly influencing the E-field is the distance between coil and cortex which has been shown to inversely correlate with E-field strength exponentially. (Danner et al., 2012; Julkunen et al., 2012; Trillenberg et al., 2012).

Such influences cannot be accounted for based on spatial information alone. Therefore, EnTMS - unlike LnTMS - utilizes on-line calculation of the induced E-field based on a mathematical model applied to a spherical head model using live data (Nadeem et al., 2003; Ravazzani et al., 1996). The spherical head model coarsely represents the different layers of the human anatomy and includes physical factors such as the above-described tissue connectivity. The fitting spherical head model for each single stimulation is chosen on-line and based on the properties of the patient's skull at each stimulation site. The spherical head model has been shown to be in good accordance to a realistic head-shaped model as long as stimulation is not applied in far frontal or occipital areas. As motor mapping primarily targets areas in or near BA6 and BA4 (M1, PMC, SMA), the spherical head model can be regarded as well-suited for this indication (Brodmann, 1909; Hamalainen & Sarvas, 1989).

Aside of the spatial coil information delivered by the tracking system, the calculation also includes additional coil characteristics such as winding geometry and coil temperature as well as stimulator output (Ruohonen & Karhu, 2010). Based on this calculation, the E-field is projected on the patient's MRI. The stimulation focal point is defined by the point of maximal calculated E-field strength and displayed on the patient's MRI with a visual marker e.g. an arrow depicting the calculated E-field's destination at the focal point.

1.4.3.5. Benefits of nTMS

The importance of sufficient tools for functional preoperative diagnostics has been well established. Currently, fMRI marks the most widely used technique for identification of cortical site of human motor function prior to tumor surgery (Krivosheya et al., 2016; Reiser et al., 2017). Yet, fMRI like MEG passively detects general changes in cell activity following voluntary activities such as speech or muscle movement. Both methods lack information about the actual involvement of these areas in the specific activity due to their passive nature.

nTMS on the other hand actively induces focal changes in neuron activity. Therefore, changes in e.g. motor activity following nTMS are a direct result of the cortical activation at the specific site. This makes nTMS the only non-invasive method that can give evidence on the causality between cortical activation and function whereas MEG or fMRI only identify cortical areas generally involved in but not causal for said function (Krings et al., 2001, 2001; Najib et al., 2011). Also, as fMRI is based on the process of neurovascular coupling, one main hindrance of using fMRI for functional diagnostics prior to tumor surgery is the tumor-induced dysfunction of neurovascular coupling in the surrounding tissue. This effect has been shown to significantly interfere with the identification of functional areas in patients suffering from brain tumors and hence affect fMRI reliability (Hou et al., 2006; Mark et al., 2015; Rutten & Ramsey, 2010; Sollmann et al., 2013). nTMS on the other hand is not affected by the dysfunction of neurovascular coupling.

Utilizing up-to-date neuronavigation systems, nTMS can stimulate the cortex with an accuracy comparable to both intraoperative DCS as well as preoperative fMRI while providing otherwise unavailable information about the causality of the identified cortical areas for a specific function. Therefore, nTMS has the potential of being a highly useful tool for non-invasive, preoperative functional diagnostics (Coburger et al., 2013; Forster et al., 2011; Krieg et al., 2014; Krieg et al., 2015; Picht et al., 2009; Picht et al., 2011; Picht et al., 2016; Sollmann et al., 2016; Sollmann et al., 2016; Takahashi et al., 2012; Tarapore et al., 2012; Weiss et al., 2013).

1.5. Aim of this study

With rising evidence for its benefits, nTMS has been increasingly used in the preoperative setting for tumor surgery (Krieg et al., 2014). The first commercial nTMS device for motor mapping has been approved by the United States food and drug administration (FDA) and marked for European conformity (Conformité Européenne; CE) in 2009 followed by the first module for speech mapping in 2012.

Nevertheless, nTMS remains highly dependent on its neuronavigation system to provide for appropriate accuracy and repeatability (Julkunen et al., 2009). As stated above, neuronavigation can currently be performed based on line or electric-field navigation. As different as those two techniques are regarding their assumptions of the induced electric field, they have so far never been compared to each other concerning their effects on the mapping process.

Comparing both techniques for the first time, main aim of the study was to assess whether the usage of different navigation techniques lead to a significant effect on the mapping process overall. Clinical differences were assessed using workflow and applicability parameters as well as quantitative stimulation parameters. As procedures were conducted by a prior naïve operator, learning curves for either technique could be depicted as well.

2. MATERIALS AND METHODS

2.1. Ethical considerations

Adhering to the rules for experiments on human subjects determined in the Declaration of Helsinki in 1964, our study protocol was presented to the ethical committee of the Klinikum rechts der Isar (RdI) and found to be in line with the committee's ethical standards (registration number: 249/15s). All patients provided written informed consent before undergoing the nTMS procedure following an extensive informative conversation with a doctor involved in the study. All data was anonymized to ensure no reference can be made to the patient's identities. As the mappings were performed as a part of the preoperative diagnostics, only data acquired with the FDA-approved and CE-marked EnTMS device was used for any patient-related further procedures.

2.2. Study design

The study was designed as a prospective, non-randomized crossover study. Motor mappings were conducted on patients with brain tumors as part of the routine preoperative procedure using two different nTMS devices that were based on either line- or electric-field navigation. Each patient was planned to receive complete motor mappings of both hemispheres with both devices consecutively. Both mappings were conducted in one session on the same day. During and following each motor mapping, timings and further characteristics were noted for later comparison.

To avoid systemic bias in favor of the EnTMS based system established at our study group, a formerly naïve operator conducted all motor mappings included in this study. The operator received extensive training by representatives of either system's manufacturers before beginning data collection to ensure for neutral conditions. During the data collection phase, the operator received no support by the EnTMS-trained members of the study group. To further minimize systemic bias, the sequence in which the mappings were performed was alternated for each patient. As the LnTMS device was a temporary loan, data acquisition time frame was restricted to six weeks in total.

Patient data included in the study was restricted to gender, age, handedness, tumor identity and site as well as tumor malignancy according to the World Health Organization (WHO) grading system. Gliomas were subdivided into low-grade glioma (LGG, grade I and II) and high-grade glioma (HGG, grade III, IV) (Louis et al., 2007; Sanai et al., 2011).

2.3. Patient cohort

As nTMS motor mapping is a regular part of the preoperative procedure at the RdI's neurosurgical department, patient acquisition was performed during clinical routine, with the decision for nTMS motor mapping being purely based on clinical indication.

Inclusion criteria for this study were:

- Age above 18 years
- Signed informed consent following extensive informative conversation
- Tumor location in a supposedly motor-eloquent region diagnosed by preoperative MRI

Exclusion criteria were:

- Age below 18 years
- Presence of metallic hardware near the stimulation site (e.g. cochlear implants, internal pulse generators, medication pumps, implanted brain electrodes)
- Pregnancy
- Non-treated recent history of epilepsy

2.4. Magnetic resonance imaging

The study only used imaging data acquired during the clinical routine preoperative procedure. No additional sequences or procedures were conducted. Cranial MRI (cMRI) was performed on a 3-Tesla scanner (Achieva 3T, Philips Medical Systems, The Netherlands B.V.) with an 8-channel phased array head coil. Contrast enhancement was achieved using intravenous gadopentate dimeglumine (Magnograf, Marotrast GmbH, Jena, Germany).

From the available sequences, the study used a fluid attenuated inversion recovery (FLAIR) sequence (TR/TE: 12,000/140 ms, voxel size: 0.9 × 0.9 × 4 mm3, acquisition time: 3 min) and a 3-dimensional T1-weighted magnetization prepared rapid gradient echo (MPRAGE) sequence (TR/TE: 9/4 ms, 1 mm^3 isovoxel covering the whole head, acquisition time: 6 min 58 s) as well as DTI sequences with fifteen orthogonal diffusion directions (TR/TE 10,737/55 ms, spatial resolution of 2 × 2 × 2 mm3, b-values of 0 and 800, acquisition time: 6 min 26 s). Images were exported using the DICOM standard (Sollmann et al., 2016).

2.5. nTMS setups

2.5.1. System arrangement

For the duration of the study's data acquisition phase (September 2015 until November 2015), both nTMS devices were permanently mounted in the dedicated study room to avoid technical errors due to assembly errors of the mobile LnTMS device. System setup was not modified by the operator and all devices were used strictly adhering to the terms stated by the instructors.

2.5.2. LnTMS setup

LnTMS motor mappings were conducted using a mobile version of the ANT Visor2 XT 3D system (ANT Neuro, Enschede, The Netherlands). The system was provided, delivered and mounted by the Inomed GmbH (Inomed Medizintechnik GmbH, Emmendingen, Germany). TMS pulses were delivered by a Magstim 200² stimulator connected to a Magstim Double 70mm Alpha figure-of-8 coil (The Magstim Company Ltd, Whitland, Carmarthenshire, UK; inner coil diameter 70mm). To enable for spatial tracking, all instruments as well as the patient's head were equipped with infrared reflecting spheres.
Infrared tracking was performed by a Polaris NDi Spectra tracking device (Polaris Spectra, Waterloo, Ontario, Canada). EMG was recorded using a TMSi Mobi mini EMG device (TMS international, Oldenzaal, The Netherlands) connected to Asmuth ASF40C Ag/AgCl-electrodes (Asmuth GmbH Medizintechnik, Minden, Germany). The EMG could be set to adapt several high- and low-pass filters to optimize EMG quality.

2.5.3. EnTMS setup

For the conductance of the EnTMS motor mappings, the Nexstim eXimia 4.3 system (Nexstim Oy, Helsinki, Finland) established at the study group was used. The system included a built-in proprietary stimulator connected to a Nexstim Focal Coil with an inner coil diameter of 70mm. Again, instruments as well as the patient's head were marked with infrared reflecting spheres. Infrared tracking was performed using a Polaris Spectra tracking device. EMG was recorded by an integrated proprietary Nexstim EMG device connected to Neuroline 720 Ag/AgCl-electrodes (Ambu GmbH, Bad Nauheim, Germany)

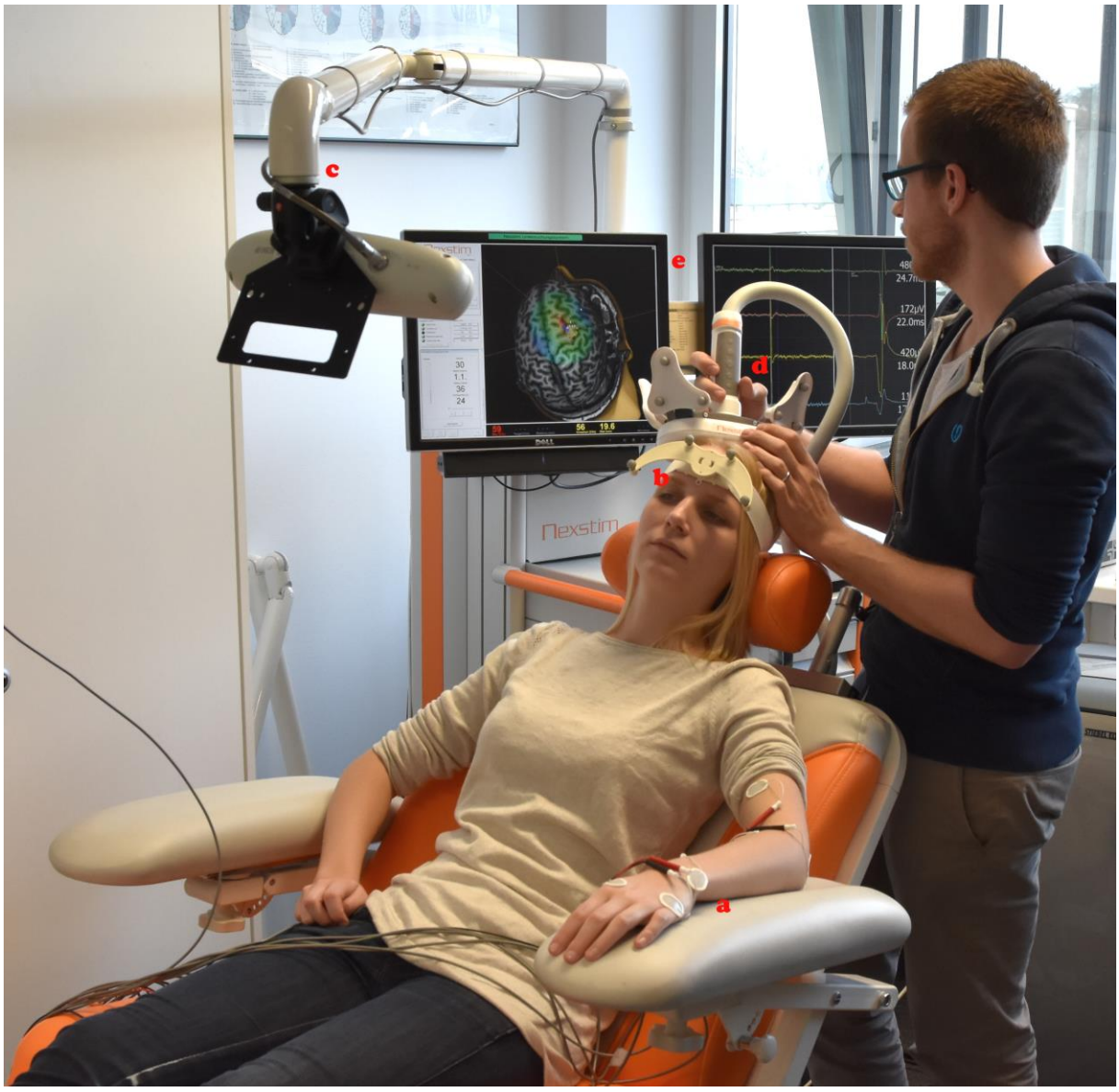

Figure 7 Setup of the EnTMS based system.

a) EMG electrodes placed on the observed muscles as described in 2.7.1. with the subject placed in a padded chair. b) Headband with attached reflecting spheres. c) optical tracking unit. d) Stimulation coil with attached reflective spheres. e) EnTMS system user interface with navigation display on the left and EMG on the right.

2.6. MRI implementation and co-registration

2.6.1. MRI import

Preliminary to motor mappings on either device, the patient's cMRI scans were imported into the navigation software of each system. Both mappings were conducted using the same MPRAGE sequence with contrast enhancement (exported in the DICOM format). Both systems integrated the MRI to generate a 3D model of the patient's skull and brain. The EnTMS based system allowed for continuous peeling of the 3D model to depict the cortex surface. The LnTMS device used a contrast-recognition algorithm to automatically depict the cortical surface characterized by the sharp contrast in signal intensity at the cortex-CSF transition. The cortical surface could be sufficiently depicted for further stimulation target determination with either software. Yet, as the LnTMS method did not include information about the thickness of the overlying tissue, stimulations could not be adjusted to be targeted at the same depth. For EnTMS targeting, peeling depth was set to 20-25 mm.

Figure 8 Display of the EnTMS device's software after import of a healthy subject's (non-contrast-enhanced) MRI. Note the first row with the original sagittal, coronal and axial scans on the top and the computed 3D model on the bottom left. Peeling depth was set to 21.7 mm on the left side control.

2.6.2. Co-registration

Following successful MRI import, co-registration of the MRI with the spatial information delivered by the tracking systems was performed. In both cases, the first step consisted of marking three fiducial spots on the patient's MRI. In our study protocol, both sides' crura of helix as well as the nasion were chosen as fiducial spots. Afterwards, the operator fastened system specific headbands with reflecting spheres to the patient's heads tightly. Patients were instructed to notify the operator should they notice the headband moving to avoid unnoticed systematic registration errors as the headband's spheres represent the patient's head to the tracking device. In case of accidental headband movement, registration could be repeated at any given time during the mapping process without loss of prior information. Each device's digitization pen which was also marked with reflective spheres was then used to present the above-mentioned anatomical landmarks to the tracking device. From this point on, spatial information and MRI coordinates could be aligned.

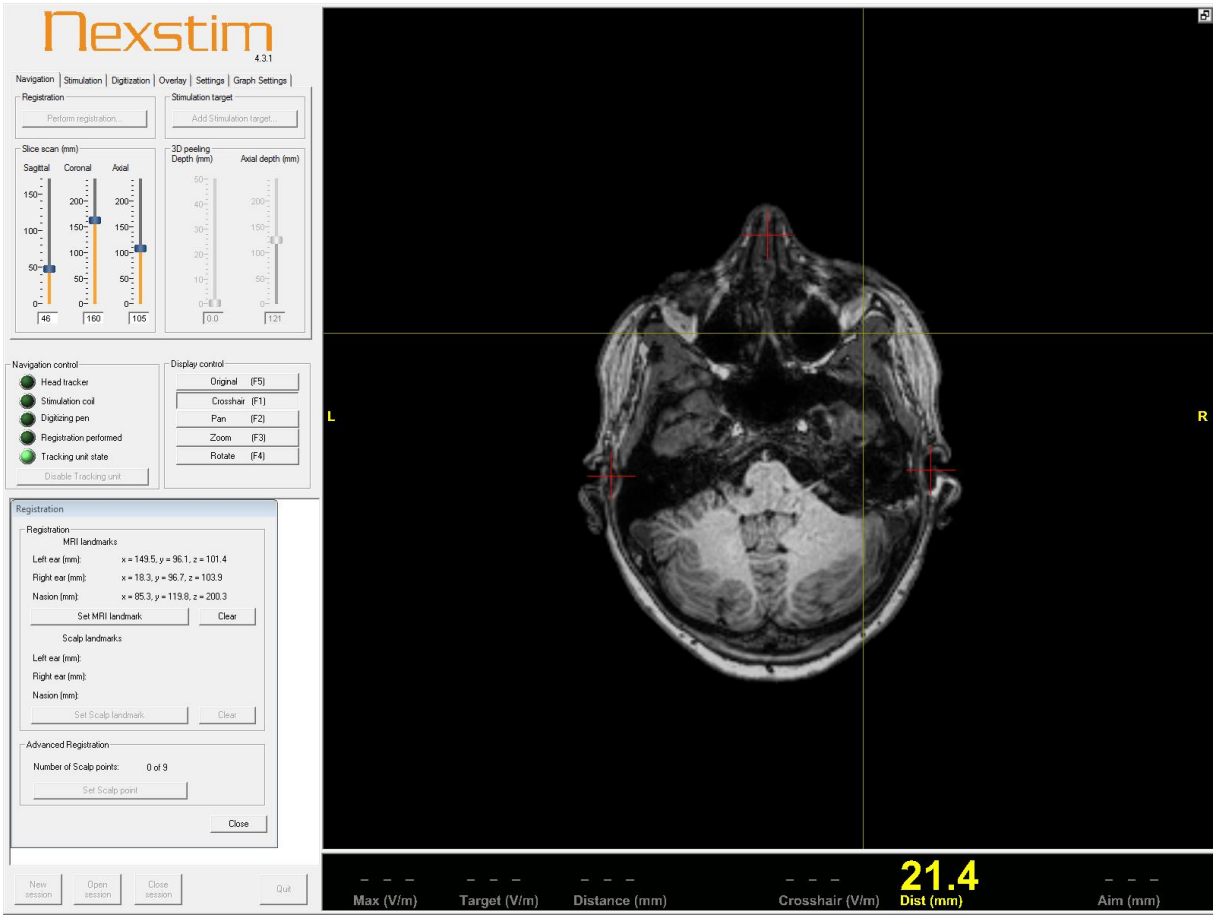

Figure 9 Display of the EnTMS device's software with the fiducial spots entered into the system. Note the markers' MRI coordinates displayed on the bottom left.

To further enhance registration accuracy, both devices utilized additional fiducial area-based methods. On the EnTMS device, nine areas on the patient's 3D skull model were depicted by the software that had to be spatially presented by the operator. The LnTMS device had the operator moving the pen freely on the patient's skull marking 50 to 99 single points from which a fiducial area was generated.

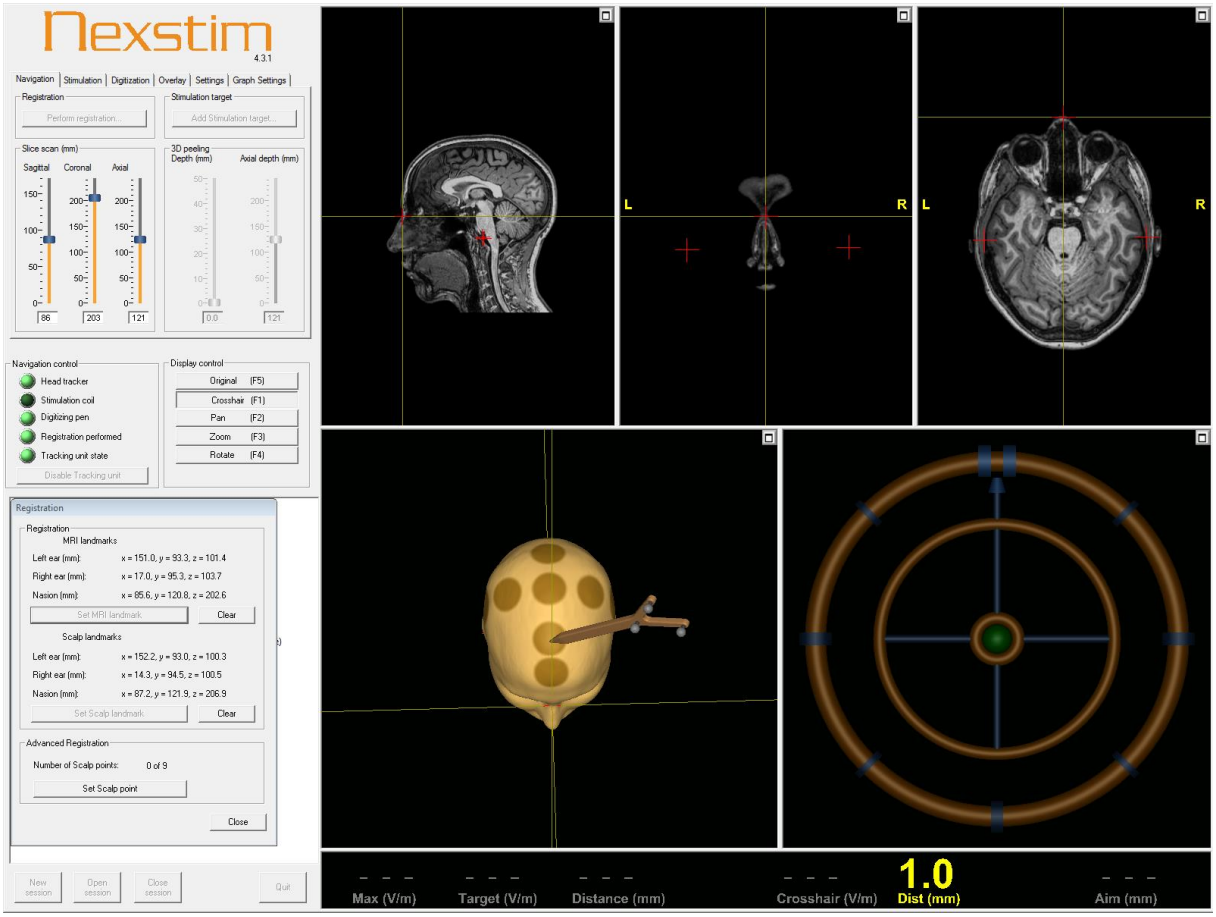

Figure 10 Display of the EnTMS device's software after spatial representation of the fiducial spots. Note the bottom left display now also showing the fiducial spots' spatial coordinates and the fiducial areas presented for spatial presentation. The current position of the digitization pen is projected onto the model based on fiducial spot co-registration.

The LnTMS device included an additional registration step in which the digitization pen was held to a fiducial label on the coil to ensure correct placement of the coil's reflective spheres.

2.7. Motor mapping

2.7.1. Basic principles

Preliminary to motor mappings, patients were again informed about the content of the procedure and patient handedness was assessed via the Edinburgh Handedness Inventory (EHI) (Oldfield, 1971). Further, each patient's degree of paresis of the upper and lower extremities was objectified using the British Medical Research Council (BMRC) scale (O'Brien, 2010). In our case, paresis was defined as a muscle strength of less than 5/5 in at least one extremity. Paresis was classified as mild when muscle strength was 4/5, and severe for all cases of muscle strength <4/5.

In general, all the following steps were conducted analogously on each device strictly adhering to the protocol. If certain steps of the procedure could not be undertaken identically, this will be noted explicitly. If not noted, the execution of a procedure was kept strictly identical to ensure for comparative conditions and avoid possible structural bias. For either device, the mapping process was executed completely before repetition on the other device.

On each device, motor mappings were conducted adhering to the then up-to-date protocol established at the study group (Bulubas et al., 2016; Krieg et al., 2012; Krieg et al., 2012; Krieg et al., 2013; Picht et al., 2009; Sollmann et al., 2016; Takahashi et al., 2013; Tarapore et al., 2012; Wassermann et al., 2008). Mapping was started on the tumor-sided or ipsilateral hemisphere followed by the non-affected or contralateral hemisphere. The operator was instructed to adhere strictly to the below described procedure for both complete mappings. Information about e.g. regions of highest excitability gained in the first mapping were not used to improve the second mapping to minimize possible bias due to mapping sequence. During the whole mapping process, the patient was placed in a padded seat. Patients were instructed to relax as best as possible.

EMG electrodes were placed on the patient's target muscles. Following protocol, UE muscles observed were the abductor pollicis brevis (APB), the abductor digiti minimi (ADM), the flexor carpi radialis (FCR) and the biceps brachii (BCS) muscles. LE muscles observed were the tibialis anterior (TA) and the gastrocnemius (GCN) muscles. The grounding electrode was placed on the patient's elbow. EMG cables were placed separately to avoid interference due to cable crossing etc. Extremities were placed to ensure ideal EMG conditions by passively flexing the observed muscles. EMG optimization was repeated until EMG background noise was clearly below 50 µV in amplitude.

Before each stimulation, coil position and orientation were optimized to ensure for ideal E-field strength and direction at the focal point. In EnTMS, this process was assisted by the navigation system. As the EnTMS approach allowed for on-line calculation as well as simulation of the induced electric field, lower field strengths due to suboptimal coil positioning could be detected

by the software. In this case, the arrow depicting focal point and E-field direction turned semi-transparent until coil orientation was corrected by the user. In line with actual findings concerning optimized coil location, E-field direction as depicted by the arrow's direction was adjusted to be perpendicular to the neighboring sulcus (Rossini et al., 2015; Ruohonen & Karhu, 2010; Saisanen et al., 2008; Thielscher et al., 2011; Thielscher & Wichmann, 2009). As the LnTMS device did not include an explicit calculation of the E-field, coil optimization was performed without direct feedback by the system prior to stimulation. The operator was advised to keep the coil midline directed perpendicular to the closest sulcus and the winding plane tangential to the skull. On both devices, no stimuli were placed inside tumorous tissue.

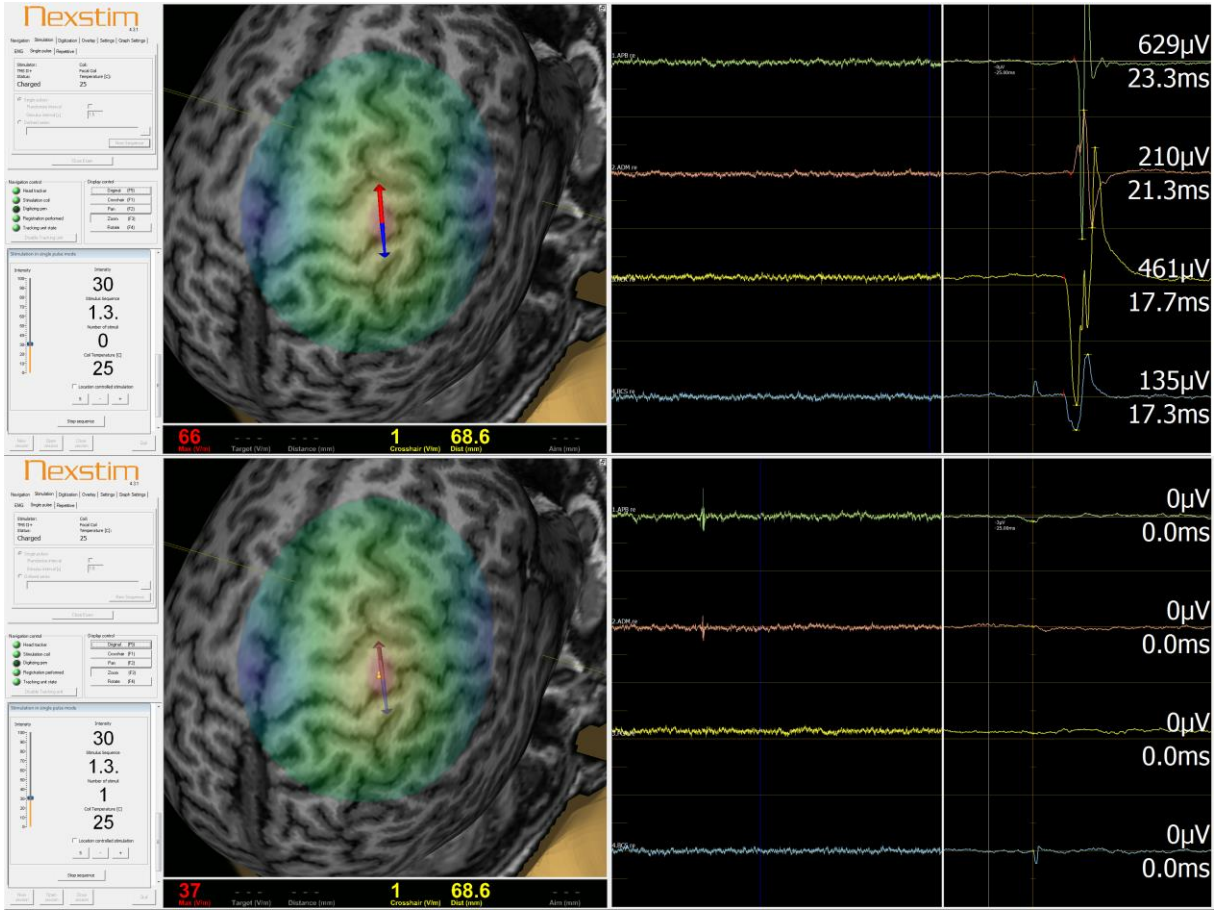

Figure 11 Stimulations of a healthy subject on the EnTMS device with (top) and without (bottom) optimization of coil positioning. Corresponding MEP responses are depicted on the right. The EnTMS device indicates suboptimal coil placement by rendering the target marker transparent. Note that even though all other factors such as coil geometry and temperature, coil-cortex distance, E-field orientation and stimulation intensity remain unchanged, calculated E-field-strengths (bottom left on the display, 66 V/m with optimal coil placement, 36 V/m without) and resultant MEP answers vary heavily.

2.7.2. Hotspot localization and motor threshold determination

As cortical excitability through nTMS varies both inter- and intra-individually, nTMS stimulation strength has to be determined individually in order to allow for comparable mapping conditions (Karhu et al., 2014; Sollmann et al., 2013; Wassermann, 2002; Ziemann et al., 1996). To do so, the so-called resting motor threshold (RMT) depicted by the percentage of the maximum stimulator output (%MO) was assessed for each hemisphere and each device. The RMT has been shown to correlate with the degree of cortical excitability. As the designation resting motor threshold implicates, its measured is based on MEP generation in a resting muscle, while the active motor threshold (AMT) is determined during weak voluntary muscle action and is usually lower than the RMT. (Day et al., 1991; Di Lazzaro et al., 1998; Temesi et al., 2014). Adhering to the study protocol, RMT was determined from either the APB or ADM muscles following location of the hotspot.

In a first step, the neuronavigation system's display was centered to the ipsilateral central sulcus. The cortical area most likely suited for hand muscle stimulation was identified using the above-described anatomical characteristics (Omega-sign, PPFM). Fitting the basic principle of somatotopy, the hotspot is most often located in or near this location (Niskanen et al., 2010). Nevertheless, as extensively described above, variations regularly occur which is why an exact location of the hotspot through nTMS is indispensable (Ahdab et al., 2016; Sollmann et al., 2013).
Starting at the identified area, a coarse first set of stimulations was applied to identify the so-called hotspot showing the highest APB- or ADM-MEP amplitude resulting of constant intensity nTMS. Stimulation intensity was increased until MEP responses with an amplitude of >100µV were achieved. As higher intensity stimulations tend to be less focal, stimulation intensity was reduced when MEP amplitude exceeded 600 µv (Esser et al., 2005; Najib et al., 2011; Rossini et al., 2015; Sollmann et al., 2013).

Following identification of the hotspot, optimal angulation for stimulation was assessed prior to RMT determination. In this context, angulation was defined as the angle between E-field direction at the focal point and the closest neighboring sulcus. The EnTMS system's target repetition mode was not utilized during the study as the LnTMS device did not include a target repetition mode. After visual identification of the to-be repeated stimulus, the operator repeated the original stimulus with unchanged coil orientation and location while varying the stimuli angulation. In this manner, stimuli were repeated with the original angulation (90°) as well as 45°/135° and 0°/180° angulations.

With both hotspot location and ideal angulation identified, RMT determination was then performed. The RMT was defined as the minimal stimulation intensity resulting in a MEP response exceeding an amplitude of 50µV in 5 out of 10 cases. As stated above either the APB or the ADM muscles were used for RMT determination. Stimuli were directed at the hotspot using optimal coil orientation and angulation as prior determined. Stimulation intensity was manually modified depending on the MEP. Again, automatized assistant tools available on the EnTMS device were not used in order to avoid bias in favor of the EnTMS device. (Rossini et al., 2015; Ruohonen & Karhu, 2010).

2.7.3. Upper and lower extremity mapping

Following RMT determination, the actual mapping process was performed, starting with the UE. For UE mapping, stimulation intensity was set to 110 % of the RMT. Mapping was begun at the hotspot. Starting here, stimulations were delivered in every single direction. For every direction, stimulation was continued until two adjacent stimulations resulted in MEP response amplitudes of <50µV in all muscles observed. Distance between single stimulations was kept at 3-5mm. Coil orientation was kept optimal adhering to the above described principles with the E-field directed perpendicular to the closest neighboring sulcus. Again, tumorous tissue was excluded from the mapping procedure keeping a safe distance of approximately 3mm. By continuing that pattern in all directions, a complete map of the cortical representation site of the UE muscles with a negative border consisting of 2 negative stimulation sites was produced. After complete mapping of the UE representation area, mapping was continued for the LE muscles. The cortical representation sites for LE muscles are most likely located in the paramedian cortical border reaching into the interhemispheric fissure and therefore less prone to stimulation. To account for this difference, stimulation intensity was set to 130% of the RMT and E-field direction was kept perpendicular to the interhemispheric fissure during LE mapping. When stimulation proved insufficient for inducing any LE MEP with an amplitude of >50µV over the whole frontotemporal and adjacent temporal lobe, stimulation intensity was increased in steps of 2%MO until a motor response could be evoked. When LE MEP could be sufficiently evoked, a LE motor map was produced in the same way as described for the UE.

Following completion of LE mapping on the ipsilateral hemisphere, the same procedure was repeated on the contralateral hemisphere starting with the identification of the hotspot. After completion of the second hemisphere's mapping, patients were asked to rate discomfort felt during the whole mapping process via the numeric rating scale for pain (NRS) (Hawker et al., 2011). Further discomfort such as nausea or vertigo was explicitly prompted and noted as well as other adverse events. Then, the procedure was analogously repeated on the other device except for the differences noted above.

2.8. Post-hoc analysis and export

Following complete mapping of both hemispheres, mapping results were examined and analyzed using both system's integrated software. Each stimulation included in the UE and LE mapping was singularly reviewed and evaluated. Depending on the corresponding MEP, stimulation spots were assigned specific markers on the corresponding MRI. Criteria for a stimulation spot being assessed as motor-positive were set as following (Kallioniemi et al., 2015; Ruohonen & Karhu, 2010; Saisanen et al., 2008):

- Amplitude of >50µV in at least one of the observed muscle's MEP
- Clear visual distinction as a single MEP from background noise
- MEP latency <30ms for UE

If a stimulation failed to conform with at least one of these criteria, it was regarded as motor-negative. After analysis, the motor-positive stimulation site markers together formed a so-called motor map for the observed muscles.

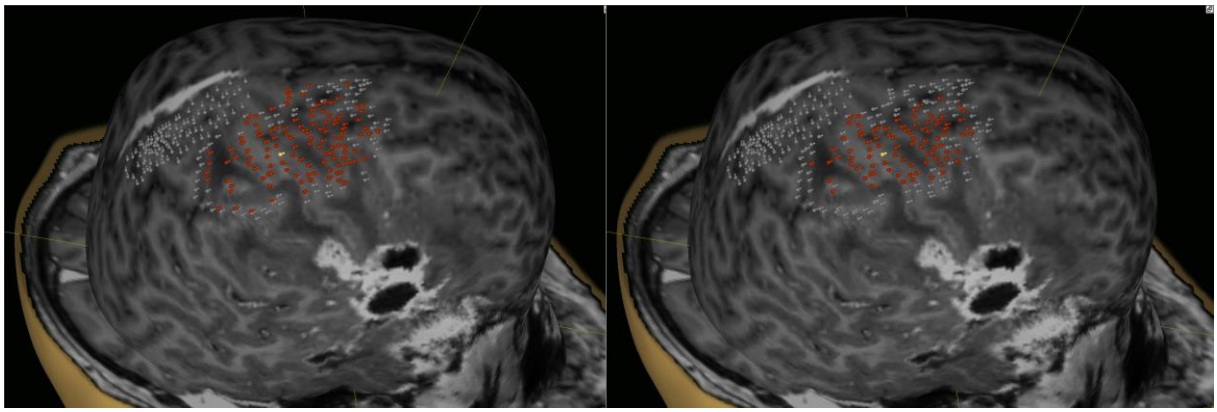

Figure 12 Display of stimulation spots following a complete mapping of the upper and lower extremity of a patient's tumor sided hemisphere on the EnTMS based device before (left) and after (right) analysis. A stimulation spot marked in grey is classified as motor negative. A stimulation spot marked in red or yellow is marked as motor positive while the different colors represent different MEP amplitudes. This color coding is not included in the final motor map which only distinguishes between positive and negative spots. Note that while the criterion of two negative spots bordering the mapping area was not achieved based on the system's automatic positive/negative classification, false positive stimulation spots were clearly identifiable as such during the mapping process and mapping was not continued further in that direction. Fittingly, the post analysis motor map does feature a double negative border as required by the protocol.

Additional to mapping analysis, quantitative stimulation factors concerning mapping characteristics were noted for later comparison. Factors included in the comparison were the RMT value, MEP amplitude at the hotspot, overall count of stimulations included in each part of the mapping process and the count of motor-positive stimulation spots following analysis on either technique. The motor-positive stimulation count only included stimuli that were marked as motor-positive after post-hoc analysis. The positive response rate was calculated using both the motor-positive stimulation count as well as the UE and LE overall stimulation count:

$$\text{Positive response rate } [\%] = \frac{\sum \text{ Motor} - \text{positive stimulation count}}{\sum \text{ Overall stimulation count in UE and LE mapping}} * 100$$

Values were noted and calculated separately for each hemisphere as well as separately for either UE, LE or both extremities.

Following analysis of all stimuli, MRI export was conducted by both systems. The exported MRI included the motor-positive markers as well as the registration markers of the original MRI allowing for anew co-registration during fiber tracking or possibly in the operation room prior to surgery. In this study, the MRI was combined with diffusion-tensor imaging (DTI) to facilitate for fiber tracking (FT) of the CST. Additional motor maps only including a hemisphere's hotspot were also exported for further analysis.

2.9. Motor map analysis and tractography

2.9.1. Setup

To allow for intraoperative usage of the EnTMS motor maps, the exports were imported into the clinic's established neuronavigation system. To further compare both techniques' spatial map properties as well as their eligibility for fiber tracking of the CST, LnTMS motor maps were imported as well. Again avoiding systemic bias, the sequence in which procedures were conducted was alternated for each patient. Neuronavigation implementation and tractography was conducted for both devices' ipsi- and contralateral hemisphere maps. Yet, adhering to our study protocol, only the ipsilateral EnTMS motor map was saved and further used for intraoperative neuronavigation while the LnTMS motor maps were discarded after complete analysis.

Neuronavigation was performed using a BrainLAB iPlan Net Server® (BrainLAB iPlan Net Cranial 3.0.1; BrainLAB AG, Feldkirchen, Germany). Motor maps were directly imported from a local device. The corresponding DTI and MPRAGE sequences created in the same original MRI session were imported from the clinic's DICOM server. After successful import, eddy current correction was applied to ensure optimal conditions for fiber tracking. Following this, image fusion was performed to compensate shifts of head position between different sequences. Motor maps were then set to overlay the original structural MPRAGE sequence.

2.9.2. Motor map analysis

Spatial hotspot analysis was performed using both device's motor and hotspot maps. Therefore, both motor hotspot map exports as well as the underlying MPRAGE sequence were again imported into the BrainLab software and fused for optimal overlap. Then, using the system's integrated spatial analysis tools, spatial distance between hotspots was measured in mm based on axial slides. As both system's exports projected the hotspot onto several subsequent slides, the middle slide of each projection was used for analysis. Afterwards hotspot location was assessed, using the original MPRAGE sequence. Finally, distance from either hotspot to the center of the visually identified hand knob was measured in mm. As the analysis did not use the cortical surface models generated by the system but instead used the original structural sequence, possible differences due to varying brain reconstructions of both systems could be avoided. Distances were measured depicting solely the radial distance between both spots without respect to the direction in which location differed. Concerning the measurement in relation to the anatomic hand knob, ipsilateral and contralateral hemispheres

were compared separately as distances were measured based on structural landmarks which could be affected by the lesion present on the ipsilateral side.

Finally, both hemisphere's complete motor maps were again imported into the system and fused with the original MPRAGE sequence. Motor map areas were then created via the system's ROI creation tool with no rim added to the stimulation spots. Area between the motor-positive spots was manually added to the ROI. Areas were assessed for both their spatial extent in cm², their spatial resolution and their ratio of overlap. Spatial resolution was defined as following:

$$\text{Spatial motor map resolution } [\frac{1}{\text{cm}^2}] = \frac{\sum \text{ Positive motor map stimulation spots}}{\text{Motor map area } [\text{cm}^2]}$$

2.9.3. CST tractography

Tractography of the CST was conducted using two included ROIs. In a first step, a three-dimensional ROI was generated using the motor-positive spots marked on the motor map as a basis. First, a rim was created for each positive spot surrounding said spot in a distance of 2 mm. Then, areas where the spots or their rims overlapped were fused to form a single, ideally continuous ROI that encompasses all positive spots. The second ROI was created manually by the operator and visually placed in the ipsilateral brainstem at the height of the tentorium cerebelli above the decussatio pyramidalis (Krieg et al., 2012; C.-H. Park et al., 2013; Seo & Jang, 2013; Sollmann et al., 2016; Weiss et al., 2015). Minimal fiber length to be included in the analysis was set to 110mm. FA threshold was set to 0.2 at the beginning of the analysis and consecutively reduced in steps of 0.01 when the analysis did not yield a satisfying depiction of the CST according to the operator's visual impression. Following successful CST tractography, the count of fibers included in the analysis was noted as well as the FA value leading to successful CST depiction.

2.10. Measurement of time durations and learning curves

Time durations were measured during all steps of the mapping process for later comparison of both techniques.
Timings for the import of the patient's MRI into the system - referred to as "MRI import" - and co-registration of the MRI with the spatial information of the tracking device - referred to as "registration" - were combined to form the "preparation for motor mapping" timing.
Durations of the coarse mapping around the hotspot needed to localize the hotspot were noted as "hotspot mapping" while time needed for the determination of the RMT was referred to as "RMT determination". UE and LE motor mappings were depicted as "UE mapping" and "LE mapping". Starting with the hotspot mapping time, these timings were summed up to form the "complete motor mapping" time. All individual timings were noted separately for each hemisphere.

Timing for post-hoc analysis of the mapping was referred to as "post-hoc analysis" and again depicted separately for either hemisphere. Finally, the duration for the implementation of either techniques' map into the neuronavigation software with additional tractography of the CST was depicted as "neuronavigation/tractography".

Complete motor mapping time in s as well as the above-described stimulation count was further used to calculate the mapping speed as following:

$$\text{Mapping speed } [\frac{1}{s}] = \frac{\sum \text{ Overall stimulations}}{\text{complete motor mapping time } [s]}$$

Analogously, mapping speed was also calculated for separate parts of the procedure, such as RMT determination and hotspot search, or UE/LE mapping.

To illustrate and compare learning effects over time, step durations and stimulation speed were plotted in relation to the consecutive patient number. Then, a linear regression method was used to depict eventual trends and their significance. Significance of each trend was evaluated via the significance of the trend's deviation from zero. Also, the trend's mean slope derived from its underlying linear equation (y=m*x+t) was used to depict trend direction and strength.

To discern between navigation dependent and navigation independent factors, step durations were divided into navigation independent and navigation dependent timings.

On the one hand, navigation independent timings included all non-navigated steps of the process (Preliminary steps, post-hoc analysis and export, neuronavigation and tractography; only including complete mappings). The evolution of said timings was used to illustrate the overall rise in routine and general technical learning effect while operating both the nTMS systems' and the neuronavigation system's user interfaces (UI) etc. The specific learning effect for navigation dependent tasks on the other hand was illustrated using both the complete duration for the mapping of both hemispheres as well as the stimulation speed during motor mapping.

2.11. Statistical analysis

Statistical analysis of the data gathered in this study was conducted via the GraphPad Prism software (GraphPad Prism 7.02, La Jolla, CA, USA). Measures are presented as mean values ± standard deviation with all ranges provided. The above described quantitative stimulation parameters (RMT value, MEP amplitude at the hotspot, Overall stimulation count per mapping, positive stimuli per mapping, positive response rate) were compared using Student's t-test (Student, 1908). Each comparison included the same parameter generated on either the EnTMS or the LnTMS device. Variances were deemed significant when the p-value was less than 0.05. Mapping specific NRS values as well as spatial motor map properties (Spatial extent, spatial resolution, FA value, CST Fiber Count) and step specific time durations (including mapping speed) were compared in a similar fashion. Technique specific learning curves were generated using linear regressions.

3. RESULTS

3.1. Patient collective

Following assembly of the LnTMS device by the manufacturer, data acquisition was conducted over the course of 3 months. In this period, a total of 12 patients were included in the study.

Age median was 53 years with age ranging from 30 years to 79 years. 7 of the study's patients were male, 5 were female. 11 patients were identified as right-handed according to the EHI. Tumor location was either frontal or parietal in all but one case. Regarding tumor entity, in 5 patients the tumor was identified as a glioblastoma (WHO IV°) while 4 presented with high-degree astrocytoma or oligodendroglioma (WHO III°) and the remaining 3 were suffering from intracranial metastases. 4 patients presented with mild or severe pre-existing motor deficits while 8 showed no clinical apparent deficit. The exact distribution can be seen in Table 1.

Patient #	Age [a]	Gender	Handedness [EHI]	Tumor side	Tumor location	WHO°	Motor deficit
1	49	M	80	Bilateral	Parietal	IV	Mild
2	51	F	100	R	Frontal	III	None
3	58	F	90	L	Frontal	M	None
4	76	M	90	L	Parietal	III	None
5	37	M	70	R	Frontal	IV	Mild
6	79	F	100	R	Parietal	M	None
7	30	M	30	L	Frontal	III	Severe
8	65	F	100	R	Parietal	M	Mild
9	56	M	70	R	Frontal	IV	None
10	37	M	90	R	Temporal	IV	None
11	45	F	100	L	Parietal	IV	None
12	42	M	100	L	Frontal	III	None

Table 1 Patient collective baseline data. Note: Patient numbers are not sorted chronologically for reasons of anonymization. Handedness is depicted using the Edinburgh Handedness Index [EHI]. Tumor grading is depicted using the WHO scale.

3.2. Technical errors

All patients consented to the complete mapping of both hemispheres. Yet, due to technical errors on the nTMS devices, complete mappings including both hemisphere's UE and LE areas could not be conducted on all patients.

On the EnTMS device, 11 patients received full mappings of both hemispheres. One patient only received a complete mapping of the ipsilateral hemisphere resulting in a complete mapping rate of 91.7%. On the LnTMS device, only six patients underwent full motor mappings of both hemispheres, resulting in a complete mapping rate of 50.0%. Two patients received a complete mapping of the ipsilateral hemisphere. In the remaining four cases, mapping could not be conducted at all.

The incomplete EnTMS mapping was due to the EMG showing a periodic interference with an amplitude of up to 100µV and a frequency of 50-60Hz. This interference was later found to stem from the system's power supply cable and the EMG connector cable lying too closely side by side. On the LnTMS device, two mappings could not be conducted due to the EMG showing an irregular interference with an amplitude of up to 2V. This error could be resolved by applying a low-pass filter even though the source could not be determined. In one case, the LnTMS device's EMG did not deliver a signal. Here, a defective power supply unit could be determined and eliminated as error source. In the remaining cases on the LnTMS device, the connection between stimulator and navigation system could not be established twice. Finally, the tracking system did not recognize the coil in one case. The problem was resolved by a change of the connection adapter.

All errors were purely hardware based and could be fully resolved. Mappings were not conducted until an error was resolved to avoid false deterioration of mappings due to hardware errors. When an error was noticed during a mapping, mapping was not continued for the same reason.

3.3. Pain and discomfort

Both EnTMS and LnTMS motor mapping were well tolerated by all patients. Aside of pain, no further adverse effects or events were observed during the study.

Pain and discomfort as depicted via NRS was restricted to none to mild temporary pain (≤ 3 NRS) on both devices without significant differences between both techniques. Pain range was slightly higher on the LnTMS device for both hemispheres (LnTMS range: 0-3; EnTMS range: 0-2). Pain was restricted to the stimulation timeframe and did not persist.

	EnTMS [NRS]	**LnTMS [NRS]**	**p**
Discomfort			
Ipsilateral	0.3 ± 0.6	0.9 ± 1.1	0.1262
Contralateral	0.3 ± 0.5	0.4 ± 0.8	0.6027

Table 2 Patient discomfort during nTMS with range depicted in brackets. Note: In this study, the hemisphere on which the tumor is located is referred to as ipsilateral.

3.4. Quantitative stimulation parameters

3.4.1. Resting motor threshold and hotspot motor-evoked potentials

Comparison for general stimulation parameters yielded a significantly higher RMT on the LnTMS device. When not discriminating for ipsi- or contralateral hemisphere, RMT averaged to 37.8 ± 7.5 %MSO on the EnTMS device versus 53.6 ± 8.1 %MSO on the LnTMS device ($p<0.0001$). MEP amplitude at the hotspot did not vary significantly, averaging to 715.8 ± 624.4 µV for EnTMS and 640.4 ± 619.1 µV for the LnTMS device, again not discriminating between ipsi- and contralateral hemisphere ($p=0.7171$). For the discriminated values, see Table 6 below.

	EnTMS	LnTMS	P
Resting Motor threshold [%MSO]			
Ipsilateral	37.2 ± 8.6	52.9 ± 9.1	0.0011
Contralateral	38.6 ± 6.3	54.4 ± 7.4	0.0002
MEP amplitude at the Hotspot [µV]			
Ipsilateral	774.0 ± 644.3	558.3 ± 347.1	0.4000
Contralateral	652.4 ± 626.5	734.3 ± 856.0	0.8174

Table 3 RMT and hotspot MEP values differentiated for site of stimulation. Note: In this study, the hemisphere on which the tumor is located is referred to as ipsilateral.

3.4.2. Stimulation count

Stimulation counts were noted separately for each part of the mapping process again allowing for discriminate analysis of individual mapping parts. Inter-system analysis yielded significantly larger counts for EnTMS concerning both overall stimulation count as well as positive stimulation count.

Overall stimulation count included both positive and negative stimulations during all parts of the mapping process. In total, overall stimulation count averaged to 617.0 ± 136.7 stimulations for EnTMS versus 409.0 ± 120.4 stimulations for LnTMS ($p=0.0026$).

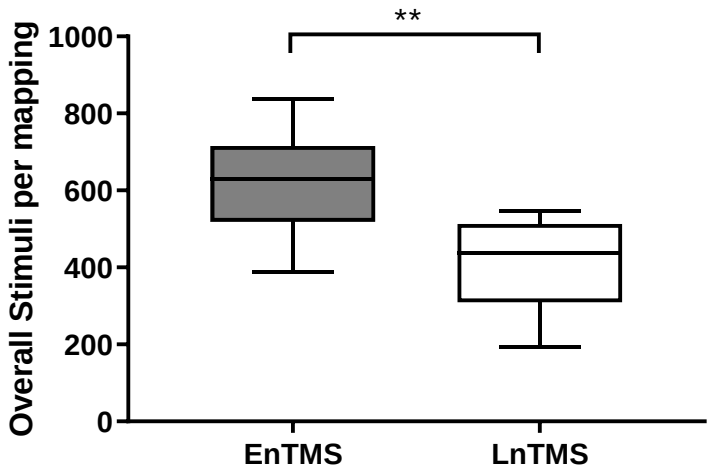

*Figure 13 Boxplot depicting the different overall stimulation counts included in complete motor mappings of both hemispheres. ** represents p=0.0026*

Positive stimulation counts per motor mapping of both hemispheres averaged to 231.9 ± 57.0 stimulations on EnTMS versus 58.5 ± 27.6 stimulations on LnTMS (p<0.0001).

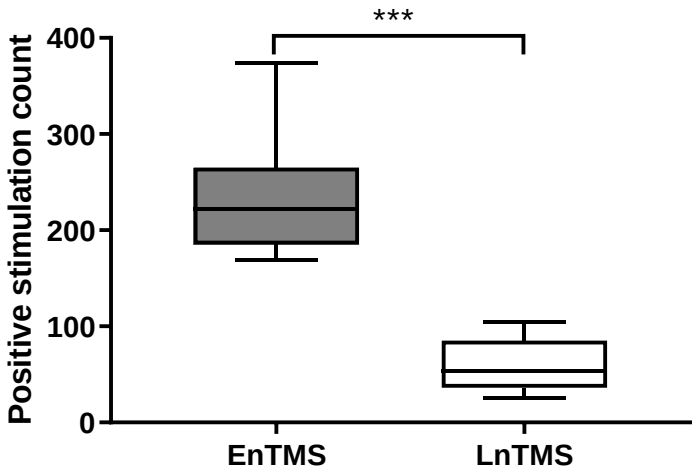

*Figure 14 Boxplot depicting different counts for motor-positive stimulations included in complete motor mappings of both hemispheres. *** represents p<0.0001*

	EnTMS	LnTMS	p
Overall stimulation count			
Ipsilateral	341.3 ± 60.0	218.8 ± 33.5	0.0001
Contralateral	300.7 ± 77.4	217.4 ± 111.7	0.0789
Bilateral	617.0 ± 136.7	409.0 ± 120.4	0.0026
Positive stimulation count			
Ipsilateral	128.3 ± 35.0	41.3 ± 26.8	<0.0001
Contralateral	113.1 ± 24.5	19.7 ± 8.7	<0.0001
Bilateral	231.9 ± 57.0	58.5 ± 27.6	<0.0001

Table 4 Overall and positive stimulation counts of the mapping process. Only completed steps were included in the analysis. Note: In this study, the hemisphere on which the tumor is located is referred to as ipsilateral.

3.4.3. Positive response rate

Additional to the overall and positive stimulation counts, the resultant positive response rates varied significantly as well. Without differentiation for ipsi- or contralateral mapping, overall positive response rate was 38.5 ± 8.9% on the EnTMS device versus 16.2 ± 12.4 % on the LnTMS device (p=0.0002).

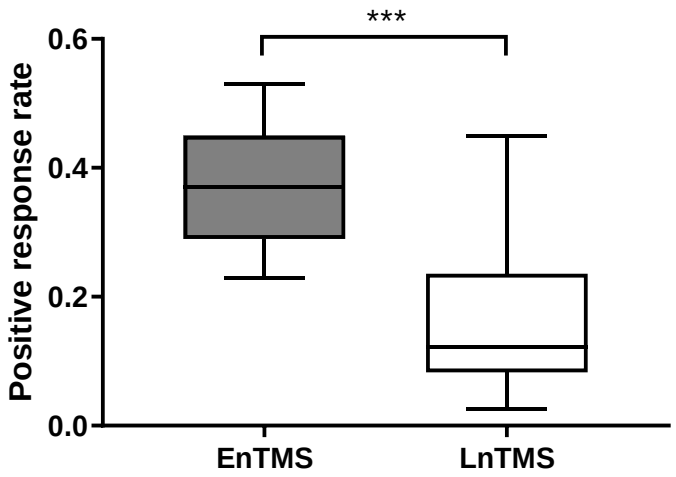

*Figure 15 Boxplot depicting different positive response rates in both hemispheres' mapping. *** represents p=0.0002*

	EnTMS [%]	LnTMS [%]	p
Positive response rate			
Ipsilateral	38.0 ± 9.2	20.0 ± 14.4	0.0031
Contralateral	39.0 ± 9.1	11.9 ± 8.6	<0.0001
Overall	38.5 ± 8.9	16.2 ± 12.4	<0.0001

Table 5 Positive response rates for either hemisphere's and the overall mapping process. Only completed steps were included in the analysis. Note: In this study, the hemisphere on which the tumor is located is referred to as ipsilateral.

3.5. Motor map analysis

3.5.1. Hotspot distance and location

Spatial hotspot comparison was performed intra-individually for each hemisphere. On the ipsilateral hemisphere, distance between both system's hotspots was 8.3 ± 4.4 mm ranging from 3.8 to 15.1 mm. Contralateral distance was 8.6 ± 4.5 mm ranging from 2.2 to 15.5 mm. Distance did not vary significantly between ipsi- and contralateral hemisphere (p=0.9124). Overall, intra-individual inter-system hotspot distance averaged to 8.4 ± 4.3 mm. As illustrated in table 10, hotspots were located in the same gyri in all but 2 cases.

Patient #	Ipsilateral Hotspot EnTMS	Ipsilateral Hotspot LnTMS	Contralateral Hotspot EnTMS	Contralateral Hotspot LnTMS
1	mPrG	mPrG	mPrG	mPrG
2	mPrG		vPrG	
3	mPrG		mPrG	
4	mPrG		mPrG	
5	mPrG	dPrG	mPrG	mPrG
6	mPoG		mPoG	
7	vPrG	dPrG	vPrG	mPrG
8	mPoG	mPoG		
9	anG	anG	mPrG	mPrG
10	mPoG	mPoG	mPrG	mPrG
11	mPrG	mPrG	mPrG	mPrG
12	mPrG	mPrG	mPrG	mPrG

Table 6 Hotspot location depicted by underlying gyrus. vPrG = ventral precentral gyrus; mPrG = medial precentral gyrus; dPrG = dorsal precentral gyrus; anG = angular gyrus, vPoG = ventral occipital gyrus, mPoG = medial occipital gyrus

Distances between the hand knob and the hotspot varied in part significantly. On the ipsilateral hemisphere, distance to the EnTMS hotspot was shorter in comparison, averaging to 9.3 ± 4.7 mm while LnTMS hotspot distance averaged to 15.4 ± 5.4 mm (p=0.0221). On the contralateral side, the difference was inversed with EnTMS distance averaging to 13.3 ± 8.1 mm and LnTMS distance averaging to 11.2 ± 7.2 mm (p=0.5769).

3.5.2. Motor map extent and spatial resolution

Spatial motor map extent was compared for all cases of successful and complete motor map creation per hemisphere as well as overall. On the ipsilateral hemisphere, EnTMS yielded significantly larger motor maps than LnTMS (EnTMS: 23.26 ± 8.31 cm³, LnTMS 9.43 ± 4.33 cm³, p=0.0006). Similar results were found when comparing motor maps of the contralateral hemisphere (EnTMS: 17.82 ± 3.46 cm³, LnTMS 7.81 ± 6.29 cm³, p=0.0011), as well as when comparing without indifference for mapping site (EnTMS: 20.68 ± 6.90 cm³, LnTMS 8.67 ± 5.20 cm³, p<0.0001).

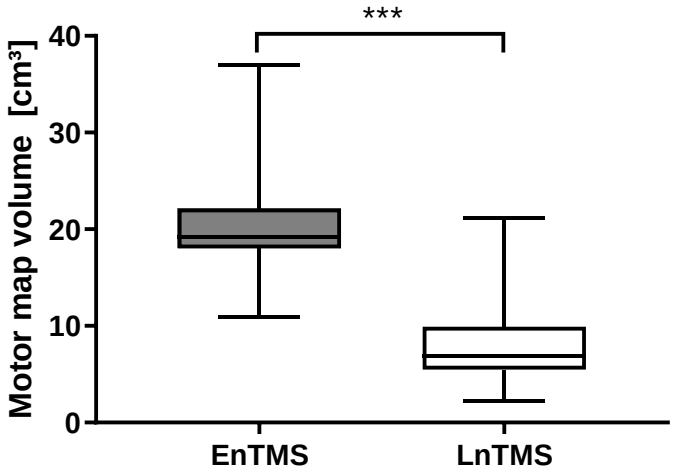

*Figure 16 Boxplot depicting different motor map volumes without distinction for site of stimulation. *** represents p<0.0001*

Ipsilateral motor map resolution was 5.72 ± 1.38 Stimuli per cm³ on the EnTMS device while LnTMS based mapping resulted in a resolution of 4.39 ± 2.53 Stimuli per cm³. These resolutions did not differ significantly (p=0.1751). When regarding the contralateral hemisphere, resolutions varied significantly with EnTMS based mapping resulting in a resolution of 6.25 ± 1.22 Stimuli per cm³ while LnTMS resolution was 2.99 ± 0.92 Stimuli per cm³ (p<0.0001). Overall values without discrimination for site of stimulation significantly varied as well (EnTMS: 5.97 ± 1.30 Stimuli per cm³, LnTMS 3.74 ± 2.02 Stimuli per cm³, p=0.0005).

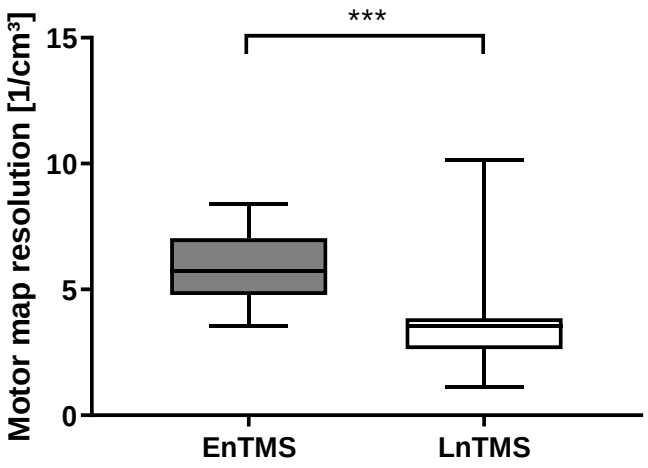

*Figure 17 Boxplot depicting different motor map resolutions without distinction for site of stimulation. *** represents p=0.0005*

3.5.3. Motor map overlap

Motor maps overlapped in all cases. On the ipsilateral hemisphere, motor maps completely overlapped in 6 out of 8 cases and partially overlapped in 2 out of 8 cases. As for the contralateral hemisphere, complete overlap occurred in 2 out of 7 cases, partial overlap in 5 out of 7 cases.

	Complete overlap	Partial overlap
Ipsilateral	6	2
Contralateral	2	5
Overall	8	7

Table 7 Motor map overlap. Note: In this study, the hemisphere on which the tumor is located is referred to as ipsilateral.

3.6. CST tractography

Fiber tracking of the CST could be successfully conducted in all cases of completed motor mappings. Results were visually similar as e.g. seen in figure 16. Both average FA threshold as well as mean numbers of identified CST fibers did not vary significantly when using either technique's motor maps (see Table 8).

	EnTMS	LnTMS	P
FA threshold			
Ipsilateral	0.2 ± 0.1	0.2 ± 0.0	0.6220
Contralateral	0.2 ± 0.1	0.2 ± 0.1	0.8971
CST fiber count			
Ipsilateral	831.4 ± 883.1	989.6 ± 990.3	0.7250
Contralateral	340.0 ±452.2	998.4 ±1610.0	0.2555

Table 8 Fiber tracking thresholds and resultant fiber counts for mapping of the CST. Note: In this study, the hemisphere on which the tumor is located is referred to as ipsilateral.

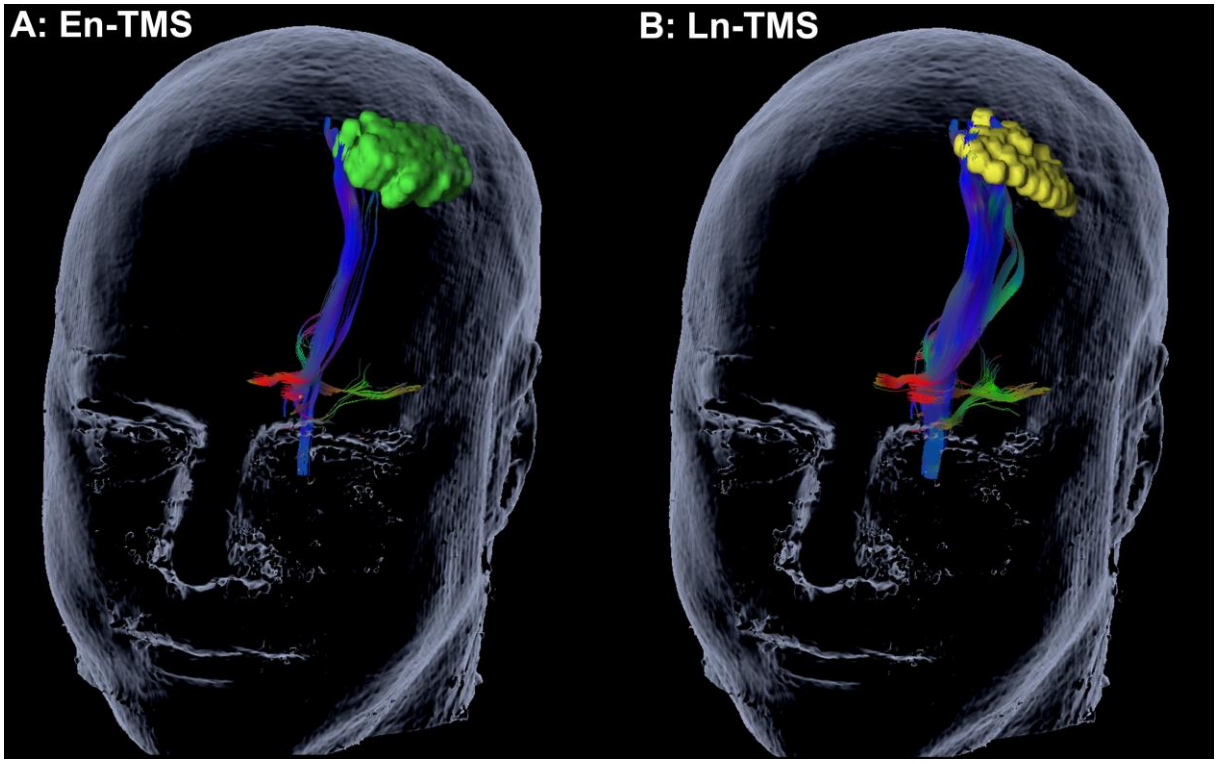

Figure 18 Exemplary CST fiber tracking on the same patient and hemisphere using EnTMS and LnTMS motor maps as a basis. (Sollmann et al., 2016)

3.7. Time durations and learning curves

3.7.1. Step durations

Duration timings were compared based on the above described classification of single steps of the mapping procedure. Comparison was done between techniques and not between hemispheres. Values were recorded separately for both techniques. In cases of incomplete mappings, only steps that have been fully completed were included in the analysis.

Regarding tasks preliminary to the motor mapping, no significant difference between the techniques could be found.

As for the motor mapping itself, single steps of the procedure again did not vary significantly except for the contralateral UE mapping duration which was significantly shorter on the LnTMS based system. Overall, single motor mapping step durations did not show homogenous trends favoring one technique. When regarding average durations of each mapping session, the LnTMS mapping durations were shorter on both hemispheres albeit failing to show significance. When combining both values to form the average duration for mappings of both hemispheres, LnTMS mapping duration was significantly shorter averaging to 1799.3 ± 5489.5 s while EnTMS mapping took 2651.0 ± 906.5 s on average ($p=0.0264$).

Post-hoc analysis for both hemispheres was significantly shorter on the EnTMS device while neuronavigation timings did not vary significantly when using either system's exports. When combining preliminary task durations and post-hoc analysis duration, the so-called non-navigated system duration can be obtained. This duration includes all steps that are performed on either device but not dependent on the neuronavigation technique. Non-navigated duration was 1175.1 ± 628.7 s on the EnTMS device and 1500.0 ± 855.2 s on the LnTMS device. Again, the variance failed to show significance ($p=0.3005$).

Overall duration for all steps included was again shorter when using the LnTMS system respectively its exports while again failing to show significance.

		EnTMS [s]	LnTMS [s]	p
Preparation for motor mapping				
MRI import		115.0 ± 53.8	424.5 ± 652.2	0.1156
Registration		97.3 ± 69.8	190.1 ± 211.8	0.1651
Preparation for motor mapping		212.3 ± 84.4	598.8 ± 846.5	0.1297
Motor mapping				
Ipsilateral	Hotspot mapping	466.4 ± 305.7	503.5 ± 332.3	0.8002
	RMT determination	214.6 ± 202.4	138.0 ± 64.5	0.3177
	UE mapping	853.8 ± 326.0	557.5 ± 298.9	0.0546
	LE mapping	375.9 ± 58.4	451.4 ± 216.7	0.2615
	Average motor mapping	1229.8 ± 348.3	1008.9 ± 380.1	0.1968
Contralateral	Hotspot mapping	490.9 ± 450.4	733.6 ± 585.4	0.3204
	RMT determination	185.9 ± 176.9	126.0 ± 56.3	0.4023
	UE mapping	832.2 ± 455.3	376.8 ± 55.6	0.0324
	LE mapping	307.3 ± 88.2	346.0 ± 185.8	0.5635
	Average motor mapping	1130.5 ± 446.1	722.8 ± 200.0	0.0529
Average motor mapping of both hemispheres		2651.0 ± 906.5	1799.3 ± 5489.5	0.0264
Post-hoc analysis				
Ipsilateral		583.2 ± 324.1	853.4 ± 428.4	0.1252
Contralateral		414.2 ± 261.0	664.7 ± 158.7	0.0504
Complete post-hoc analysis of both hemispheres		502.4 ± 301.65	772.5 ± 343.4	0.0169
Non-navigated system duration				
Preparation & post-hoc analysis		1175.1 ± 628.7	1500.0 ± 855.2	0.3005
Neuronavigation / tractography				
Ipsilateral		271.2 ± 136.4	249.9 ± 84.1	0.7045
Contralateral		216.9 ± 91.3	251.7 ± 97.0	0.4735
Complete bilateral neuronavigation / tractography		245.5 ± 117.4	250.7 ± 87.0	0.1709
Overall duration				
Preparation & motor mapping & post-hoc analysis & neuronavigation / tractography		5131.2 ± 1533.3	3837.7 ± 2035.8	0.0926

Table 9 Time durations for single steps of the mapping process depicted in s. Note. In this study, the hemisphere on which the tumor is located is referred to as ipsilateral.

As stated above, values include step timings from completed parts of incomplete mapping sessions. Incomplete mappings were also included in the average durations. Therefore, while the above values do depict the average duration of all mappings included in this study, they are distorted by the inclusion of in part considerably shorter incomplete mappings.

To depict comparable values without distortion by incomplete mappings, a modified calculation was used for the summed-up values. This calculation only utilized data from both system's complete mappings. For the calculation of the bilateral mapping duration, only complete bilateral mappings were included. This modified calculation yielded corrected bilateral motor mapping durations of 3150.8 ± 295.5 s for LnTMS versus 2902.0 ± 711.9 s for EnTMS. The corrected ipsi- and contralateral mapping durations did not show a homogenous trend in favor of one device. Regarding the whole mapping process including all preliminary and subsequent parts, corrected durations did not vary significantly.

	EnTMS [s]	**LnTMS [s]**	**p**
Complete motor mapping durations			
Ipsilateral	1803.0 ± 564.4	1650.4 ± 450.2	0.5594
Contralateral	1306.5 ± 284.7	1471.3 ± 662.2	0.5877
Both hemispheres	2902.0 ± 711.9	3150.9 ± 295.5	0.4474
Overall duration	4184.4 ± 865.7	4890.6 ± 1063.5	0.1673

Table 10 Mapping and overall durations only including complete mappings.

Note: Mean values from single hemisphere durations do not add up to bilateral mapping duration because only bilateral mappings were included for the calculation of the bilateral duration. In this study, the hemisphere on which the tumor is located is referred to as ipsilateral.

3.7.2. Mapping speed

Mapping speed was depicted by calculating the count of stimulations per s of mapping time. As stimulation counts and timings were recorded separately for each step, mapping speed could be divided as well.

Mapping speed was slightly lower during hotspot search and RMT determination compared to UE and LE mapping on both devices. Mapping speed average for ipsilateral mapping was significantly different with an average of 0.22 ± 0.09 stimulations per s using EnTMS while LnTMS mapping speed averaged to 0.14 ± 0.03 stimulations per s (p=0.0221). Similar findings were observed for the contralateral mapping as shown in the table below. Combined, overall mapping speed was significantly higher as well with EnTMS averaging at 0.23 ± 0.07 Stimulations per s and LnTMS averaging to 0.15 ± 0.02 Stimulations per s (p=0.0027).

	EnTMS [1/s]	**LnTMS [1/s]**	**p**
Mapping speed			
Ipsilateral	0.22 ± 0.09	0.14 ± 0.03	0.0221
Contralateral	0.27 ± 0.06	0.17 ± 0.02	0.0051
Both hemispheres	0.23 ± 0.07	0.15 ± 0.02	0.0027

Table 11 Mapping speed for different parts of the mapping process Note: In this study, the hemisphere on which the tumor is located is referred to as ipsilateral.

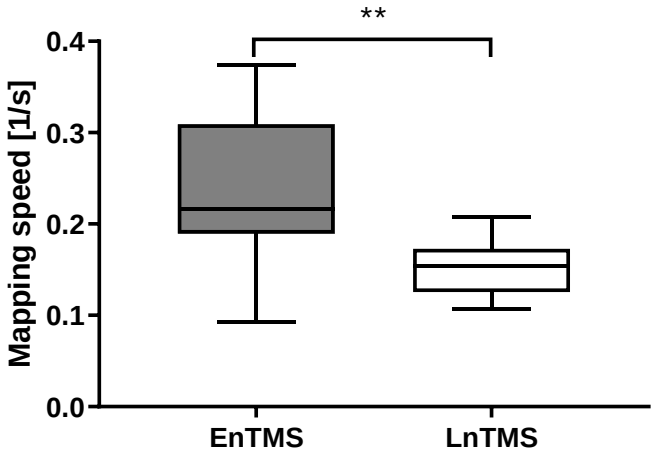

*Figure 19 Boxplot depicting the overall mapping speed of both systems. The difference between both systems is significant. ** represents p=0.0027*

3.7.3. Learning curves

Regarding the general technical learning effect depicted by navigation independent timings, illustration of the linear regression yielded negative trends with similar slopes (EnTMS: -101.2, LnTMS: -121.2) for both systems. Both trends were found to be significant non-zero (EnTMS: p=0.0479; LnTMS: p=0.0287).

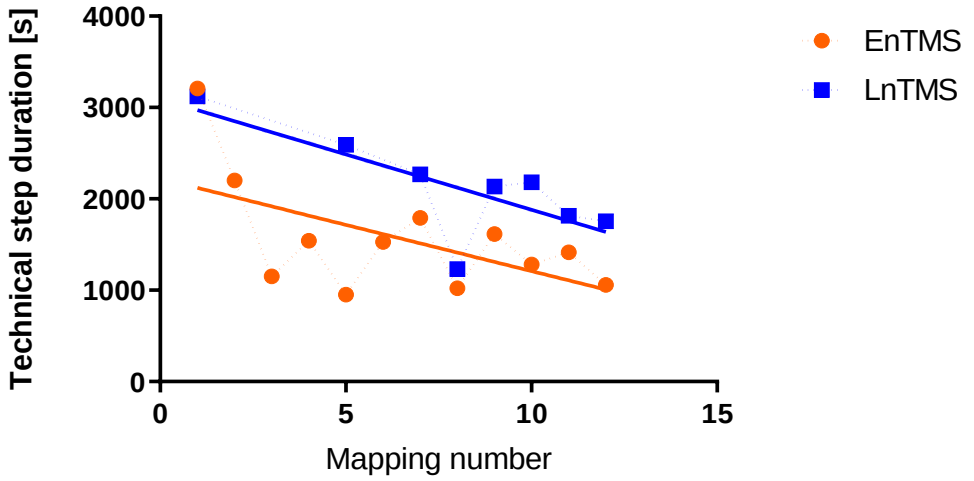

Figure 20 Evolution of navigation independent timings.
Note: Bold lines depict the linear regression result (R^2 for EnTMS:0.3367, R^2 for LnTMS: 0.5775), dotted lines are not meant to represent values but serve for better readability. (Sollmann et al., 2016)

For the changes in complete bilateral motor mapping duration, linear regression yielded a negative trend for EnTMS (slope: -224.6) and a positive trend for LnTMS (slope: +65.30). The Analysis found the EnTMS trend to be significantly non-zero, while the LnTMS trend failed to show significance (EnTMS: p=0.0092; LnTMS: p=0.0535).

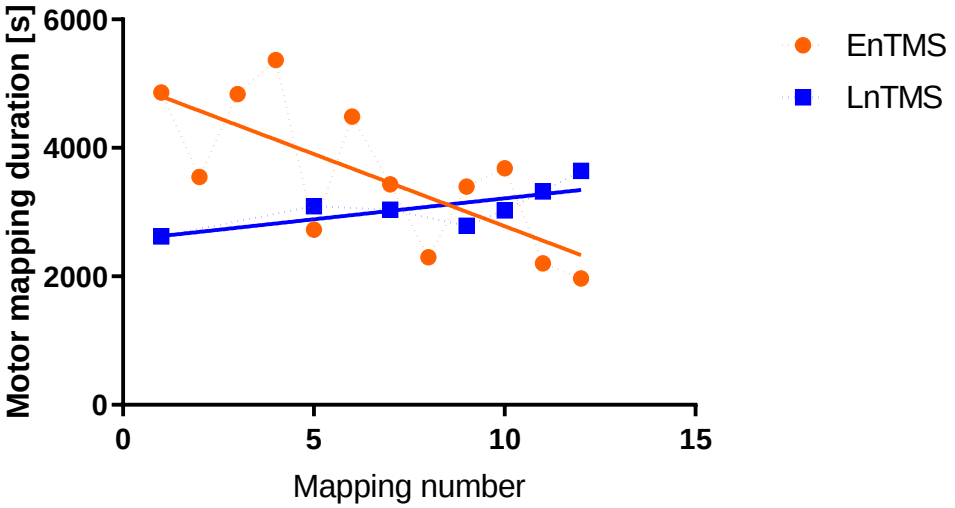

Figure 21 Evolution of complete motor mapping duration for both hemispheres.
Note: Bold lines depict the linear regression result (R^2 for EnTMS:0.5086, R^2 for LnTMS: 0.5586), dotted lines are not meant to represent values but serve for better readability. (Sollmann et al., 2016)

For the stimulation speed, linear regression yielded a trend towards an increase in mapping speed over time for both devices. The trend for EnTMS had a slope of +0.019 and was found to be significant non-zero (p=0.0008). LnTMS speed trend had a slope of +0.004 and was found to be not significantly deviant from zero (p=0.0691).

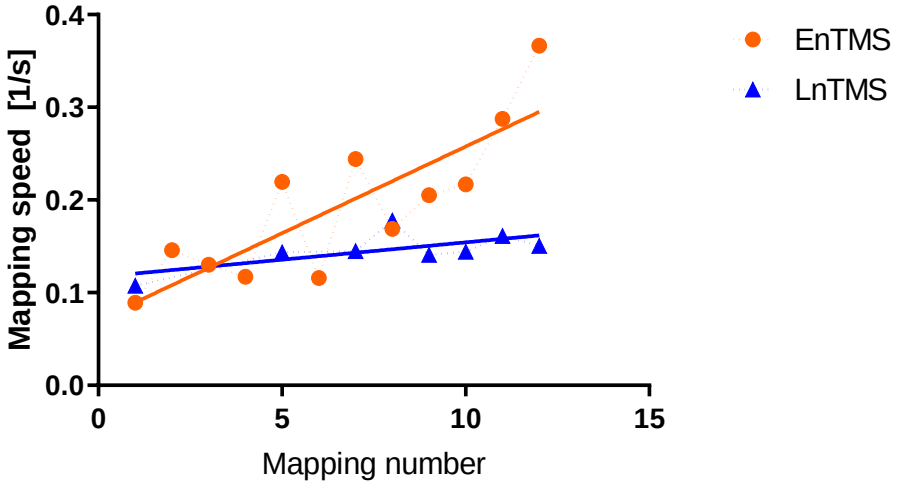

Figure 22 Evolution of stimulation speed.
Note: Bold lines depict the linear regression result (R^2 for EnTMS:0.6922, R^2 for LnTMS: 0.4489), dotted lines are not meant to represent values but serve for better readability. (Sollmann et al., 2016)

4. DISCUSSION

4.1. Overview

To refine recent findings about nTMS, this dissertation serves to investigate whether the usage of different neuronavigation guidance techniques for nTMS has a significant effect on clinical characteristics of the diagnostic process of pre surgical motor mapping in patients suffering from brain tumors.

Complete motor mappings could be conducted using both EnTMS as well as LnTMS for neuronavigation. In total, 12 patients were included in the study. Stimulations were well tolerated without occurrence of severe adverse effects or abortion due to navigational insufficiency. Hardware errors lead to different counts of mappings conducted for either device, but none of the hardware-errors were software related or stemmed from the neuronavigation device. Also, no mappings were conducted while unresolved hardware error persisted. When comparing mapping characteristics, significant differences between both techniques could be observed. Differences were most distinct regarding motor-positive response rates as well as the absolute counts of motor-positive stimulation points per mapping and mapping speed. These results significantly varied towards increased values when using EnTMS (*See Fig. 13/18/19*). Learning curves depicting both navigation-dependent as well as navigation-independent steps of the process could be created as well. Neuronavigation method was again shown to be influential concerning the learning process of navigation-dependent tasks. Using an EnTMS based system lead to more distinct improvements (*See Fig. 14-16*). Navigation-independent parameters depict either system's underlying technical properties and usability. These parameters did not vary significantly. A spatial analysis of the resultant motor maps showed that both techniques located the hotspot in the same gyrus in all but two cases (*See Table 10*). Radial distance between hotspots identified by either system was <1cm on average. Motor maps overlapped in all cases while the spatial extent of the motor maps as well as the spatial resolution varied significantly, again favoring EnTMS (*See Fig. 21, 22, Table 11*).

4.2. Clinical applicability

One of the aims of this study was the assessment of the general clinical applicability of both EnTMS and LnTMS in the context of pre-surgical cortical motor mapping. Clinical applicability includes both, the navigational techniques' influences on the practical parts of the clinical procedure as well as the effects on the patient.

Regarding the influence on the mapping process, even though error rates varied significantly between both systems, none of the errors were resultant from the navigation technique. All errors were purely hardware based. Not taking these unrelated hardware errors into consideration, both navigation techniques allowed for the conduction of complete motor mappings. On a special note, no mapping had to be aborted due to neuronavigation insufficiency resulting in e.g. impossibility of Hotspot location or RMT determination. As mapping was not proceeded once hardware errors arose until these errors were resolved, it can be assumed that the data included in this study was not biased by faulty hardware. Ultimately, both navigation techniques showed equal levels of overall applicability, meaning that mappings overall could be performed and completed using both EnTMS and/or LnTMS.

Patient relaxation is of crucial importance for the conductance of nTMS motor mapping as reliant MEP answers can only be deducted when MEG interference due to involuntary muscle contraction is minimized (Karhu et al., 2014; Rossi et al., 2009; Saisanen, 2011). Factors derogatory to patient relaxation are therefore to be minimized in nTMS. One of these factors is pain perceived during the examination.

Both devices' mapping procedures were well tolerated with patients reporting mild to no levels of discomfort or pain depicted by NRS (*See Table 2*). Differences between devices were non-significant with pain during LnTMS motor mapping ranging slightly higher than on the EnTMS device. A recent study by Tarapore et al. including 733 neurosurgical patients undergoing preoperative cortical mapping via nTMS found similar results with only 0.4% of the patients reporting pain of >3 NRS (Tarapore et al., 2016). In our study, patient discomfort was restricted to the duration of the examination and did not persist.

Aside of non-persistent discomfort, no adverse events were observed on either device. Again, these findings are in line with Tarapore et al.'s findings on 733 patients as well as further findings on 258 healthy subjects (Tarapore et al., 2016; Tarapore et al., 2016).

It should be noted that Tarapore et al. only used EnTMS based devices for cortical mapping during their studies. Still, this study found no significant difference between EnTMS and LnTMS based cortical mapping regarding patient tolerability and safety. Both systems' findings were

in line with Tarapore et al.'s and further authors' findings on the high safety and well tolerability of nTMS (Rossi et al., 2009).

Another factor of comparison was either technique's suitability for further analysis as well as further utilization. As motor maps used in an intraoperative setting were purely EnTMS-based, no comparison could be made regarding that characteristic. Post-hoc analysis was not included in the comparison as the analysis' criteria do not include navigation-dependent factors (*See 2.8.*). Therefore, comparison of the technique's suitability for post-hoc utilization was achieved via nTMS motor map-based DTI-FT of the CST.
The combination of nTMS derived motor maps with DTI-FT has been shown to provide for superior accuracy of CST depiction compared to conventional anatomic ROI placement and provide for superior postoperative outcome (Forster et al., 2015; Frey et al., 2012; Krieg et al., 2012; Krieg et al., 2012; Sollmann et al., 2016; Weiss et al., 2015). As this advantage is reliant on the validity and size of the motor maps created by nTMS, different navigation techniques could lead to inferior quality of the CST depiction e.g. indicated by higher FA values or lower fiber counts due to incorrect ROI placement. When reviewing the data gathered in this study, both techniques appeared equally well suited for that task. No significant difference resultant from the usage of either technique's motor maps could be found (*See Table 9*). Both technique's motor maps allowed for successful depiction of the CST in all cases of complete hemispheric motor mapping. FA thresholds used for CST depiction as well as count of fibers included in the CST-model did not vary significantly. Overall, CST models were found to be visually similar. As only EnTMS derived data was used intra-operatively, an analysis concerning the validity of the CST depiction could not be made.

Differences in navigation technique did not lead to significant differences concerning the clinical applicability of both systems. In either case, complete motor mappings could be conducted in a fashion that was safe for and well tolerated by the patient. Motor maps could further be incorporated in the DTI-FT of the CST for both devices without a significant effect on the process.

4.3. Workflow

Another aim of the study was to depict the navigation technique's influence on the workflow of the mapping process. As the general mapping procedure was identical on either system (*See 2.6.-2.9.*), differences in the suitability of either technique could have led to different amounts of time to achieve the same goal on either system. Gross practical insufficiencies of a neuronavigation technique would hence clinically manifest themselves in the form of increased navigation-dependent timings.

As for the duration of a complete mapping session, the efficiency of the modified calculation could be well demonstrated. Initially, averaged bilateral mapping duration was significantly shorter on the LnTMS device. Yet, as stated above this was due to distortion of the averaged durations by the incorporation of incomplete mappings. LnTMS mappings included a higher number of incomplete mappings. These incomplete mapping timings heavily deviated from the actual mean timing for complete mappings. This was shown by the standard deviation of 5489.5 s for the bilateral mapping duration on the LnTMS device (mean duration 1799.3 s, EnTMS standard deviation 906.5 s). When viewing the corrected calculations, LnTMS bilateral mapping standard deviation was reduced to 295.5 s depicting a more homogenous and non-distorted distribution. Corrected calculations did not vary significantly in favor of either technique.
As for the overall timings including neuronavigation implementation and CST tracking, no significant difference between both techniques could be observed either. Based on these findings, both techniques could be deemed equally well suited for the tasks performed during motor mapping. Yet, using absolute timings for this purpose only gives information about how long it took to complete all procedures during a certain step. This would leave out quantitative factors that reflect the quality of these procedures. Still, a procedure's overall duration is an important factor in today's clinical daily routine. Therefore, the fact that both systems took comparable absolute amounts of time for the examination also deserves consideration when evaluating both techniques' eligibility for clinical usage.

Non-navigated system durations unlike e.g. mapping durations do not include such quantitative factors and are not influenced by the navigation method. Therefore, these values serve well at depicting a system's general functionality. Factors influencing functionality include the usability and overall design of the system as well as hardware quality. As stated above, non-navigated system durations did not vary significantly. Therefore, both systems' overall general functionality can be regarded as similar. Further, navigation-dependent steps can be deemed not systematically biased by differences in either system's general functionality.

To account for the above-mentioned quantitative differences during navigation-dependent steps of the workflow, mapping speed depicted by stimulations per s was generated. This parameter was chosen as it incorporates both the time duration for the mapping steps of the process as well as the quantitative stimulation counts depicting differences in process quality. Moreover, the interval between two stimulations is mostly generated by the time it takes to relocate and reorient the coil to ensure for optimal stimulation properties. These tasks are mainly dependent on the neuronavigation technique and not influenced by other parts of the system. Therefore, potential differences in mapping speed are very likely to stem from the neuronavigation technique's differences. (Karhu et al., 2014; Picht et al., 2011; Rossini et al., 2015). As mappings were aborted as soon as hardware errors were noted and not continued under suboptimal conditions, mapping speed was not assumed to be affected by the errors. Therefore, it was not necessary to exclude incomplete mappings from the calculation.

Mapping speed was significantly higher when using the EnTMS for neuronavigation. This effect was present on both ipsi- and contralateral hemispheres as well as when combining both hemispheres' values to form the overall speed. As described above, differences in mapping speed between both systems are very likely to be due to the difference in the underlying neuronavigation technique. This connection seems even more plausible when taking into consideration that both systems' general functionality has been shown to be comparable to each other.

When looking to explain this difference, one should again review the differences between both techniques' approach to neuronavigation. In EnTMS, the neuronavigation unit calculates and simulates the E-field on-line. Therefore, suboptimal coil orientation can be detected by the system as the calculated E-field strength will be below the simulated optimal E-field strength. As stated above, the system indicates this case by rendering the E-field direction marker transparent. Using this information, correction of coil placement and orientation can be assisted by the system as successful correction is immediately confirmed by the user interface. Furthermore, the operator does not need to look at the coil while operating it but instead keeps watching the system monitor while correcting coil placement and/or orientation until the UI confirms correct placement/orientation. Therefore, accidental changes in one spatial factor while correcting the other factor e.g. by shifting the coil while correcting its orientation to the skull can directly be detected and avoided as well (Danner et al., 2008; Krings et al., 2001; Ruohonen & Ilmoniemi, 1999; Saisanen, 2011; Thielscher & Wichmann, 2009).
Line navigation does not provide for visual feedback concerning (sub)optimal coil placement as the E-field is merely projected instead of calculated/simulated under ideal conditions. Therefore, suboptimal coil placement cannot be identified without the operator looking at the

coil and checking for optimal placement himself, losing vision of the system UI while doing so. As the operator does not have vision of the neuronavigation system's interface while correcting coil orientation, coil position needs to be checked again after reorientation preliminary to each stimulation to avoid unintended coil shifting.
Both manual optimization as well as reaffirmation of correct coil positioning preliminary to each stimulation are likely to increase the interval between two stimulations when performed based on the operator's visual impression of the coil on the patient's skull. Therefore, these differences between both techniques are likely to at least partially cause the different findings for both system's mapping speeds.

In addition to absolute values of overall timings and mapping speed, the evolution of both values over time could be presented. As the study protocol included a naïve operator, these developments depicted the formerly inexperienced operator's learning curve when conducting mappings on both devices. To depict the underlying learning effect of said curves, a linear regression analysis was performed (Mayo et al., 2016; Terzi et al., 2016). Navigation-dependent and navigation-independent durations were compared to each other separately as they represent different aspects of the learning process.

Navigation-independent timings were assessed to depict the learning curve concerning general operation of both the hard- and software as well as the handling of the resultant motor map. To do so, the navigation independent system timings as well as the time taken for neuronavigation and CST tractography were included in the calculation. Aside of depicting general learning effects, this analysis served to check for possible bias due to different mapping counts. If the operator's general learning effect were less distinct e.g. due to the lower count of overall mappings on the LnTMS device, the resultant learning curve would be less steep as well.
In this context, a significant learning effect could be depicted for both devices. Furthermore, the effect was well distinctive as depicted by the slope of the linear regression. As a matter of fact, the technical learning effect was more distinctive on the LnTMS device, even though the LnTMS device had a lower count of complete mapping performed on. As these timings depict the general operation of the device without influence by differences in neuronavigation it seems appropriate to deduce that the operator's general learning effect was comparably distinctive when operating either device.

To assess the learning effect for navigation dependent factors, absolute duration of complete motor mappings as well as motor mapping speed were used. As stated above, these timings are mainly influenced by the neuronavigation technique and are both relevant for the daily

clinical routine. An underlying general bias concerning the learning effects due to e.g. navigation-independent insufficiencies or inferior general learning effects for either system seems unlikely as both systems' navigation-independent timings were reduced by a comparatively equal degree.

Regarding complete motor mapping duration, a significant learning effect could only be depicted for the EnTMS device whereas LnTMS mapping durations in fact presented with a significant albeit flat-angled trend towards an increase in mapping duration. Similar observation could be made when analyzing mapping speed: A significant trend towards increased EnTMS mapping speeds with rising experience was found while no significant change in mapping speed over time could be depicted for the LnTMS device.

These findings fit well to the above-described findings of superior absolute values and can be well explained by the underlying differences in navigation. As stated above, the E-field calculation and simulation underlying EnTMS provide with superior capabilities for optimization of coil positioning and orientation. Yet, the operator needs to learn how to make use of these advantages. Fittingly, mapping speed as depicted in *Fig. 16* was almost identical for both EnTMS and LnTMS during the first mapping. As the operator's experience and skill rise, he learns how to increasingly make use of the advantages of EnTMS. Fittingly, LnTMS speed does not show a significant trend towards reduced or increased timings as LnTMS does not provide for additional methods for optimization of coil positioning and orientation that can be adapted with increased experience.

Overall, both techniques facilitated for the conductance of motor mappings within comparatively similar timeframes. No significant differences could be found concerning both navigation-dependent as well as navigation-independent overall durations. Furthermore, a significant learning effect could be well depicted concerning the general operation of both devices' hard- and software as well as the further analysis of either technique's motor maps. Yet, when regarding mapping speed as well as the evolution of navigation-dependent timings and mapping speed over the course of time, significant differences in favor of the EnTMS device were found. These are most likely to stem from the superior capabilities for optimization of coil positioning and orientation preliminary to each stimulation offered by EnTMS that can be increasingly made use of with rising experience.

Technical disparities let aside, this study marks one of the first times that the learning process for cortical motor mappings in a clinical setting has been described. As this study was able to show, overall durations significantly decrease even after a low number of mappings conducted and with no onset delay. Even though navigation-dependent step improvement was present only when using EnTMS, the general learning effect was present on both devices. Given the presumed increase in usage and implementation of nTMS, details about the duration and

course of the incorporation process in a clinical setting can prove useful for clinics that plan to newly implement nTMS devices into their neurosurgical departments (Sollmann et al., 2017). As the operator in this study did not receive any support by the nTMS-trained members of the study group, learning processes can be assumed to be comparable for departments with no preceding experience concerning nTMS. Yet, the author strongly advises an intensive training to be conducted either by representatives of the system manufacturers as done for this study, or possibly by highly nTMS trained members of other departments prior to conducting nTMS in a clinical setting. As shown in this study, these trainings can be sufficiently performed within the duration of a single day.

4.4. Quantitative stimulation parameters

Quantitative stimulation parameters serve to further depict navigation-dependent differences between the mapping process on either system. While technically those factors could also be part of the workflow analysis, they are not time-based and serve to analyze different parameters and will therefore be discussed separately.

Regarding the counts of stimulations, both overall count of stimulations applied in the mapping process without regard to MEP response as well as the count of only motor-positive stimulations were compared. In both cases, significant differences were observed with EnTMS based motor mapping providing for both higher counts of positive stimulations as well as higher stimulation counts overall. The count of positive responses per mapping correlates with the sensitivity of the examination. Of course, as no comparison to the gold standard of DCS was included in the study protocol, differences in either technique's sensitivity can ultimately only be estimated. Yet, EnTMS has already been repeatedly shown to be comparable if not analogous to DCS concerning both techniques' high levels of sensitivity and specificity when used for cortical motor mapping (Coburger et al., 2013; Forster et al., 2011; Krieg et al., 2012; Krieg et al., 2013; Krieg et al., 2014; Picht et al., 2011; Takahashi et al., 2012; Takahashi et al., 2013). Therefore, differences in positive response count are more likely to stem from inferior sensitivity on the LnTMS device than from false-positive spots on the EnTMS device.

Differences in sensitivity are likely to stem from two main factors – differences in targeting accuracy and differences in stimulation efficiency. Regarding the prior, the underlying differences regarding the projection of the assumed stimulation site in EnTMS and LnTMS are likely to influence targeting accuracy. LnTMS solely uses spatial data for the projection of the E-field while ignoring e.g. the electromagnetic properties of the overlying and surrounding tissues. Yet, these factors have been found to influence the shape and strength of the resulting E-field (Esser et al., 2005; Rattay, 1999; Thielscher et al., 2011). Ignoring these factors in the projection of the stimulation site hence ignores significant parameters that influence the E-field. Without these factors, the E-field maximum or stimulation site cannot accurately be depicted. Yet, sensitivity of an examination that is based on the electrophysiologic reaction to cortical stimulation logically depends on the correct identification of the site of stimulation as otherwise no reliable conclusion can be drawn from the measured electrophysiologic reaction. LnTMS can by theory therefore be assumed to lead a decrease in stimulation sensitivity fitting well with the above findings. Further, stimulation site and direction are to be set in a gyrus's border zone and perpendicular to its border to the CSF to allow for optimal stimulation efficiency. An

inaccurate depiction of the stimulation site would not allow for this essential factor of stimulation optimization and therefore also lead to a decrease in stimulation efficiency.

Efficiency of nTMS can generally be depicted via the relationship between stimulation intensity and cortical response (Julkunen et al., 2009). Therefore, the RMT would seem practical for comparing either technique's stimulation efficiency, as the RMT by definition is a stimulation intensity resulting in a predefined cortical reaction that was created under otherwise constant (ideal) conditions (Rossini et al., 1994; Saisanen et al., 2008; Temesi et al., 2014). Thus, significantly different RMT values as present in this study could be a representation of differences in nTMS efficiency. Yet, these values have been obtained using different stimulators and coils. As the RMT is depicted via %MO, it is dependent on the stimulation unit's maximum output. A comparison by %MO-based RMT generated using different systems should not be conducted without exact knowledge of these values. Instead, especially in that case the %MO value should be replaced by the computed electric field strength required for successful stimulation (Danner et al., 2008; Julkunen et al., 2012; Saisanen, 2011; Stokes et al., 2007; Temesi et al., 2014). LnTMS by definition does not include computation of the estimated E-field. Therefore, a comparison of efficiency based on these values was not possible within the scope of this study either.
When analyzing hotspot search and RMT determination, MEP elicited at the hotspot during hotspot search did not vary significantly when using either LnTMS or EnTMS for stimulation and did not show a homogenous trend in favor of either technique. Even though these MEP were created using non-standardized stimulator intensities and therefore unfit for the comparison of stimulation efficiency, they do show that both technical approaches are generally capable of eliciting equally distinct MEP responses and therefore ultimately stimulating the cortex at comparable strengths.

As E-field strength based RMT values were not available for usage as indicators for either technique's stimulation efficiency, the positive response rate was assessed in their place. This approach adheres to an inversed version of the principle underlying the comparison of RMT values described above (Picht et al., 2011; Tarapore et al., 2012). In this approach, the intensity-response relationship was depicted using varying cortical responses after constant stimulation of similarly excitable cortical areas. This was achieved by using the different techniques under otherwise unchanged conditions on the same patient, starting at the same cortical area and following the same protocol. While one might argue that this method should be restricted to UE/LE mapping values only as these values were generated using constant stimulation intensities of 110 respectively 130 % of either technique's RMT, the Hotspot search

and RMT determination also followed the same protocol and lead to an equal cortical stimulation depicted by the comparative MEPs of either device.

The comparison of both devices' positive response rates again yielded significant differences. In this case using EnTMS for motor mapping lead to considerably higher response rates. Again, this effect was present on each hemisphere as well as without distinction for tumor location indicating a consistently higher efficiency of stimulation when using EnTMS for motor mapping of the same patient. When interpreting positive response rates, one must consider that stimulations set in one direction by protocol were ended once two adjacent stimulations yielded negative results. Ideally, the area covered by the stimulations as well as overall stimulation counts should be equal on both devices to depict stimulation efficiency in an optimal fashion. Yet, in that case stimulation would have to be continued after reaching the double-negative border until the extent of the other device's mapping area were met. As motor function is spatially restricted to certain areas and not spread diffusely, further stimulation is likely to primarily result in further negative responses once the outer extent of the cortical representation area has been delineated. This would in the end lead to a decrease in the positive stimulation rate of the device that identified the motor-positive area as more spatially restricted as mapping had to be continued outside the motor-positive area as identifiable by the device. Therefore, our method can be assumed to falsely favor the device on which the motor-positive area was identified to be more spatially restricted. Motor-positive areas identified by EnTMS were of significantly larger spatial extent. It can therefore be assumed that the difference observed was not due to but rather despite this method's bias. Nevertheless, as E-field strength based RMT comparison was not possible due to the principle of LnTMS, stimulation efficiency can ultimately only be assumed but not ultimately proven. Further studies using standardized protocols that adjust stimulation rates and stimulation areas to be equal should be considered, as well as studies using the gold standard of DCS.

Both the significantly higher count of positive stimulations of EnTMS as well as the higher efficiency of stimulation via EnTMS suggested by the significantly higher positive response ratio fit well with the above described findings concerning mapping speed and learning curves. In both cases, the differences are likely to stem from the superior capabilities for coil positioning and orientation offered by EnTMS. In the case of quantitative stimulation parameters, it seems probable that aside of taking longer to perform, manual coil orientation without feedback by the neuronavigation system also does not enable for sufficient correction of subtle shifts and misplacements of the coil which have been shown to significantly influence stimulations results (Fox et al., 2004; S. Schmidt et al., 2015). Furthermore it has recently been found that factors such as gyral geometry or angle of passage through tissue borders further influence the E-

field (Rattay, 1999; Thielscher et al., 2011). To ensure optimal stimulation parameters, coil orientation needs to be adapted to these differences as well. Yet, this adaption can hardly be made without the usage of complex mathematical algorithms and therefore not be included in the visually controlled manual correction of coil alignment. Combined, unnoticed shifts in coil alignment and missing consideration of additional E-field-affecting factors are very likely to lead to a significant decrease stimulation efficiency as observed in this study. As stimulation using both techniques ultimately did elicit MEP of comparable amplitude, alternative navigation-independent reasons for inefficient stimulation such as a potential gross insufficiency of the LnTMS based system's stimulating unit seem unlikely. Rather, this observation further supports the theory of otherwise unnoticed suboptimal coil placement and/or orientation as RMT determination by protocol was preceded by extensive testing of coil angulation and orientation at the hotspot to ensure for ideal stimulation. By doing so, optimal coil orientation could be practically identified on the LnTMS device even without a model that pays respect to e.g. the angle of passage through tissue borders.

As the only change between both motor mappings was the switch between either device and both mappings were performed during the same session in an alternating pattern, other e.g. biological factors such as variation in cortical excitability which has been described to occur over the course of several days seem unlikely as well (N. H. Jung et al., 2010; Ly et al., 2016; van der Kamp et al., 1996).

4.5. Motor map characteristics

Motor maps mark the result of the examination and serve for intraoperative usage as well as further analysis. While the count of positive stimulations per mapping has already been analyzed in *4.4.,* it is more of a representation of the technical sensitivity of either technique. By including the spatial distribution of said points, motor maps outline the motor-positive area identified by the examination. Therefore, spatial distribution of the hotspot as well as the motor-positive spots is of vital importance as this factor determines the shape and size of the identified motor-positive area that is to be treated with care during the operation.

Findings concerning either technique's depicted locations of the hotspot were comparable for most of sessions included. Both systems identified the hotspot within the same gyrus in all but two cases. The measurement of the radial distance between both techniques' hotspots resulted in a mean distance of 8.4 ± 4.3 mm. In this context, a recent study conducted by Sollmann et al. investigated the intra-observer variability of the location of the hotspot when using the same EnTMS based system on ten healthy subjects and found it to average to 8.1 ± 3.1 mm (Sollmann et al., 2013). Even though Sollmann et al. investigated healthy subjects for their study while this study's subject were patients, the underlying technical conditions were comparable, especially as Sollmann et al. used the same EnTMS guided device for hotspot location as was used for this study. Therefore, it seems plausible to assume that the usage of different techniques for neuronavigation does not contribute to hotspot location variety in a clinically significant way and that both techniques' gross targeting function lead to comparable results regarding hotspot location. Yet, as stated above, exact stimulation accuracy is likely to also be inferior when using LnTMS based neuronavigation based on the results of this study. Nevertheless, definite conclusion about the accuracy of LnTMS cannot be made without a comparison to intraoperative DCS.

As for spatial properties of the motor maps, LnTMS based motor maps were significantly more restricted. Again, these differences were found to be significant with and without distinction for tumor side indicating a constant underlying difference between both techniques. Motor maps overlapped in all cases with the majority of motor maps overlapping completely. Spatial resolution within the motor-positive areas was again significantly inferior for LnTMS based motor maps when not discriminating for site of stimulation.

Together, these findings mark the logical conclusion of and further backing for the prior conclusions about the inefficiency of stimulation when using LnTMS. Motor maps depict

stimulation spots as either positive or negative without indicating the amplitude of the MEP. Differences due to inefficient stimulation are therefore most likely to show in the motor area's border zone. The hotspot marks the spot with the highest reactivity when exposed to nTMS with cortex reactivity decreasing with rising distance to the hotspot. When stimulating near the hotspot, differences in stimulation efficiency are hence expressed as lower yet still positive MEP amplitudes which are not included in the information delivered by the motor map. With rising distance to the hotspot, cortical reactivity gets lower and suboptimal coil alignment now leads to motor-negative answers whereas superior coil alignment still leads to an E-field strong enough to elicit a MEP-positive response. This results in the observed significantly lowered resolution of LnTMS based motor maps. Since the probability of two adjacent negative responses in the (still motor-positive) border zone logically also increases, mapping in a certain direction is stopped earlier leading to spatially significantly more restricted motor maps on the LnTMS device.

Of course, these findings need to ultimately be confirmed by comparison of LnTMS to DCS. Yet, given the already shown high accordance of EnTMS to DCS and the consistency as well as the distinctiveness of the differences between LnTMS and EnTMS results, a systematic tendency towards inefficient stimulation using LnTMS seems more than likely based on the results of this study (Coburger et al., 2013; M.-T. Forster et al., 2011; S. M. Krieg et al., 2013; S. M. Krieg et al., 2014; S. M. Krieg, Ringel et al., 2012; T. Picht et al., 2011; S. Takahashi et al., 2012; S. Takahashi et al., 2013)(Coburger et al., 2013; M.-T. Forster et al., 2011; S. M. Krieg et al., 2013; S. M. Krieg et al., 2014; S. M. Krieg, Ringel et al., 2012; T. Picht et al., 2011; S. Takahashi et al., 2012; S. Takahashi et al., 2013).

4.6. Limitations

While this study provides coherent and significant results in favor of EnTMS compared to classic LnTMS, one must consider the limitations that went along with this study.
The main limitation of this study was its low patient count of only 12 patients which was even further diminished due to unexpected hardware errors. This was due to the study protocol requiring the examination to be performed on patients instead of healthy subjects while also being temporally limited. Yet, despite low patient count, our main results were deemed significant using Student's t-test, which has been shown to be feasible for sample sizes as used in our study and less (de Winter, J. C.F., 2013; Student, 1908). Still, to depict both techniques' differences even further and more distinct, additional studies including a larger number of patients should be conducted.

Another limitation that went along with this study's protocol was the design of the nTMS devices used for comparison. Ideally, to be able to unequivocally depict the dependence between navigation technique and mapping characteristics, all other factors of influence should be identical. Therefore, an ideal setup would have consisted of a single nTMS device in which the navigational system could be switched to use either EnTMS or LnTMS for neuronavigation with all other parts unaffected. Yet at the time of the study there was no such system available. As the EnTMS-based and CE certified system was used in the general clinical routine and thus not to be modified, the provision of a second device was the only option. Still, as shown by our results, both devices were comparable concerning general characteristics as well as their stimulating capacity. Hardware errors on the LnTMS based device did not hinder the operator's general learning effect on that device. Nevertheless, for the design of further comparative studies, a choice of two devices using the same stimulating unit would e.g. allow for the comparison of %MO-based RMT values for further comparison of either technique's stimulating efficiency.

Also, as the study's primary focus was clinical characteristics of the mapping process, it did not include a comparison to intraoperative DCS. Therefore, underlying differences concerning either technique's sensitivity could only be seen in relation to the proven well accordance of EnTMS with intraoperative DCS for cortical motor mapping (Coburger et al., 2013; Krieg et al., 2014; Picht et al., 2011; Tarapore et al., 2012). Moreover, difference in target accuracy could not be estimated either without DCS. To allow for an all-embracing comparison of either technique including an assumption of the accuracy of LnTMS, this study's clinical findings need to be supplemented with further results comparing LnTMS to intraoperative DCS.

5. Significance and Outlook

The avoidance of iatrogenous neurological deficits while maximizing the EOR in glioma surgery remains a challenge for neurosurgeons to date while being of major importance for patient survival (Patel et al., 2018; Sanai, Polley et al., 2011). Among other methods – mostly fMRI – nTMS is emerging as a safe and well tolerated non-invasive diagnostic procedure that according to this study is easy to learn within the course of one day (Rossi et al., 2009; P. Tarapore et al., 2016). Using nTMS, the human motor cortex can be mapped with a level of accuracy, sensitivity, specificity and repeatedly comparable to the current gold standard of intraoperative DCS (Krieg et al., 2013; Ottenhausen et al., 2015; Phiroz Tarapore et al., 2012). Furthermore, unlike established procedures such as fMRI which depicts the general involvement of certain cortical areas in neurological functions, nTMS actually illustrates causality between cortical activation and response and is not affected by tumor-induced changes in neurovascular functions (Hou et al., 2006; Karhu et al., 2014; Krieg et al., 2012; Ruohonen & Karhu, 2010).

As extensively illustrated in this thesis, neuronavigation is indispensable for the diagnostic usage of nTMS and cortical motor mapping via nTMS cannot be undertaken without respect to the individual anatomy and knowledge of the exact location of the stimulation site, especially in tumor patients (Ahdab et al., 2016; Brasil-Neto et al., 1992; Fox et al., 2004; Karhu et al., 2014; Krings et al., 2001; Ruohonen et al., 1998; Tofts & Branston, 1991; Wu et al., 2015; Yousry et al., 1997). The usage of neuronavigation for cortical stimulation of the motor cortex leads to significant improvements in stimulation accuracy as well as stimulation efficiency and repeatability (Julkunen et al., 2009).

Moreover, other TMS settings such as e.g. the treatment of depression via rTMS or motor function rehabilitation following a stroke are also dependent on the correct assessment of the RMT for stimulation intensity standardization (Blumberger et al., 2016; Du et al., 2016; Kennedy et al., 2009; Lefaucheur et al., 2014). Yet, RMT reliability can be assumed to suffer greatly without neuronavigation as hotspot location has been shown to deviate significantly from its presumed position in both healthy subjects and patients (Ahdab et al., 2016; Bulubas et al., 2016). Further, therapeutic rTMS can be assumed to suffer from the lack of neuronavigation as non-navigated TMS stimulation sites have repeatedly been found to deviate significantly from their target in the dorsolateral prefrontal cortex (DLPFC) in the psychiatric setting (Ahdab et al., 2010; Fitzgerald et al., 2009; Herwig et al., 2001; Moirand et al., 2015; Nauczyciel et al., 2011; Wall et al., 2016).

Currently, there are two neuronavigation techniques available, LnTMS and EnTMS. Even though both techniques use different techniques for nTMS guidance and are based on different assumptions concerning E-field properties, they have so far been subsumed as nTMS. Yet, based on recent findings and in line with our findings these differences are likely to significantly affect the mapping process as well as mapping results (Esser et al., 2005; Fox et al., 2004; Thielscher et al., 2011).

Only the EnTMS based system used in this study is approved and commercially available for preoperative diagnostic usage outside of clinical studies. With rising evidence for the feasibility of nTMS as well as increasing numbers of clinics that implement nTMS setups (J. Jung et al., 2019; Sollmann et al., 2017), the quantity and variety of commercially available nTMS devices are going to rise as well. These newly developed nTMS devices are likely to use either classic LnTMS or newly developed alternative methods for neuronavigation as the current method of EnTMS is protected by a key technology patent. The assessment and comparison of these upcoming systems' clinical feasibility requires comprehensive knowledge of the clinical implications caused by differences of the underlying navigational techniques. Pioneering in the assessment of these differences, this study marks the first systematic comparison of EnTMS and LnTMS in a clinical setting for cortical motor mapping using two commercially available devices explicitly designed for that indication.

Further, this study was the first to assess learning curves for a naïve operator of nTMS conducting motor mappings in a routine preoperative setting. These findings will prove beneficial for those clinics newly implementing nTMS into their daily routine as well as clinics expanding their nTMS departments.

Based on the results of this study and in line with theoretical considerations, differences in neuronavigation have a significant effect on the clinical parameters of the mapping process as well as on the resultant motor maps. While no definite conclusion on the efficiency of LnTMS based stimulation can be drawn from this study, an underlying inferiority of LnTMS based stimulation seems plausible. Yet, to be able to assess this topic correctly, this study should be supplemented by DCS based studies. Based on the results of this study, a distinction between different methods of neuronavigation – such as LnTMS and EnTMS – should be made when describing nTMS based study results as well as possible upcoming new models of nTMS,

6. Conclusions

This study's findings are consistent with the academic consensus about the multitude of influences on the E-field induced by nTMS (Danner et al., 2012; Fox et al., 2004; Julkunen et al., 2012; Karhu et al., 2014; Niskanen et al., 2010; Saisanen et al., 2008; S. Schmidt et al., 2015; Stokes et al., 2007; Thielscher et al., 2011). Since LnTMS does not include these effects into the projection of the E-field, suboptimal coil alignment cannot be identified automatically by an LnTMS based system leading to inefficient stimulation. Further, manual correction of coil alignment leads to lower LnTMS mapping speed. The inefficient stimulation leads to LnTMS based motor maps being more spatially restricted since border zone areas with lower reactivity are identified as motor-negative while EnTMS based motor mapping which has been shown to highly accord with DCS still identifies the same regions to be motor-positive (Krieg et al., 2012; Krieg et al., 2013; Krieg et al., 2014; Picht et al., 2009; Picht et al., 2011; Takahashi et al., 2012; Takahashi et al., 2013).

Preoperative motor mapping via EnTMS has been shown to lead to a significant improvement in patient outcome as well as an increase in extent of resection paired with a decrease in craniotomy size (Frey et al., 2014; Krieg et al., 2014; Krieg et al., 2015; Rizzo et al., 2014; Takahashi et al., 2013). These assets are dependent on the quality of the navigation technique underlying nTMS data. E.g. a decrease in craniotomy size can only be achieved when intraoperative DCS can be assumed to not outline the motor-positive area within a considerably larger cortical field than nTMS. Based to the findings of this study, classical LnTMS therefore does not seem well suited for preoperative diagnostics.

This study found motor mapping characteristics and results to be significantly influenced by the underlying navigational method. Hence, nTMS results should be described with reference to the underlying navigational technique. EnTMS based findings should not be adapted to other nTMS devices until the equality of both navigational techniques has been assessed.

7. Summary

7.1. English

For patients suffering from intracranial tumors, primary resection of the tumor is the primary aim as it has been shown to lead to the largest increase in survival rate. Maximum extent of resection whilst avoiding iatrogenous neurological deficits is one of the main factors that influence long-term survival rates. To facilitate for this aim, the surgeon needs information about the functional activity of the brain tissue surrounding the tumor. nTMS has the potential to accurately and reliantly provide for said information while being non-invasive and well-tolerated by the patient. The feasibility of nTMS heavily relies on the functionality of the underlying neuronavigation technique. Currently, there are two techniques for neuronavigation that use difference approaches and assumption for depicting the E-field induced by nTMS on the cortex. These two techniques are classical line navigation and the more recently developed electric field navigation. So far, these two techniques have been subsumed under the term nTMS. Yet, based on theoretical differences between both techniques, it seems likely that their practical results differ as well.

This study compared EnTMS and LnTMS for the first time. The comparison was performed in a clinical setting and based on characteristics of the mapping process as well as quantitative and spatial properties of the resultant motor maps. During a timeframe of 6 weeks, 12 patients that suffered from intracranial tumors underwent cortical motor mapping via both methods prior to surgery. Examinations were conducted by a formerly naïve operator to avoid systematical bias as well as to be able to depict learning curves for either technique. Either system's motor maps were further tested for their suitability for implementation into the clinic's neuronavigation system as well as DTI FT of the CST.

Overall, complete motor mappings could be conducted within comparable timeframes and were well tolerated by the patients. The motor-positive area could be outlined in all cases excluding hardware errors. Both devices were capable of stimulating the cortex with comparable strength. A general learning effect could be observed on both devices while navigation-dependent timings only improved on the EnTMS device. Implementation into the neuronavigation software and DTI FT of the CST could be conducted in all cases excluding hardware errors.

Regarding quantitative mapping characteristics as well as spatial motor map properties, significant and distinctive differences in favor of EnTMS were observed. Navigation-dependent mapping parameters such as mapping speed, count of overall stimulations, count of stimulations leading to a positive MEP response as well as the positive response rates were

significantly higher using EnTMS. EnTMS based motor maps identified the motor-positive area as spatially less restricted.
With EnTMS proven to be comparable to the gold standard of intraoperative DCS, these consistent differences are likely to stem from inferior sensitivity of the LnTMS-based device. In line with current consensus about the influence of coil placement on nTMS efficiency, these findings are best explained by insufficient stimulation due to missing optimization of coil placement and to result of underlying insufficiencies of LnTMS.

As shown by this study, the usage of different navigation techniques leads to significant differences in clinical mapping characteristics and resultant motor map properties even at low patient counts. These differences should be considered when describing nTMS results. Furthermore, findings observed using EnTMS-based devices should not be adapted for other nTMS techniques without testing for either technique's comparability. Further studies including a systematic comparison of EnTMS to LnTMS based on larger counts of patients as well as studies comparing LnTMS to the gold standard of intraoperative DCS could further refine these findings.

7.2. Deutsch

Die primäre Tumorresektion stellt aufgrund ihres Effektes auf das Gesamtüberleben die Erstlinientherapie intrakranieller Tumore dar. Dieser Effekt ist maßgeblich von der Maximierung des Resektionsausmaßes unter Vermeidung iatrogener neurologischer Defizite abhängig. Hierzu benötigt der Chirurg detailliertes und verlässliches Wissen über die funktionelle Aktivität des den Tumor umgebenden Hirngewebes. Die navigierte transkranielle Magnetstimulation (nTMS) stellt eine sichere und zuverlässige Methode zur exakten, nicht-invasiven Diagnostik ebendieser Aktivität dar. Hierzu ist sie aber maßgeblich auf die Funktionalität des angeschlossenen Neronavigationssystems angewiesen. Derzeit existieren zwei Ansätze der Neuronavigation, die Liniennavigation (LnTMS) und die E-Feld-Navigation (EnTMS). Beide Techniken basieren auf fundamental unterschiedlichen Annahmen über das durch nTMS auf dem Kortex induzierte E-Feld. Trotz unterschiedlicher Ansätze wurden diese beiden Techniken bislang dennoch unter dem Begriff nTMS subsumiert. Es erscheint jedoch naheliegend, dass sich die deutlichen Unterschiede der theoretischen Grundlagen dieser beiden Techniken auch auf deren Ergebnisse in der klinischen Praxis auswirken.

Diese Studie stellt den ersten systematischen Vergleich zwischen EnTMS und LnTMS in einem klinischen Setting dar. Der Vergleich erfolgte über einen Zeitraum von 6 Wochen im Rahmen der routinemäßigen präoperativen Diagnostik einer neurochirurgischen Klinik an insgesamt 12 Patienten mit Tumoren im Bereich des Motorkortex. Der Untersucher wies keinerlei Vorkenntnisse im Umgang mit den Techniken auf. Hierdurch wurde eine Verzerrung der Ergebnisse hin zu dem in der Arbeitsgruppe etablierten EnTMS basierten Gerät verhindert. Zudem ermöglichte dies die Untersuchung des Lerneffekts beider Techniken. Der Vergleich umfasste sowohl qualitative als auch quantitative Faktoren der Untersuchung. Zudem wurden die resultierenden Kartierungen der motorischen Funktion auf dem Kortex ausgewertet. Die angefertigten Motorkarten wurden zudem auf ihre Eignung zur Integration und weiteren Verwendung im klinikeigenen Neuronavigationssystem sowie zur Darstellung der Kortikospinalen Bahn (CST) mittels Diffusions-Tensor Bildgebung basierter Faserdarstellung (DTI FT) geprüft.

Motorkartierungen konnten auf beiden Geräten innerhalb vergleichbarer Zeiträume durchgeführt werden und wurden von den Patienten gut vertragen. Das motorisch aktive Areal konnte in allen Fällen einer vollständigen Untersuchung ohne Hardwarefehler vollständig dargestellt werden. Zudem waren beide Geräte in der Lage, den Kortex mit vergleichbarer Stärke zu stimulieren. Ein allgemeiner, navigationsunabhängiger technischer Lerneffekt konnte auf beiden Geräten beobachtet werden, wohingegen die navigationsabhängigen Zeiten

sich nur auf dem EnTMS-Gerät verbesserten. Die Implementierung der angefertigten Karten in die Neuronavigationssoftware und die Darstellung des CST konnte in allen Fällen erfolgreicher Kartierung durchgeführt werden. Beim Vergleich der quantitativen Faktoren beider Untersuchungen sowie bei der Analyse der angefertigten Motorkarten konnten signifikante Unterschiede zu Gunsten der EnTMS beobachtet werden. Navigationsabhängige Parameter wie die Stimulationsgeschwindigkeit, die Anzahl der Gesamtstimulationen, die Anzahl der Stimulationen, die zu einem positiven motorisch evozierten Potenzial (MEP) führen, sowie die Quote an Stimulationen mit positiver MEP-Antwort waren allesamt im Falle der EnTMS-basierten Kartierung signifikant erhöht. EnTMS-basierte Motorkarten identifizierten den motorisch positiven Bereich zudem als räumlich größer.

In mehreren Studien konnte demonstriert werden, dass die Sensitivität der EnTMS mit der des Goldstandards der intraoperativen direkten kortikalen Stimulation (DCS) vergleichbar ist. Angesicht der deutlich und einheitlich zugunsten der EnTMS ausfallenden Ergebnisse dieser Studie erscheint eine geringere Sensitivität des LnTMS-basierten Geräts plausibel. In Anbetracht des erheblichen Einflusses der Positionierung der TMS Spule auf die Effizienz der nTMS, sowie die Vielzahl der hierbei zu berücksichtigen Faktoren erscheint es am wahrscheinlichsten, dass dieser Unterschied aus einer unzureichenden Optimierung der Spulenpositionierung zurückzuführen ist. Hierbei kann die inkorrekte Positionierung technikbedingt nicht vom LnTMS basierten System erkannt beziehungsweise mit Hilfe der LnTMS nur unzureichend korrigiert werden.

Wie aus den Ergebnissen dieser Studie hervorgeht, führt die Verwendung unterschiedlicher Navigationstechniken bereits bei geringen Patientenzahlen zu signifikanten Unterschieden des Untersuchungsablaufs und der angefertigten Motorkarten. Diese Unterschiede sollten bei der zukünftigen Beschreibung von nTMS-Ergebnissen berücksichtigt werden. Darüber hinaus sollten Beobachtungen, die auf EnTMS-basierten Geräten beruhen nicht auf andere nTMS-Techniken übertragen werden, ohne zuvor die Vergleichbarkeit der zugrundeliegenden Navigationstechniken zu testen.

Die Ergebnisse dieser ersten Studie können mittels weiterer systematischer Vergleiche zwischen EnTMS und LnTMS an einer größeren Zahl an Patienten sowie einem Vergleich zwischen der LnTMS und der intraoperativen DCS verfeinert werden. Hierdurch würde zudem eine endgültige Aussage über die Genauigkeit der Stimulation mittels LnTMS ermöglicht.

8. References

Ahdab, R., Ayache, S. S., Brugieres, P., Farhat, W. H., & Lefaucheur, J. P. (2016). The Hand Motor Hotspot is not Always Located in the Hand Knob: A Neuronavigated Transcranial Magnetic Stimulation Study. *Brain Topography*, *29*(4), 590–597. https://doi.org/10.1007/s10548-016-0486-2

Ahdab, R., Ayache, S. S., Brugieres, P., Goujon, C., & Lefaucheur, J. P. (2010). Comparison of "standard" and "navigated" procedures of TMS coil positioning over motor, premotor and prefrontal targets in patients with chronic pain and depression. *Neurophysiologie Clinique = Clinical Neurophysiology*, *40*(1), 27–36. https://doi.org/10.1016/j.neucli.2010.01.001

Aksu, F., Steinmetz, H., Steinmetz, M. Sitzer, H., & Sitzer, M. (Eds.) (2011). *Lehrbuch neurologie* (1. Auflage). Munich, Germany: Urban & Fischer. Retrieved from http://search.ebscohost.com/login.aspx?direct=true&scope=site&db=nlebk&AN=807979

Anderson, R. J., Hoy, K. E., Daskalakis, Z., & Fitzgerald, P. B. (2016). Repetitive transcranial magnetic stimulation for treatment resistant depression: Re-establishing connections. *Clinical Neurophysiology : Official Journal of the International Federation of Clinical Neurophysiology*, *127*(11), 3394–3405. https://doi.org/10.1016/j.clinph.2016.08.015

Bankman, I. N. (Ed.) (2000). *Academic Press series in biomedical engineering*. *Handbook of medical imaging: Processing and analysis*. San Diego, CA: Academic Press. Retrieved from http://search.ebscohost.com/login.aspx?direct=true&scope=site&db=nlebk&db=nlabk&AN=248870

Barbosa, B. J. A. P., Mariano, E. D., Batista, C. M., Marie, S. K. N., Teixeira, M. J., Pereira, C. U., Tatagiba, M. S., & Lepski, G. A. (2015). Intraoperative assistive technologies and extent of resection in glioma surgery: A systematic review of prospective controlled studies. *Neurosurgical Review*, *38*(2), 217-26; discussion 226-7. https://doi.org/10.1007/s10143-014-0592-0

Barker, A. T., Freeston, I. L., Jabinous, R., & Jarratt, J. A. (1986). Clinical evaluation of conduction time measurements in central motor pathways using magnetic stimulation of human brain. *Lancet (London, England)*, *1*(8493), 1325–1326.

Barker, A. T., Jalinous, R., & Freeston, I. L. (1985). Non-invasive magnetic stimulation of human motor cortex. *The Lancet*, *325*(8437), 1106–1107. https://doi.org/10.1016/S0140-6736(85)92413-4

Basser, P. J., Mattiello, J., & LeBihan, D. (1994). MR diffusion tensor spectroscopy and imaging. *Biophysical Journal*, *66*(1), 259–267. https://doi.org/10.1016/S0006-3495(94)80775-1

Basser, P. J., Pajevic, S., Pierpaoli, C., Duda, J., & Aldroubi, A. (2000). In vivo fiber tractography using DT-MRI data. *Magnetic Resonance in Medicine*, *44*(4), 625–632.

Basser, P. J., & Pierpaoli, C. (2011). Microstructural and physiological features of tissues elucidated by quantitative-diffusion-tensor MRI. 1996. *Journal of Magnetic Resonance (San Diego, Calif. : 1997)*, *213*(2), 560–570. https://doi.org/10.1016/j.jmr.2011.09.022

Behe, M., Kauffmann, G., Sauer, R., & Weber, W. (Eds.) (2013). *Radiologie: Bildgebende Verfahren, Strahlentherapie, nuklearmedizin und strahlenschutz* (4., völlig überarbeitete Auflage). Munich, Germany: Urban & Fischer.

Blagden, S. P., Charman, S. C., Sharples, L. D., Magee, L. R. A., & Gilligan, D. (2003). Performance status score: Do patients and their oncologists agree? *British Journal of Cancer*, *89*(6), 1022–1027. https://doi.org/10.1038/sj.bjc.6601231

Blumberger, D. M., Maller, J. J., Thomson, L., Mulsant, B. H., Rajji, T. K., Maher, M., Brown, P. E., Downar, J., Vila-Rodriguez, F., Fitzgerald, P. B., & Daskalakis, Z. (2016). Unilateral and bilateral MRI-targeted repetitive transcranial magnetic stimulation for treatment-resistant depression: A randomized controlled study. *Journal of Psychiatry & Neuroscience : JPN*, *41*(4), E58-66.

Blystad, I., Warntjes, J. B. M., Smedby, Ö., Lundberg, P., Larsson, E.-M., & Tisell, A. (2017). Quantitative MRI for analysis of peritumoral edema in malignant gliomas. *PloS One*, *12*(5). https://doi.org/10.1371/journal.pone.0177135

Boling, W., & Olivier, A. (2004). Localization of hand sensory function to the pli de passage moyen of Broca. *Journal of Neurosurgery*, *101*(2), 278–283. https://doi.org/10.3171/jns.2004.101.2.0278

Boling, W., Olivier, A., Bittar, R. G., & Reutens, D. (1999). Localization of hand motor activation in Broca's pli de passage moyen. *Journal of Neurosurgery*, *91*(6), 903–910. https://doi.org/10.3171/jns.1999.91.6.0903

Branco, D. M., Coelho, T. M., Branco, B. M., Schmidt, L., Calcagnotto, M. E., Portuguez, M., Neto, E. P., Paglioli, E., Palmini, A., Lima, J. V., & Da Costa, J. C. (2003). Functional variability of the human cortical motor map: Electrical stimulation findings in perirolandic epilepsy surgery. *Journal of Clinical Neurophysiology : Official Publication of the American Electroencephalographic Society*, *20*(1), 17–25.

Brasil-Neto, J. P., Cohen, L. G., Panizza, M., Nilsson, J., Roth, B. J., & Hallett, M. (1992). Optimal focal transcranial magnetic activation of the human motor cortex: effects of coil

orientation, shape of the induced current pulse, and stimulus intensity. *J Clin Neurophysiol*, *9*(1), 132–136. Retrieved from http://www.ncbi.nlm.nih.gov/pubmed/1552001

Brodmann, K. (1909). *Vergleichende Lokalisationslehre der Grosshirnrinde: In ihren Prinzipien dargestellt auf Grund des Zellenbaues*. Leipzig: Barth.

Brown, R. W. (2014). *Magnetic resonance imaging: Physical principles and sequence design* (Second edition). Hoboken, New Jersey: Wiley-Blackwell.

Bulubas, L., Sabih, J., Wohlschlaeger, A., Sollmann, N., Hauck, T., Ille, S., Ringel, F., Meyer, B., & Krieg, S. M. (2016). Motor areas of the frontal cortex in patients with motor eloquent brain lesions. *Journal of Neurosurgery*, 1–12. https://doi.org/10.3171/2015.11.JNS152103

Buonomano, D. V., & Merzenich, M. M. (1998). Cortical plasticity: From synapses to maps. *Annual Review of Neuroscience*, *21*, 149–186. https://doi.org/10.1146/annurev.neuro.21.1.149

Capelle, L., Fontaine, D., Mandonnet, E., Taillandier, L., Golmard, J. L., Bauchet, L., Pallud, J., Peruzzi, P., Baron, M. H., Kujas, M., Guyotat, J., Guillevin, R., Frenay, M., Taillibert, S., Colin, P., Rigau, V., Vandenbos, F., Pinelli, C., & Duffau, H. [H.] (2013). Spontaneous and therapeutic prognostic factors in adult hemispheric World Health Organization Grade II gliomas: A series of 1097 cases: Clinical article. *Journal of Neurosurgery*, *118*(6), 1157–1168. https://doi.org/10.3171/2013.1.JNS121

Casarotto, S., Romero Lauro, L. J., Bellina, V., Casali, A. G., Rosanova, M., Pigorini, A., Defendi, S., Mariotti, M., & Massimini, M. (2010). Eeg responses to TMS are sensitive to changes in the perturbation parameters and repeatable over time. *PloS One*, *5*(4), e10281. https://doi.org/10.1371/journal.pone.0010281

Chen, R., Cohen, L. G., & Hallett, M. (2002). Nervous system reorganization following injury. *Neuroscience*, *111*(4), 761–773.

Coburger, J., Musahl, C., Henkes, H., Horvath-Rizea, D., Bittl, M., Weissbach, C., & Hopf, N. (2013). Comparison of navigated transcranial magnetic stimulation and functional magnetic resonance imaging for preoperative mapping in rolandic tumor surgery. *Neurosurgical Review*, *36*(1), 65-75; discussion 75-6. https://doi.org/10.1007/s10143-012-0413-2

Cohen, L. G., Roth, B. J., Nilsson, J., Dang, N., Panizza, M., Bandinelli, S., Friauf, W., & Hallett, M. (1990). Effects of coil design on delivery of focal magnetic stimulation. Technical considerations. *Electroencephalography and Clinical Neurophysiology*, *75*(4), 350–357.

Conway, N., Tanigawa, N., Meyer, B., & Krieg, S. M. (2016). 363 Cortical Plasticity of Motor-Eloquent Areas Measured by Navigated Transcranial Magnetic Stimulation in Glioma

Patients. *Neurosurgery*, *63 Suppl 1*, 207–208. https://doi.org/10.1227/01.neu.0000489851.39946.4c

Dai, W., Pi, Y.-L., Ni, Z., Tan, X.-Y., Zhang, J.-D., & Wu, Y. (2016). Maintenance of balance between motor cortical excitation and inhibition after long-term training. *Neuroscience*, *336*, 114–122. https://doi.org/10.1016/j.neuroscience.2016.08.053

Danner, N., Julkunen, P., Kononen, M., Saisanen, L., Nurkkala, J., & Karhu, J. (2008). Navigated transcranial magnetic stimulation and computed electric field strength reduce stimulator-dependent differences in the motor threshold. *Journal of Neuroscience Methods*, *174*(1), 116–122. https://doi.org/10.1016/j.jneumeth.2008.06.032

Danner, N., Kononen, M., Saisanen, L., Laitinen, R., Mervaala, E., & Julkunen, P. (2012). Effect of individual anatomy on resting motor threshold-computed electric field as a measure of cortical excitability. *Journal of Neuroscience Methods*, *203*(2), 298–304. https://doi.org/10.1016/j.jneumeth.2011.10.004

Darvas, F., Pantazis, D., Kucukaltun-Yildirim, E., & Leahy, R. M. (2004). Mapping human brain function with MEG and EEG: Methods and validation. *NeuroImage*, *23 Suppl 1*, S289-99. https://doi.org/10.1016/j.neuroimage.2004.07.014

Day, B. L., Dressler, D., Maertens de Noordhout, A., Marsden, C. D., Nakashima, K., Rothwell, J. C., & Thompson, P. D. (1989). Electric and magnetic stimulation of human motor cortex: Surface EMG and single motor unit responses. *The Journal of Physiology*, *412*, 449–473.

Day, B. L., Riescher, H., Struppler, A., Rothwell, J. C., & Marsden, C. D. (1991). Changes in the response to magnetic and electrical stimulation of the motor cortex following muscle stretch in man. *The Journal of Physiology*, *433*, 41–57.

De Winter, J. C.F. (2013). Using the Student's "t"-Test with Extremely Small Sample Sizes. *Practical Assessment, Research & Evaluation*, *18*(10).

Demtröder, W. (2013). *Experimentalphysik 2: Elektrizität und Optik* (6., überarb. u. akt. Aufl. 2013). *Springer-Lehrbuch*. Berlin Heidelberg: Springer Berlin Heidelberg. Retrieved from http://dx.doi.org/10.1007/978-3-642-29944-5

Di Lazzaro, V. [V.], Restuccia, D., Oliviero, A., Profice, P., Ferrara, L., Insola, A., Mazzone, P., Tonali, P., & Rothwell, J. C. (1998). Effects of voluntary contraction on descending volleys evoked by transcranial stimulation in conscious humans. *The Journal of Physiology*, *508 (Pt 2)*, 625–633.

Du, J., Tian, L., Liu, W., Hu, J., Xu, G., Ma, M., Fan, X., Ye, R., Jiang, Y., Yin, Q., Zhu, W., Xiong, Y., Yang, F., & Liu, X. (2016). Effects of repetitive transcranial magnetic stimulation on motor recovery and motor cortex excitability in patients with stroke: A randomized

controlled trial. *European Journal of Neurology*, *23*(11), 1666–1672. https://doi.org/10.1111/ene.13105

Duffau, H. [H.] (2005). Lessons from brain mapping in surgery for low-grade glioma: Insights into associations between tumour and brain plasticity. *The Lancet Neurology*, *4*(8), 476–486. https://doi.org/10.1016/S1474-4422(05)70140-X

Duffau, H. [H.] (2008). Brain plasticity and tumors. In J. D. Pickard, N. Akalan, C. Rocco, V. V. Dolenc, J. L. Antunes, J. J. A. Mooij, . . . M. Sin (Eds.), *Advances and Technical Standards in Neurosurgery: Vol. 33. Advances and Technical Standards in Neurosurgery 33* (1st ed., Vol. 33, pp. 3–33). s.l.: Springer Verlag Wien.

Duffau, H. [H.], Lopes, M., Arthuis, F., Bitar, A., Sichez, J. P., van Effenterre, R., & Capelle, L. (2005). Contribution of intraoperative electrical stimulations in surgery of low grade gliomas: A comparative study between two series without (1985-96) and with (1996-2003) functional mapping in the same institution. *Journal of Neurology, Neurosurgery, and Psychiatry*, *76*(6), 845–851. https://doi.org/10.1136/jnnp.2004.048520

Duffau, H. [Hugues] (2012). *Brain Mapping: From Neural Basis of Cognition to Surgical Applications*. Vienna: Springer-Verlag Vienna.

Epstein, C. M., Schwartzberg, D. G., Davey, K. R., & Sudderth, D. B. (1990). Localizing the site of magnetic brain stimulation in humans. *Neurology*, *40*(4), 666–670.

Esser, S. K., Hill, S. L., & Tononi, G. (2005). Modeling the effects of transcranial magnetic stimulation on cortical circuits. *Journal of Neurophysiology*, *94*(1), 622–639. https://doi.org/10.1152/jn.01230.2004

Ettinger, G. J., Grimson, W. E., Leventon, M. E., Kikinis, R., Gugino, V., Cote, W., Karapelou, M., Aglio, L., Shenton, M. E., Potts, G., & Alexander, E. (1996). Non-invasive Functional Brain Mapping using Registered Transcranial Magnetic Stimulation, 32–41.

Farrell, D. F., Burbank, N., Lettich, E., & Ojemann, G. A. (2007). Individual variation in human motor-sensory (rolandic) cortex. *Journal of Clinical Neurophysiology : Official Publication of the American Electroencephalographic Society*, *24*(3), 286–293. https://doi.org/10.1097/WNP.0b013e31803bb59a

Fink, D. G., & Christiansen, D. (Eds.) (1989). *Electronics engineers' handbook* (3. ed.). New York: McGraw-Hill.

Fitzgerald, P. B., Hoy, K., McQueen, S., Maller, J. J., Herring, S., Segrave, R., Bailey, M., Been, G., Kulkarni, J., & Daskalakis, Z. (2009). A randomized trial of rTMS targeted with MRI based neuro-navigation in treatment-resistant depression. *Neuropsychopharmacology : Official Publication of the American College of Neuropsychopharmacology*, *34*(5), 1255–1262. https://doi.org/10.1038/npp.2008.233

Fitzpatrick, J. M., Hill, D. L., & Maurer, C. R. (2000). Image Registration. In I. N. Bankman (Ed.), *Academic Press series in biomedical engineering. Handbook of medical imaging: Processing and analysis* (pp. 451–501). San Diego, CA: Academic Press. Retrieved from http://www.sciencedirect.com.eaccess.ub.tum.de/science/book/9780120777907#ancpart4

Fleming, M. K., Sorinola, I. O., Di Newham, J., Roberts-Lewis, S. F., & Bergmann, J. H. M. (2012). The effect of coil type and navigation on the reliability of transcranial magnetic stimulation. *IEEE Transactions on Neural Systems and Rehabilitation Engineering : A Publication of the IEEE Engineering in Medicine and Biology Society*, *20*(5), 617–625. https://doi.org/10.1109/TNSRE.2012.2202692

Fließbach, T. (2012). *Elektrodynamik: Lehrbuch zur Theoretischen Physik II* (6th ed.). Heidelberg: Spektrum Akademischer Verlag. Retrieved from http://dx.doi.org/10.1007/978-3-8274-3036-6

Forster, M. T., Hattingen, E., Senft, C., Gasser, T., Seifert, V., & Szelenyi, A. (2011). Navigated transcranial magnetic stimulation and functional magnetic resonance imaging: Advanced adjuncts in preoperative planning for central region tumors. *Neurosurgery*, *68*(5), 1317-24; discussion 1324-5. https://doi.org/10.1227/NEU.0b013e31820b528c

Forster, M. T., Hoecker, A. C., Kang, J. S., Quick, J., Seifert, V., Hattingen, E., Hilker, R., & Weise, L. M. (2015). Does navigated transcranial stimulation increase the accuracy of tractography? A prospective clinical trial based on intraoperative motor evoked potential monitoring during deep brain stimulation. *Neurosurgery*, *76*(6), 766-75; discussion 775-6. https://doi.org/10.1227/NEU.0000000000000715

Forster, M. T., Senft, C., Hattingen, E., Lorei, M., Seifert, V., & Szelenyi, A. (2012). Motor cortex evaluation by nTMS after surgery of central region tumors: A feasibility study. *Acta Neurochirurgica*, *154*(8), 1351–1359. https://doi.org/10.1007/s00701-012-1403-4

Fox, P. T., Narayana, S., Tandon, N., Sandoval, H., Fox, S. P., Kochunov, P., & Lancaster, J. L. (2004). Column-based model of electric field excitation of cerebral cortex. *Human Brain Mapping*, *22*(1), 1–14. https://doi.org/10.1002/hbm.20006

Frey, D., Schilt, S., Strack, V., Zdunczyk, A., Rosler, J., Niraula, B., Vajkoczy, P., & Picht, T. (2014). Navigated transcranial magnetic stimulation improves the treatment outcome in patients with brain tumors in motor eloquent locations. *Neuro-Oncology*, *16*(10), 1365–1372. https://doi.org/10.1093/neuonc/nou110

Frey, D., Strack, V., Wiener, E., Jussen, D., Vajkoczy, P., & Picht, T. (2012). A new approach for corticospinal tract reconstruction based on navigated transcranial stimulation and standardized fractional anisotropy values. *NeuroImage*, *62*(3), 1600–1609. https://doi.org/10.1016/j.neuroimage.2012.05.059

Gray, H., & Lewis, W. H. (1918). *Anatomy of the human body*. Philadelphia: Lea & Febiger. Retrieved from http://www.bartleby.com/107/ https://doi.org/10.5962/bhl.title.20311

Gugino, L. D., Romero, J. R., Aglio, L., Titone, D., Ramirez, M., Pascual-Leone, A., Grimson, E., Weisenfeld, N., Kikinis, R., & Shenton, M. E. (2001). Transcranial magnetic stimulation coregistered with MRI: A comparison of a guided versus blind stimulation technique and its effect on evoked compound muscle action potentials. *Clinical Neurophysiology : Official Journal of the International Federation of Clinical Neurophysiology*, *112*(10), 1781–1792.

Gupta, A., & Dwivedi, T. (2017). A Simplified Overview of World Health Organization Classification Update of Central Nervous System Tumors 2016. *Journal of Neurosciences in Rural Practice*, *8*(4), 629–641. https://doi.org/10.4103/jnrp.jnrp_168_17

Hamalainen, M. S., & Sarvas, J. (1989). Realistic conductivity geometry model of the human head for interpretation of neuromagnetic data. *IEEE Transactions on Bio-Medical Engineering*, *36*(2), 165–171. https://doi.org/10.1109/10.16463

Hamalainen, M. S., & Sarvas, J. (1989). Realistic conductivity geometry model of the human head for interpretation of neuromagnetic data. *IEEE Transactions on Bio-Medical Engineering*, *36*(2), 165–171. https://doi.org/10.1109/10.16463

Hannula, H. Nexstim NBS solution for pre-surgical mapping - differentiators 5January2016.

Hawker, G. A., Mian, S., Kendzerska, T., & French, M. (2011). Measures of adult pain: Visual Analog Scale for Pain (VAS Pain), Numeric Rating Scale for Pain (NRS Pain), McGill Pain Questionnaire (MPQ), Short-Form McGill Pain Questionnaire (SF-MPQ), Chronic Pain Grade Scale (CPGS), Short Form-36 Bodily Pain Scale (SF-36 BPS), and Measure of Intermittent and Constant Osteoarthritis Pain (ICOAP). *Arthritis Care & Research*, *63 Suppl 11*, S240-52. https://doi.org/10.1002/acr.20543

Herwig, U., Padberg, F., Unger, J., Spitzer, M., & Schonfeldt-Lecuona, C. (2001). Transcranial magnetic stimulation in therapy studies: Examination of the reliability of "standard" coil positioning by neuronavigation. *Biological Psychiatry*, *50*(1), 58–61.

Herwig, U., Satrapi, P., & Schonfeldt-Lecuona, C. (2003). Using the International 10-20 EEG System for Positioning of Transcranial Magnetic Stimulation. *Brain Topography*, *16*(2), 95–99. https://doi.org/10.1023/B:BRAT.0000006333.93597.9d

Hou, B. L., Bradbury, M., Peck, K. K., Petrovich, N. M., Gutin, P. H., & Holodny, A. I. (2006). Effect of brain tumor neovasculature defined by rCBV on BOLD fMRI activation volume in the primary motor cortex. *NeuroImage*, *32*(2), 489–497. https://doi.org/10.1016/j.neuroimage.2006.04.188

Ille, S., Kulchytska, N., Sollmann, N., Wittig, R., Beurskens, E., Butenschoen, V. M., Ringel, F., Vajkoczy, P., Meyer, B., Picht, T., & Krieg, S. M. (2016). Hemispheric language dominance measured by repetitive navigated transcranial magnetic stimulation and postoperative course of language function in brain tumor patients. *Neuropsychologia*, *91*, 50–60. https://doi.org/10.1016/j.neuropsychologia.2016.07.025

Johnson, K. A., Baig, M., Ramsey, D., Lisanby, S. H., Avery, D., McDonald, W. M., Li, X., Bernhardt, E. R., Haynor, D. R., Holtzheimer, P. E. 3., Sackeim, H. A., George, M. S., & Nahas, Z. (2013). Prefrontal rTMS for treating depression: Location and intensity results from the OPT-TMS multi-site clinical trial. *Brain Stimulation*, *6*(2), 108–117. https://doi.org/10.1016/j.brs.2012.02.003

Julkunen, P., Saisanen, L., Danner, N., Awiszus, F., & Kononen, M. (2012). Within-subject effect of coil-to-cortex distance on cortical electric field threshold and motor evoked potentials in transcranial magnetic stimulation. *Journal of Neuroscience Methods*, *206*(2), 158–164. https://doi.org/10.1016/j.jneumeth.2012.02.020

Julkunen, P., Saisanen, L., Danner, N., Niskanen, E., Hukkanen, T., Mervaala, E., & Kononen, M. (2009). Comparison of navigated and non-navigated transcranial magnetic stimulation for motor cortex mapping, motor threshold and motor evoked potentials. *NeuroImage*, *44*(3), 790–795. https://doi.org/10.1016/j.neuroimage.2008.09.040

Jung, J., Lavrador, J.-P., Patel, S., Giamouriadis, A., Lam, J., Bhangoo, R., Ashkan, K., & Vergani, F. (2019). First United Kingdom Experience of Navigated Transcranial Magnetic Stimulation in Preoperative Mapping of Brain Tumors. *World Neurosurgery*, *122*, e1578-e1587. https://doi.org/10.1016/j.wneu.2018.11.114

Jung, N. H., Delvendahl, I., Kuhnke, N. G., Hauschke, D., Stolle, S., & Mall, V. (2010). Navigated transcranial magnetic stimulation does not decrease the variability of motor-evoked potentials. *Brain Stimulation*, *3*(2), 87–94. https://doi.org/10.1016/j.brs.2009.10.003

Kallioniemi, E., Pitkanen, M., Saisanen, L., & Julkunen, P. (2015). Onset Latency of Motor Evoked Potentials in Motor Cortical Mapping with Neuronavigated Transcranial Magnetic Stimulation. *Open Neurol J*, *9*, 62–69. https://doi.org/10.2174/1874205X01509010062

Karhu, J., Hannula, H., Laine, J., & Ruohonen, J. (2014). Navigated Transcranial Magnetic Stimulation: Principles and Protocol for Mapping the Motor Cortex. In A. Rotenberg, J. C. Horvath, & A. Pascual-Leone (Eds.), *Neuromethods. Transcranial Magnetic Stimulation* (Vol. 89, pp. 337–359). New York, NY: Springer New York. https://doi.org/10.1007/978-1-4939-0879-0_16

Karnofsky, D. A., Abelmann, W. H., Craver, L. F., & Burchenal, J. H. (1948). The use of the nitrogen mustards in the palliative treatment of carcinoma.With particular reference to

bronchogenic carcinoma. *Cancer*, *1*(4), 634–656. https://doi.org/10.1002/1097-0142(194811)1:4%3C634::AID-CNCR2820010410%3E3.0.CO;2-L

Keller, S. S., Highley, J. R., Garcia-Finana, M., Sluming, V., Rezaie, R., & Roberts, N. (2007). Sulcal variability, stereological measurement and asymmetry of Broca's area on MR images. *Journal of Anatomy*, *211*(4), 534–555. https://doi.org/10.1111/j.1469-7580.2007.00793.x

Kennedy, S. H., Milev, R., Giacobbe, P., Ramasubbu, R., Lam, R. W., Parikh, S. V., Patten, S. B., & Ravindran, A. V. (2009). Canadian Network for Mood and Anxiety Treatments (CANMAT) Clinical guidelines for the management of major depressive disorder in adults. Iv. Neurostimulation therapies. *Journal of Affective Disorders*, *117 Suppl 1*, S44-53. https://doi.org/10.1016/j.jad.2009.06.039

Khan, M. N., Sharma, A. M., Pitz, M., Loewen, S. K., Quon, H., Poulin, A., & Essig, M. (2016). High-grade glioma management and response assessment-recent advances and current challenges. *Current Oncology (Toronto, Ont.)*, *23*(4), e383-91. https://doi.org/10.3747/co.23.3082

Kim, W. J., Hahn, S. J., Kim, W. S., & Paik, N. J. (2016). Neuronavigation-guided Repetitive Transcranial Magnetic Stimulation for Aphasia. *J Vis Exp.* Advance online publication. https://doi.org/10.3791/53345

Kocak, M., Ulmer, J. L., Sahin Ugurel, M., Gaggl, W., & Prost, R. W. (2009). Motor homunculus: Passive mapping in healthy volunteers by using functional MR imaging--initial results. *Radiology*, *251*(2), 485–492. https://doi.org/10.1148/radiol.2512080231

Krieg, S. M., Buchmann, N., Gempt, J., Shiban, E., Meyer, B., & Ringel, F. (2012). Diffusion tensor imaging fiber tracking using navigated brain stimulation--a feasibility study. *Acta Neurochirurgica*, *154*(3), 555–563. https://doi.org/10.1007/s00701-011-1255-3

Krieg, S. M., Ringel, F., & Meyer, B. (2012). Functional guidance in intracranial tumor surgery. *Perspectives in Medicine*, *1*(1-12), 59–64. https://doi.org/10.1016/j.permed.2012.03.014

Krieg, S. M., Ringel, F., & Meyer, B. (2012). Functional guidance in intracranial tumor surgery. *New Trends in Neurosonology and Cerebral Hemodynamics – an Update*, *1*(1–12), 59–64. https://doi.org/10.1016/j.permed.2012.03.014

Krieg, S. M., Sabih, J., Bulubas, L., Obermueller, T., Negwer, C., Janssen, I., Shiban, E., Meyer, B., & Ringel, F. (2014). Preoperative motor mapping by navigated transcranial magnetic brain stimulation improves outcome for motor eloquent lesions. *Neuro-Oncology*, *16*(9), 1274–1282. https://doi.org/10.1093/neuonc/nou007

Krieg, S. M., Shiban, E., Buchmann, N., Gempt, J., Foerschler, A., Meyer, B., & Ringel, F. (2012). Utility of presurgical navigated transcranial magnetic brain stimulation for the

resection of tumors in eloquent motor areas. *Journal of Neurosurgery*, *116*(5), 994–1001. https://doi.org/10.3171/2011.12.JNS111524

Krieg, S. M., Shiban, E., Buchmann, N., Meyer, B., & Ringel, F. (2013). Presurgical navigated transcranial magnetic brain stimulation for recurrent gliomas in motor eloquent areas. *Clinical Neurophysiology : Official Journal of the International Federation of Clinical Neurophysiology*, *124*(3), 522–527. https://doi.org/10.1016/j.clinph.2012.08.011

Krieg, S. M., Sollmann, N., Obermueller, T., Sabih, J., Bulubas, L., Negwer, C., Moser, T., Droese, D., Boeckh-Behrens, T., Ringel, F., & Meyer, B. (2015). Changing the clinical course of glioma patients by preoperative motor mapping with navigated transcranial magnetic brain stimulation. *BMC Cancer*, *15*, 231. https://doi.org/10.1186/s12885-015-1258-1

Krings, T., Buchbinder, B. R., Butler, W. E., Chiappa, K. H., Jiang, H. J., Cosgrove, G. R., & Rosen, B. R. (1997). Functional magnetic resonance imaging and transcranial magnetic stimulation: Complementary approaches in the evaluation of cortical motor function. *Neurology*, *48*(5), 1406–1416.

Krings, T., Buchbinder, B. R., Butler, W. E., Chiappa, K. H., Jiang, H. J., Rosen, B. R., & Cosgrove, G. R. (1997). Stereotactic transcranial magnetic stimulation: Correlation with direct electrical cortical stimulation. *Neurosurgery*, *41*(6), 1319-25; discussion 1325-6.

Krings, T., Chiappa, K. H., Foltys, H., Reinges, M. H., Cosgrove, G. R., & Thron, A. (2001). Introducing navigated transcranial magnetic stimulation as a refined brain mapping methodology. *Neurosurgical Review*, *24*(4), 171–179.

Krivosheya, D., Prabhu, S. S., Weinberg, J. S., & Sawaya, R. (2016). Technical principles in glioma surgery and preoperative considerations. *Journal of Neuro-Oncology*, *130*(2), 243–252. https://doi.org/10.1007/s11060-016-2171-4

Lacroix, M., Abi-Said, D., Fourney, D. R., Gokaslan, Z. L., Shi, W., DeMonte, F., Lang, F. F., McCutcheon, I. E., Hassenbusch, S. J., Holland, E., Hess, K., Michael, C., Miller, D., & Sawaya, R. (2001). A multivariate analysis of 416 patients with glioblastoma multiforme: Prognosis, extent of resection, and survival. *Journal of Neurosurgery*, *95*(2), 190–198. https://doi.org/10.3171/jns.2001.95.2.0190

Langlet, C., Bastide, B., & Canu, M.-H. (2012). Hindlimb unloading affects cortical motor maps and decreases corticospinal excitability. *Experimental Neurology*, *237*(1), 211–217. https://doi.org/10.1016/j.expneurol.2012.06.018

Lassek, A. M. (1941). The pyramidal tract of the monkeys. A betz cell and pyramidal tract enumeration. *The Journal of Comparative Neurology*, *74*(2), 193–202. https://doi.org/10.1002/cne.900740202

Lefaucheur, J. P., Andre-Obadia, N., Antal, A., Ayache, S. S., Baeken, C., Benninger, D. H., Cantello, R. M., Cincotta, M., Carvalho, M. de, Ridder, D. de, Devanne, H., Di Lazzaro, V. [Vincenzo], Filipovic, S. R., Hummel, F. C., Jaaskelainen, S. K., Kimiskidis, V. K., Koch, G., Langguth, B., Nyffeler, T., Oliviero, A., Padberg, F., Poulet, E., Rossi, S., Rossini, P. M., Rothwell, J. C., Schonfeldt-Lecuona, C., Siebner, H. R., Slotema, C. W., Stagg, C. J., Valls-Sole, J., Ziemann, U., Paulus, W., & Garcia-Larrea, L. (2014). Evidence-based guidelines on the therapeutic use of repetitive transcranial magnetic stimulation (rTMS). *Clinical Neurophysiology : Official Journal of the International Federation of Clinical Neurophysiology*, *125*(11), 2150–2206. https://doi.org/10.1016/j.clinph.2014.05.021

Leroy, H.-A., Delmaire, C., Le Rhun, E., Drumez, E., Lejeune, J.-P., & Reyns, N. (2019). High-field intraoperative MRI and glioma surgery: Results after the first 100 consecutive patients. *Acta Neurochirurgica.* Advance online publication. https://doi.org/10.1007/s00701-019-03920-6

Logothetis, N. K., Pauls, J., Augath, M., Trinath, T., & Oeltermann, A. (2001). Neurophysiological investigation of the basis of the fMRI signal. *Nature*, *412*(6843), 150–157. https://doi.org/10.1038/35084005

Logothetis, N. K., & Pfeuffer, J. (2004). On the nature of the BOLD fMRI contrast mechanism. *Magnetic Resonance Imaging*, *22*(10), 1517–1531. https://doi.org/10.1016/j.mri.2004.10.018

Louis, D. N., Ohgaki, H., Wiestler, O. D., Cavenee, W. K., Burger, P. C., Jouvet, A., Scheithauer, B. W., & Kleihues, P. (2007). The 2007 WHO classification of tumours of the central nervous system. *Acta Neuropathologica*, *114*(2), 97–109. https://doi.org/10.1007/s00401-007-0243-4

Lüllmann-Rauch, R. (2009). *Taschenlehrbuch Histologie: 10 Tabellen* (3., vollst. überarb. Aufl.). Stuttgart: Thieme.

Ly, J. Q. M., Gaggioni, G., Chellappa, S. L., Papachilleos, S., Brzozowski, A., Borsu, C., Rosanova, M., Sarasso, S., Middleton, B., Luxen, A., Archer, S. N., Phillips, C., Dijk, D.-J., Maquet, P., Massimini, M., & Vandewalle, G. (2016). Circadian regulation of human cortical excitability. *Nature Communications*, *7*, 11828. https://doi.org/10.1038/ncomms11828

Mallik, A., & Weir, A. I. (2005). Nerve conduction studies: Essentials and pitfalls in practice. *Journal of Neurology, Neurosurgery, and Psychiatry*, *76 Suppl 2*, ii23-31. https://doi.org/10.1136/jnnp.2005.069138

Malmivuo, J., & Plonsey, R. (1995). *BioelectromagnetismPrinciples and Applications of Bioelectric and Biomagnetic Fields*: Oxford University Press. Retrieved from

http://www.bem.fi/book/index.htm
https://doi.org/10.1093/acprof:oso/9780195058239.001.0001

Mark, C. I., Mazerolle, E. L., & Chen, J. J. (2015). Metabolic and vascular origins of the BOLD effect: Implications for imaging pathology and resting-state brain function. *Journal of Magnetic Resonance Imaging : JMRI*, *42*(2), 231–246. https://doi.org/10.1002/jmri.24786

Marko, N. F., Weil, R. J., Schroeder, J. L., Lang, F. F., Suki, D., & Sawaya, R. (2014). Extent of resection of glioblastoma revisited: Personalized survival modeling facilitates more accurate survival prediction and supports a maximum-safe-resection approach to surgery. *Journal of Clinical Oncology : Official Journal of the American Society of Clinical Oncology*, *32*(8), 774–782. https://doi.org/10.1200/JCO.2013.51.8886

Martino, J., Honma, S. M., Findlay, A. M., Guggisberg, A. G., Owen, J. P., Kirsch, H. E., Berger, M. S., & Nagarajan, S. S. (2011). Resting functional connectivity in patients with brain tumors in eloquent areas. *Annals of Neurology*, *69*(3), 521–532. https://doi.org/10.1002/ana.22167

Maurer, S., Tanigawa, N., Sollmann, N., Hauck, T., Ille, S., Boeckh-Behrens, T., Meyer, B., & Krieg, S. M. (2015). Non-invasive mapping of calculation function by repetitive navigated transcranial magnetic stimulation. *Brain Structure & Function.* Advance online publication. https://doi.org/10.1007/s00429-015-1136-2

Maxwell, J. C. (1865). A Dynamical Theory of the Electromagnetic Field. *Philosophical Transactions of the Royal Society of London*, *155*(0), 459–512. https://doi.org/10.1098/rstl.1865.0008

Mayo, B. C., Massel, D. H., Bohl, D. D., Long, W. W., Modi, K. D., & Singh, K. (2016). Anterior Cervical Discectomy and Fusion: The Surgical Learning Curve. *Spine*, *41*(20), 1580–1585. https://doi.org/10.1097/BRS.0000000000001588

Mehta, A. D., & Klein, G. (2010). Clinical utility of functional magnetic resonance imaging for brain mapping in epilepsy surgery. *Epilepsy Research*, *89*(1), 126–132. https://doi.org/10.1016/j.eplepsyres.2009.12.001

Mills, K. R., Boniface, S. J., & Schubert, M. (1992). Magnetic brain stimulation with a double coil: The importance of coil orientation. *Electroencephalography and Clinical Neurophysiology/Evoked Potentials Section*, *85*(1), 17–21. https://doi.org/10.1016/0168-5597(92)90096-T

Mohammadi, S., Moller, H. E., Kugel, H., Muller, D. K., & Deppe, M. (2010). Correcting eddy current and motion effects by affine whole-brain registrations: Evaluation of three-dimensional distortions and comparison with slicewise correction. *Magnetic Resonance in Medicine*, *64*(4), 1047–1056. https://doi.org/10.1002/mrm.22501

Moirand, R., Brunelin, J., & Poulet, E. (2015). Apport de l'imagerie dans le traitement des pathologies psychiatriques par stimulation magnétique transcrânienne répétée (rTMS). *Annales Médico-Psychologiques, Revue Psychiatrique*, *173*(3), 263–266. https://doi.org/10.1016/j.amp.2015.02.001

Mylius, V., Ayache, S. S., Ahdab, R., Farhat, W. H., Zouari, H. G., Belke, M., Brugieres, P., Wehrmann, E., Krakow, K., Timmesfeld, N., Schmidt, S., Oertel, W. H., Knake, S., & Lefaucheur, J. P. (2013). Definition of DLPFC and M1 according to anatomical landmarks for navigated brain stimulation: Inter-rater reliability, accuracy, and influence of gender and age. *NeuroImage*, *78*, 224–232. https://doi.org/10.1016/j.neuroimage.2013.03.061

Nadeem, M., Thorlin, T., Gandhi, O. P., & Persson, M. (2003). Computation of electric and magnetic stimulation in human head using the 3-D impedance method. *IEEE Transactions on Bio-Medical Engineering*, *50*(7), 900–907. https://doi.org/10.1109/TBME.2003.813548

Najib, U., Bashir, S., Edwards, D., Rotenberg, A., & Pascual-Leone, A. (2011). Transcranial Brain Stimulation: Clinical Applications and Future Directions. *Neurosurgery Clinics of North America*, *22*(2), 233-ix. https://doi.org/10.1016/j.nec.2011.01.002

Nauczyciel, C., Hellier, P., Morandi, X., Blestel, S., Drapier, D., Ferre, J. C., Barillot, C., & Millet, B. (2011). Assessment of standard coil positioning in transcranial magnetic stimulation in depression. *Psychiatry Research*, *186*(2-3), 232–238. https://doi.org/10.1016/j.psychres.2010.06.012

Ngomo, S., Leonard, G., & Mercier, C. (2012). Influence of the amount of use on hand motor cortex representation: Effects of immobilization and motor training. *Neuroscience*, *220*, 208–214. https://doi.org/10.1016/j.neuroscience.2012.06.018

Nieminen, J. O., Koponen, L. M., & Ilmoniemi, R. J. (2015). Experimental Characterization of the Electric Field Distribution Induced by TMS Devices. *Brain Stimulation*, *8*(3), 582–589. https://doi.org/10.1016/j.brs.2015.01.004

Niskanen, E., Julkunen, P., Saisanen, L., Vanninen, R., Karjalainen, P., & Kononen, M. (2010). Group-level variations in motor representation areas of thenar and anterior tibial muscles: Navigated Transcranial Magnetic Stimulation Study. *Hum Brain Mapp*, *31*(8), 1272–1280. https://doi.org/10.1002/hbm.20942

Noirhomme, Q., Ferrant, M., Vandermeeren, Y., Olivier, E., Macq, B., & Cuisenaire, O. (2004). Registration and real-time visualization of transcranial magnetic stimulation with 3-D MR images. *IEEE Transactions on Bio-Medical Engineering*, *51*(11), 1994–2005. https://doi.org/10.1109/TBME.2004.834266

O'Brien, M. (2010). *Aids to the examination of the peripheral nervous system* (Fifth edition, second reprint). Edinburgh: Saunders Elsevier.

Ogawa, S. [S.], Lee, T. M., Kay, A. R., & Tank, D. W. (1990). Brain magnetic resonance imaging with contrast dependent on blood oxygenation. *Proceedings of the National Academy of Sciences of the United States of America*, *87*(24), 9868–9872.

Ogawa, S. [Seiji], Lee, T. M., Nayak, A. S., & Glynn, P. (1990). Oxygenation-sensitive contrast in magnetic resonance image of rodent brain at high magnetic fields. *Magnetic Resonance in Medicine*, *14*(1), 68–78. https://doi.org/10.1002/mrm.1910140108

Oken, M. M., Creech, R. H., Tormey, D. C., Horton, J., Davis, T. E., McFadden, E. T., & Carbone, P. P. (1982). Toxicity and response criteria of the Eastern Cooperative Oncology Group. *American Journal of Clinical Oncology*, *5*(6), 649–655.

Oldfield, R. C. (1971). The assessment and analysis of handedness: The Edinburgh inventory. *Neuropsychologia*, *9*(1), 97–113.

Opitz, A., Windhoff, M., Heidemann, R. M., Turner, R., & Thielscher, A. (2011). How the brain tissue shapes the electric field induced by transcranial magnetic stimulation. *NeuroImage*, *58*(3), 849–859. https://doi.org/10.1016/j.neuroimage.2011.06.069

Ostrom, Q. T., Gittleman, H., Liao, P., Rouse, C., Chen, Y., Dowling, J., Wolinsky, Y., Kruchko, C., & Barnholtz-Sloan, J. (2014). Cbtrus statistical report: Primary brain and central nervous system tumors diagnosed in the United States in 2007-2011. *Neuro-Oncology*, *16 Suppl 4*, iv1-63. https://doi.org/10.1093/neuonc/nou223

Ostrom, Q. T., Gittleman, H., Liao, P., Rouse, C., Chen, Y., Dowling, J., Wolinsky, Y., Kruchko, C., & Barnholtz-Sloan, J. (2014). Cbtrus statistical report: Primary brain and central nervous system tumors diagnosed in the United States in 2007-2011. *Neuro-Oncology*, *16 Suppl 4*, iv1-63. https://doi.org/10.1093/neuonc/nou223

Ottenhausen, M., Krieg, S. M., Meyer, B., & Ringel, F. (2015). Functional preoperative and intraoperative mapping and monitoring: Increasing safety and efficacy in glioma surgery. *Neurosurgical Focus*, *38*(1), E3. https://doi.org/10.3171/2014.10.FOCUS14611

Park, C.-H., Kou, N., Boudrias, M.-H., Playford, E. D., & Ward, N. S. (2013). Assessing a standardised approach to measuring corticospinal integrity after stroke with DTI. *NeuroImage. Clinical*, *2*, 521–533. https://doi.org/10.1016/j.nicl.2013.04.002

Park, M. C., Goldman, M. A., Park, M. J., & Friehs, G. M. (2007). Neuroanatomical localization of the 'precentral knob' with computed tomography imaging. *Stereotact Funct Neurosurg*, *85*(4), 158–161. https://doi.org/10.1159/000099074

Patel, C. K., Vemaraju, R., Glasbey, J., Shires, J., Northmore, T., Zaben, M., & Hayhurst, C. (2018). Trends in peri-operative performance status following resection of high grade glioma and brain metastases: The impact on survival. *Clin Neurol Neurosurg*, *164*, 67–71. https://doi.org/10.1016/j.clineuro.2017.11.016

Penfield, W., & Boldrey, E. (1937). Somatic motor and sensory representation in the cerebral cortex of man as studied by electrical stimulation. *Brain*, *60*(4), 389–443. https://doi.org/10.1093/brain/60.4.389

Penfield, W., Rasmussen, T., & National Institute on Drug Abuse (1950). *The cerebral cortex of man: A clinical study of localization of function*. New York: Macmillan.

Penhune, V. B., & Steele, C. J. (2012). Parallel contributions of cerebellar, striatal and M1 mechanisms to motor sequence learning. *Behavioural Brain Research*, *226*(2), 579–591. https://doi.org/10.1016/j.bbr.2011.09.044

Péus, D., Newcomb, N., & Hofer, S. (2013). Appraisal of the Karnofsky Performance Status and proposal of a simple algorithmic system for its evaluation. *BMC Medical Informatics and Decision Making*, *13*, 72. https://doi.org/10.1186/1472-6947-13-72

Picht, T., Frey, D., Thieme, S., Kliesch, S., & Vajkoczy, P. (2016). Presurgical navigated TMS motor cortex mapping improves outcome in glioblastoma surgery: A controlled observational study. *Journal of Neuro-Oncology*, *126*(3), 535–543. https://doi.org/10.1007/s11060-015-1993-9

Picht, T., Mularski, S., Kuehn, B., Vajkoczy, P., Kombos, T., & Suess, O. (2009). Navigated transcranial magnetic stimulation for preoperative functional diagnostics in brain tumor surgery. *Neurosurgery*, *65*(6 Suppl), 93-8; discussion 98-9. https://doi.org/10.1227/01.NEU.0000348009.22750.59

Picht, T., Schmidt, S., Brandt, S. [Stephan], Frey, D., Hannula, H., Neuvonen, T., Karhu, J., Vajkoczy, P., & Suess, O. (2011). Preoperative functional mapping for rolandic brain tumor surgery: Comparison of navigated transcranial magnetic stimulation to direct cortical stimulation. *Neurosurgery*, *69*(3), 581-8; discussion 588. https://doi.org/10.1227/NEU.0b013e3182181b89

Pickard, J. D., Akalan, N., Rocco, C., Dolenc, V. V., Antunes, J. L., Mooij, J. J. A., . . . Sin, M. (Eds.) (2008). *Advances and Technical Standards in Neurosurgery: Vol. 33*. *Advances and Technical Standards in Neurosurgery 33* (1. Aufl.). s.l.: Springer Verlag Wien. Retrieved from http://search.ebscohost.com/login.aspx?direct=true&scope=site&db=nlebk&db=nlabk&AN=229228

Potts, G. F., Gugino, L. D., Leventon, M. E., Grimson, W. E., Kikinis, R., Cote, W., Alexander, E., Anderson, J. E., Ettinger, G. J., Aglio, L. S., & Shenton, M. E. (1998). Visual hemifield mapping using transcranial magnetic stimulation coregistered with cortical surfaces derived from magnetic resonance images. *Journal of Clinical Neurophysiology : Official Publication of the American Electroencephalographic Society*, *15*(4), 344–350.

Raffin, E., & Siebner, H. R. (2019). Use-Dependent Plasticity in Human Primary Motor Hand Area: Synergistic Interplay Between Training and Immobilization. *Cerebral Cortex*, *29*(1), 356–371. https://doi.org/10.1093/cercor/bhy226

Ranck, J. B., JR (1975). Which elements are excited in electrical stimulation of mammalian central nervous system: A review. *Brain Research*, *98*(3), 417–440.

Rattay, F. (1999). The basic mechanism for the electrical stimulation of the nervous system. *Neuroscience*, *89*(2), 335–346.

Ravazzani, P., Ruohonen, J., Grandori, F., & Tognola, G. (1996). Magnetic stimulation of the nervous system: Induced electric field in unbounded, semi-infinite, spherical, and cylindrical media. *Annals of Biomedical Engineering*, *24*(5), 606–616.

Reiser, M., Kuhn, F.-P., & Debus, J. (2017). *Radiologie* (4., vollständig überarbeitete Auflage). *Duale Reihe*. Stuttgart: Thieme.

Rizzo, V., Terranova, C., Conti, A., Germanò, A., Alafaci, C., Raffa, G., Girlanda, P., Tomasello, F., & Quartarone, A. (2014). Preoperative functional mapping for rolandic brain tumor surgery. *Neuroscience Letters*, *583*, 136–141. https://doi.org/10.1016/j.neulet.2014.09.017

Rizzo, V., Terranova, C., Conti, A., Germanò, A., Alafaci, C., Raffa, G., Girlanda, P., Tomasello, F., & Quartarone, A. (2014). Preoperative functional mapping for rolandic brain tumor surgery. *Neuroscience Letters*, *583*, 136–141. https://doi.org/10.1016/j.neulet.2014.09.017

Roelz, R., Strohmaier, D., Jabbarli, R., Kraeutle, R., Egger, K., Coenen, V. A., Weyerbrock, A., & Reinacher, P. C. (2016). Residual Tumor Volume as Best Outcome Predictor in Low Grade Glioma - A Nine-Years Near-Randomized Survey of Surgery vs. Biopsy. *Scientific Reports*, *6*, 32286. https://doi.org/10.1038/srep32286

Rossi, S., Hallett, M., Rossini, P. M., & Pascual-Leone, A. (2009). Safety, ethical considerations, and application guidelines for the use of transcranial magnetic stimulation in clinical practice and research. *Clinical Neurophysiology : Official Journal of the International Federation of Clinical Neurophysiology*, *120*(12), 2008–2039. https://doi.org/10.1016/j.clinph.2009.08.016

Rossini, P. M., Barker, A. T., Berardelli, A., Caramia, M. D., Caruso, G., Cracco, R. Q., Dimitrijevic, M. R., Hallett, M., Katayama, Y., & Lucking, C. H. (1994). Non-invasive electrical and magnetic stimulation of the brain, spinal cord and roots: Basic principles and procedures for routine clinical application. Report of an IFCN committee. *Electroencephalography and Clinical Neurophysiology*, *91*(2), 79–92.

Rossini, P. M., Burke, D., Chen, R., Cohen, L. G., Daskalakis, Z., Di Iorio, R., Di Lazzaro, V. [V.], Ferreri, F., Fitzgerald, P. B., George, M. S., Hallett, M., Lefaucheur, J. P., Langguth, B., Matsumoto, H., Miniussi, C., Nitsche, M. A., Pascual-Leone, A., Paulus, W., Rossi, S., Rothwell, J. C., Siebner, H. R., Ugawa, Y., Walsh, V., & Ziemann, U. (2015). Non-invasive electrical and magnetic stimulation of the brain, spinal cord, roots and peripheral nerves: Basic principles and procedures for routine clinical and research application. An updated report from an I.F.C.N. Committee. *Clinical Neurophysiology : Official Journal of the International Federation of Clinical Neurophysiology*, *126*(6), 1071–1107. https://doi.org/10.1016/j.clinph.2015.02.001

Rotenberg, A., Horvath, J. C., & Pascual-Leone, A. (Eds.) (2014). *Neuromethods*. *Transcranial Magnetic Stimulation*. New York, NY: Springer New York. https://doi.org/10.1007/978-1-4939-0879-0

Roth, B. J., Saypol, J. M., Hallett, M., & Cohen, L. G. (1991). A theoretical calculation of the electric field induced in the cortex during magnetic stimulation. *Electroencephalography and Clinical Neurophysiology*, *81*(1), 47–56.

Roux, F.-E., Durand, J.-B., Djidjeli, I., Moyse, E., & Giussani, C. (2016). Variability of intraoperative electrostimulation parameters in conscious individuals: Language cortex. *Journal of Neurosurgery*, 1–12. https://doi.org/10.3171/2016.4.JNS152434

Ruh, A., Scherer, H., & Kiselev, V. G. (2018). The larmor frequency shift in magnetically heterogeneous media depends on their mesoscopic structure. *Magnetic Resonance in Medicine*, *79*(2), 1101–1110. https://doi.org/10.1002/mrm.26753

Ruohonen, J., & Ilmoniemi, R. J. (1999). Modeling of the stimulating field generation in TMS. *Electroencephalogr Clin Neurophysiol Suppl*, *51*, 30–40. Retrieved from http://www.ncbi.nlm.nih.gov/pubmed/10590933

Ruohonen, J., & Karhu, J. (2010). Navigated transcranial magnetic stimulation. *Neurophysiologie Clinique = Clinical Neurophysiology*, *40*(1), 7–17. https://doi.org/10.1016/j.neucli.2010.01.006

Ruohonen, J., Ravazzani, P., & Grandori, F. (1998). Functional magnetic stimulation: Theory and coil optimization. *Bioelectrochemistry and Bioenergetics*, *47*(2), 213–219. https://doi.org/10.1016/S0302-4598(98)00191-3

Rushton, W. A. (1927). The effect upon the threshold for nervous excitation of the length of nerve exposed, and the angle between current and nerve. *The Journal of Physiology*, *63*(4), 357–377.

Rutten, G.-J., & Ramsey, N. F. (2010). The role of functional magnetic resonance imaging in brain surgery. *Neurosurgical Focus*, *28*(2), E4. https://doi.org/10.3171/2009.12.FOCUS09251

Sagberg, L. M., Iversen, D. H., Fyllingen, E. H., Jakola, A. S., Reinertsen, I., & Solheim, O. (2019). Brain atlas for assessing the impact of tumor location on perioperative quality of life in patients with high-grade glioma: A prospective population-based cohort study. *NeuroImage : Clinical*, *21*, 101658. https://doi.org/10.1016/j.nicl.2019.101658

Saisanen, L. (2011). *Human motor cortex function characterized by navigated transcranial magnetic stimulation* (Vol. 68). Retrieved from http://epublications.uef.fi/pub/urn_isbn_978-952-61-0504-8/urn_isbn_978-952-61-0504-8.pdf

Saisanen, L., Julkunen, P., Niskanen, E., Danner, N., Hukkanen, T., Lohioja, T., Nurkkala, J., Mervaala, E., Karhu, J., & Kononen, M. (2008). Motor potentials evoked by navigated transcranial magnetic stimulation in healthy subjects. *J Clin Neurophysiol*, *25*(6), 367–372. https://doi.org/10.1097/WNP.0b013e31818e7944

Sanai, N., Chang, S. M., & Berger, M. S. (2011). Low-grade gliomas in adults. *Journal of Neurosurgery*, *115*(5), 948–965. https://doi.org/10.3171/2011.7.JNS101238

Sanai, N., Polley, M.-Y., McDermott, M. W., Parsa, A. T., & Berger, M. S. (2011). An extent of resection threshold for newly diagnosed glioblastomas. *Journal of Neurosurgery*, *115*(1), 3–8. https://doi.org/10.3171/2011.2.JNS10998

Schmidt, R. F., Lang, F. [Florian], & Heckmann, M. (2011). *Physiologie des Menschen: Mit Pathophysiologie*. Berlin/Heidelberg: Springer Berlin Heidelberg. Retrieved from http://gbv.eblib.com/patron/FullRecord.aspx?p=3066576

Schmidt, S., Bathe-Peters, R., Fleischmann, R. [R.], Ronnefarth, M., Scholz, M., & Brandt, S. A. (2015). Nonphysiological factors in navigated TMS studies; confounding covariates and valid intracortical estimates. *Hum Brain Mapp*, *36*(1), 40–49. https://doi.org/10.1002/hbm.22611

Schünke, M., Schulte, E., Schumacher, U., & Voll, M. (2009). *Kopf, Hals und Neuroanatomie: 115 Tabellen* (2., überarb. und erw. Aufl.). *Prometheus / Michael Schünke Erik Schulte Udo Schumacher. Unter Mitarb. von Jürgen Rude. Ill. von Markus Voll Karl Wesker: Vol. 3*. Stuttgart: Thieme.

Seo, J. P., & Jang, S. H. (2013). Characteristics of corticospinal tract area according to pontine level. *Yonsei Medical Journal*, *54*(3), 785–787. https://doi.org/10.3349/ymj.2013.54.3.785

Smith, J. S., Chang, E. F., Lamborn, K. R., Chang, S. M., Prados, M. D., Cha, S., Tihan, T., Vandenberg, S., McDermott, M. W., & Berger, M. S. (2008). Role of extent of resection in the long-term outcome of low-grade hemispheric gliomas. *Journal of Clinical Oncology :*

Official Journal of the American Society of Clinical Oncology, *26*(8), 1338–1345. https://doi.org/10.1200/JCO.2007.13.9337

Sollmann, N., Giglhuber, K., Tussis, L., Meyer, B., Ringel, F., & Krieg, S. M. (2015). nTMS-based DTI fiber tracking for language pathways correlates with language function and aphasia - A case report. *Clin Neurol Neurosurg*, *136*, 25–28. https://doi.org/10.1016/j.clineuro.2015.05.023

Sollmann, N., Goblirsch-Kolb, M. F., Ille, S., Butenschoen, V. M., Boeckh-Behrens, T., Meyer, B., Ringel, F., & Krieg, S. M. (2016). Comparison between electric-field-navigated and line-navigated TMS for cortical motor mapping in patients with brain tumors. *Acta Neurochirurgica.* Advance online publication. https://doi.org/10.1007/s00701-016-2970-6

Sollmann, N., Hauck, T., Hapfelmeier, A., Meyer, B., Ringel, F., & Krieg, S. M. (2013). Intra- and interobserver variability of language mapping by navigated transcranial magnetic brain stimulation. *BMC Neuroscience*, *14*, 150. https://doi.org/10.1186/1471-2202-14-150

Sollmann, N., Hauck, T., Obermueller, T., Hapfelmeier, A., Meyer, B., Ringel, F., & Krieg, S. M. (2013). Inter- and intraobserver variability in motor mapping of the hotspot for the abductor policis brevis muscle. *BMC Neuroscience*, *14*, 94. https://doi.org/10.1186/1471-2202-14-94

Sollmann, N., Kubitscheck, A., Maurer, S., Ille, S., Hauck, T., Kirschke, J. S., Ringel, F., Meyer, B., & Krieg, S. M. (2016). Preoperative language mapping by repetitive navigated transcranial magnetic stimulation and diffusion tensor imaging fiber tracking and their comparison to intraoperative stimulation. *Neuroradiology*, *58*(8), 807–818. https://doi.org/10.1007/s00234-016-1685-y

Sollmann, N., Meyer, B., & Krieg, S. M. (2017). Implementing Functional Preoperative Mapping in the Clinical Routine of a Neurosurgical Department: Technical Note. *World Neurosurgery*, *103*, 94–105. https://doi.org/10.1016/j.wneu.2017.03.114

Sollmann, N., Negwer, C., Ille, S., Maurer, S., Hauck, T., Kirschke, J. S., Ringel, F., Meyer, B., & Krieg, S. M. (2016). Feasibility of nTMS-based DTI fiber tracking of language pathways in neurosurgical patients using a fractional anisotropy threshold. *J Neurosci Methods.* Advance online publication. https://doi.org/10.1016/j.jneumeth.2016.04.002

Sollmann, N., Negwer, C., Tussis, L., Hauck, T., Ille, S., Maurer, S., Giglhuber, K., Bauer, J. S., Ringel, F., Meyer, B., & Krieg, S. M. (2016). Interhemispheric connectivity revealed by diffusion tensor imaging fiber tracking derived from navigated transcranial magnetic stimulation maps as a sign of language function at risk in patients with brain tumors. *J Neurosurg*, 1–12. https://doi.org/10.3171/2016.1.JNS152053

Sollmann, N., Picht, T., Makela, J. P., Meyer, B., Ringel, F., & Krieg, S. M. (2013). Navigated transcranial magnetic stimulation for preoperative language mapping in a patient with a left frontoopercular glioblastoma. *Journal of Neurosurgery*, *118*(1), 175–179. https://doi.org/10.3171/2012.9.JNS121053

Stokes, M. G., Chambers, C. D., Gould, I. C., English, T., McNaught, E., McDonald, O., & Mattingley, J. B. (2007). Distance-adjusted motor threshold for transcranial magnetic stimulation. *Clinical Neurophysiology : Official Journal of the International Federation of Clinical Neurophysiology*, *118*(7), 1617–1625. https://doi.org/10.1016/j.clinph.2007.04.004

Student (1908). The probable error of a mean. *Biometrika*, *6*(1), 1–25. https://doi.org/10.1093/biomet/6.1.1

Takahashi, S., Jussen, D., Vajkoczy, P., & Picht, T. (2012). Plastic relocation of motor cortex in a patient with LGG (low grade glioma) confirmed by NBS (navigated brain stimulation). *Acta Neurochirurgica*, *154*(11), 2003-8; discussion 2008. https://doi.org/10.1007/s00701-012-1492-0

Takahashi, S., Vajkoczy, P., & Picht, T. (2013). Navigated transcranial magnetic stimulation for mapping the motor cortex in patients with rolandic brain tumors. *Neurosurgical Focus*, *34*(4), E3. https://doi.org/10.3171/2013.1.FOCUS133

Tarapore, P. E., Picht, T., Bulubas, L., Shin, Y., Kulchytska, N., Meyer, B., Berger, M. S., Nagarajan, S. S., & Krieg, S. M. (2016). Safety and tolerability of navigated TMS for preoperative mapping in neurosurgical patients. *Clin Neurophysiol*, *127*(3), 1895–1900. https://doi.org/10.1016/j.clinph.2015.11.042

Tarapore, P. E., Picht, T., Bulubas, L., Shin, Y., Kulchytska, N., Meyer, B., Nagarajan, S. S., & Krieg, S. M. (2016). Safety and tolerability of navigated TMS in healthy volunteers. *Clinical Neurophysiology : Official Journal of the International Federation of Clinical Neurophysiology*, *127*(3), 1916–1918. https://doi.org/10.1016/j.clinph.2015.11.043

Tarapore, P. E., Tate, M. C., Findlay, A. M., Honma, S. M., Mizuiri, D., Berger, M. S., & Nagarajan, S. S. (2012). Preoperative multimodal motor mapping: A comparison of magnetoencephalography imaging, navigated transcranial magnetic stimulation, and direct cortical stimulation. *Journal of Neurosurgery*, *117*(2), 354–362. https://doi.org/10.3171/2012.5.JNS112124

Teitti, S., Maatta, S., Saisanen, L., Kononen, M., Vanninen, R., Hannula, H., Mervaala, E., & Karhu, J. (2008). Non-primary motor areas in the human frontal lobe are connected directly to hand muscles. *NeuroImage*, *40*(3), 1243–1250. https://doi.org/10.1016/j.neuroimage.2007.12.065

Temesi, J., Gruet, M., Rupp, T., Verges, S., & Millet, G. Y. (2014). Resting and active motor thresholds versus stimulus-response curves to determine transcranial magnetic stimulation intensity in quadriceps femoris. *Journal of Neuroengineering and Rehabilitation*, *11*, 40. https://doi.org/10.1186/1743-0003-11-40

Terzi, H., Biler, A., Demirtas, O., Guler, O. T., Peker, N., & Kale, A. (2016). Total laparoscopic hysterectomy: Analysis of the surgical learning curve in benign conditions. *International Journal of Surgery (London, England)*, *35*, 51–57. https://doi.org/10.1016/j.ijsu.2016.09.010

Thielscher, A., & Kammer, T. (2004). Electric field properties of two commercial figure-8 coils in TMS: Calculation of focality and efficiency. *Clinical Neurophysiology : Official Journal of the International Federation of Clinical Neurophysiology*, *115*(7), 1697–1708. https://doi.org/10.1016/j.clinph.2004.02.019

Thielscher, A., Opitz, A., & Windhoff, M. (2011). Impact of the gyral geometry on the electric field induced by transcranial magnetic stimulation. *NeuroImage*, *54*(1), 234–243. https://doi.org/10.1016/j.neuroimage.2010.07.061

Thielscher, A., & Wichmann, F. A. (2009). Determining the cortical target of transcranial magnetic stimulation. *NeuroImage*, *47*(4), 1319–1330. https://doi.org/10.1016/j.neuroimage.2009.04.021

Thulborn, K. R., Waterton, J. C., Matthews, P. M., & Radda, G. K. (1982). Oxygenation dependence of the transverse relaxation time of water protons in whole blood at high field. *Biochimica Et Biophysica Acta*, *714*(2), 265–270.

Tofts, P. S., & Branston, N. M. (1991). The measurement of electric field, and the influence of surface charge, in magnetic stimulation. *Electroencephalography and Clinical Neurophysiology*, *81*(3), 238–239.

Trillenberg, P., Bremer, S., Oung, S., Erdmann, C., Schweikard, A., & Richter, L. (2012). Variation of stimulation intensity in transcranial magnetic stimulation with depth. *Journal of Neuroscience Methods*, *211*(2), 185–190. https://doi.org/10.1016/j.jneumeth.2012.09.007

Tussis, L., Sollmann, N., Boeckh-Behrens, T., Meyer, B., & Krieg, S. M. (2016). Language function distribution in left-handers: A navigated transcranial magnetic stimulation study. *Neuropsychologia*, *82*, 65–73. https://doi.org/10.1016/j.neuropsychologia.2016.01.010

Uy, J., Ridding, M. C., & Miles, T. S. (2002). Stability of Maps of Human Motor Cortex Made with Transcranial Magnetic Stimulation. *Brain Topography*, *14*(4), 293–297. https://doi.org/10.1023/A:1015752711146

Van der Kamp, W., Zwinderman, A. H., Ferrari, M. D., & van Dijk, J. G. (1996). Cortical excitability and response variability of transcranial magnetic stimulation. *Journal of Clinical*

Neurophysiology : Official Publication of the American Electroencephalographic Society, *13*(2), 164–171.

Vieth, J. (1984). Magnetoencephalography, a new function diagnostic method. *EEG-EMG Zeitschrift Fur Elektroenzephalographie, Elektromyographie Und Verwandte Gebiete*, *15*(2), 111–118.

Wager, T. D., Atlas, L. Y., Lindquist, M. A., Roy, M., Woo, C.-W., & Kross, E. (2013). An fMRI-based neurologic signature of physical pain. *The New England Journal of Medicine*, *368*(15), 1388–1397. https://doi.org/10.1056/NEJMoa1204471

Wall, C. A., Croarkin, P. E., Maroney-Smith, M. J., Haugen, L. M., Baruth, J. M., Frye, M. A., Sampson, S. M., & Port, J. D. (2016). Magnetic Resonance Imaging-Guided, Open-Label, High-Frequency Repetitive Transcranial Magnetic Stimulation for Adolescents with Major Depressive Disorder. *Journal of Child and Adolescent Psychopharmacology*, *26*(7), 582–589. https://doi.org/10.1089/cap.2015.0217

Wassermann, E. M. (2002). Variation in the response to transcranial magnetic brain stimulation in the general population. *Clinical Neurophysiology : Official Journal of the International Federation of Clinical Neurophysiology*, *113*(7), 1165–1171.

Wassermann, E. M., Epstein, C. M., & Ziemann, U. (Eds.) (2008). *Oxford handbooks series*. *The Oxford handbook of transcranial stimulation*. Oxford, New York: Oxford University Press. Retrieved from http://ovidsp.ovid.com/ovidweb.cgi?T=JS&PAGE=booktext&NEWS=N&DF=bookdb&AN=01376495/1st_Edition&XPATH=/PG(0)

Wassermann, E. M., McShane, L. M., Hallett, M., & Cohen, L. G. (1992). Noninvasive mapping of muscle representations in human motor cortex. *Electroencephalography and Clinical Neurophysiology/Evoked Potentials Section*, *85*(1), 1–8. https://doi.org/10.1016/0168-5597(92)90094-R

Weiss, C., Nettekoven, C., Rehme, A. K., Neuschmelting, V., Eisenbeis, A., Goldbrunner, R., & Grefkes, C. (2013). Mapping the hand, foot and face representations in the primary motor cortex - retest reliability of neuronavigated TMS versus functional MRI. *NeuroImage*, *66*, 531–542. https://doi.org/10.1016/j.neuroimage.2012.10.046

Weiss, C., Tursunova, I., Neuschmelting, V., Lockau, H., Nettekoven, C., Oros-Peusquens, A.-M., Stoffels, G., Rehme, A. K., Faymonville, A. M., Shah, N. J., Langen, K. J., Goldbrunner, R., & Grefkes, C. (2015). Improved nTMS- and DTI-derived CST tractography through anatomical ROI seeding on anterior pontine level compared to internal capsule. *NeuroImage. Clinical*, *7*, 424–437. https://doi.org/10.1016/j.nicl.2015.01.006

Weller, M., Wick, W., Aldape, K., Brada, M., Berger, M. S., Pfister, S. M., Nishikawa, R., Rosenthal, M., Wen, P. Y., Stupp, R., & Reifenberger, G. (2015). Glioma. *Nature Reviews Disease Primers*, *1*, 15017 EP -. https://doi.org/10.1038/nrdp.2015.17

Welsch, U., Deller, T., & Kummer, W. (2014). *Lehrbuch Histologie* (4. Auflage). München: Elsevier Urban & Fischer.

White, L. (1997). Structure of the human sensorimotor system. I: Morphology and cytoarchitecture of the central sulcus. *Cerebral Cortex*, *7*(1), 18–30. https://doi.org/10.1093/cercor/7.1.18

Wu, C.-X., Lin, G.-S., Lin, Z.-X., Zhang, J.-D., Liu, S.-Y., & Zhou, C.-F. (2015). Peritumoral edema shown by MRI predicts poor clinical outcome in glioblastoma. *World Journal of Surgical Oncology*, *13*, 97. https://doi.org/10.1186/s12957-015-0496-7

Yousry, T. A., Schmid, U. D., Alkadhi, H., Schmidt, D., Peraud, A., Buettner, A., & Winkler, P. (1997). Localization of the motor hand area to a knob on the precentral gyrus. A new landmark. *Brain : A Journal of Neurology*, *120 (Pt 1)*, 141–157.

Zdunczyk, A., Fleischmann, R. [Robert], Schulz, J., Vajkoczy, P., & Picht, T. (2013). The reliability of topographic measurements from navigated transcranial magnetic stimulation in healthy volunteers and tumor patients. *Acta Neurochirurgica*, *155*(7), 1309–1317. https://doi.org/10.1007/s00701-013-1665-5

Zdunczyk, A., Fleischmann, R. [Robert], Schulz, J., Vajkoczy, P., & Picht, T. (2013). The reliability of topographic measurements from navigated transcranial magnetic stimulation in healthy volunteers and tumor patients. *Acta Neurochirurgica*, *155*(7), 1309–1317. https://doi.org/10.1007/s00701-013-1665-5

Ziemann, U., Lonnecker, S., Steinhoff, B. J., & Paulus, W. (1996). Effects of antiepileptic drugs on motor cortex excitability in humans: A transcranial magnetic stimulation study. *Annals of Neurology*, *40*(3), 367–378. https://doi.org/10.1002/ana.410400306

9. ABBREVIATIONS

%MO	percentage of maximum stimulator output
ADM	abductor digiti minimi muscle
AMT	active motor threshold
anG	angular gyrus
APB	adductor pollicis brevis muscle
BA	Brodmann area
BCS	biceps brachii muscle
BOLD	blood oxygenation level dependent
CE	Conformité européenne
cMRI	cranial magnetic resonance image/imaging
CNS	central nervous system
CSF	corticospinal fluid
CST	corticospinal tract
CT	X-ray computed tomography
DCS	direct cortical stimulation
DLPFC	dorsolateral prefrontal cortex
dPrG	dorsal precentral gyrus
DTI	diffusion tensor imaging
DTI FT	diffusion tensor imaging fiber tracking
ECOG	Eastern Co-operative Oncology Group
EEG	electroencephalography
E-field	electric field
EHI	Edinburgh Handedness Inventory
EMG	electromyography
EnTMS	electric field navigated transcranial magnetic stimulation
EOR	extend of resection
FA	fractional anisotropy
FCR	flexor carpi radialis muscle
FDA	United States food and drug administration
FLAIR	fluid attenuated inversion recovery
fMRI	functional magnetic resonance image/imaging
FT	fiber tracking

GCN	gastrocnemius muscle
HGG	high-grade glioma
LE	lower extremity
LGG	low-grade glioma
LnTMS	line navigated transcranial magnetic stimulation
LTD	long-term depression
LTP	long term potentiation
M1	primary motor cortex
MEG	magnetoencephalography
MEP	motor-evoked potential
mPoG	medial occipital gyrus
MPRAGE	magnetization prepared rapid gradient echo
mPrG	medial precentral gyrus
MRI	magnetic resonance image/imaging
nTMS	navigated transcranial magnetic stimulation
PET	position emission tomography
PMC	premotor cortex
PPFM	pli de passage fronto-pariétal de moyen
QOL	quality of life
RdI	Klinikum Rechts der Isar
RMT	resting motor threshold
ROI	region of interest
rTMS	repetitive transcranial magnetic stimulation
S1	primary sensory cortex
SMA	supplementary motor areas
TA	tibialis anterior muscle
TES	transcranial electric stimulation
TMS	transcranial magnetic stimulation
UE	upper extremity
UI	user interface
VAS	visual analogue scale for pain
vPoG	ventral occipital gyrus
vPrG	ventral precentral gyrus
WHO	World Health Organization

10. TABLE OF FIGURES

Written consent was acquired for the usage of the previously published figures 6, 18, 20, 21, 22 prior to the publication of this thesis.

The figures of (Gray & Lewis, 1918) and (Brodmann, 1909) are used in the public domain as the copyright on both sources expired 100 years after the authors passing.

The Figures of the motor and sensory homunculi used In Figure 4 are licensed under creative commons licenses. These licenses require provision of the following details:

License used for the motor homunculus: “Attribution-ShareAlike 4.0 International”
Author: Wikimedia User *ralf@ark.in-berlin.de*
File link: *https://commons.wikimedia.org/wiki/File:Motor_homunculus.svg*
License link *https://creativecommons.org/licenses/by-sa/4.0/deed.en*
Changes made: removal of centric lines present in the original figure

License used for the sensory homunculus: “Attribution-ShareAlike 3.0 Unported”
Author: Wikimedia User *Btarsky*
File link: *https://commons.wikimedia.org/wiki/File:Sensory_Homunculus.png*
License link: *https://creativecommons.org/licenses/by-sa/3.0/deed.en*
Changes made: mirroring of the original image by 180 degrees.

11. TABLE OF TABLES

12. ACKNOWLEDGEMENTS

First, I want to thank my supervisor Prof. Dr. med. Sandro M. Krieg, whose support and guidance rendered this thesis possible in the first place. The same goes for my mentor, Dr. med. Nico Sollmann, PhD, B.A.. The constant and extensive amount of helpfulness and understanding offered by both deserves particular mention. As I have experienced before, it is far from usual to be able to ask for advice or help at any given time and receive it immediately even after the end of the study. Thanks to them, I was given the opportunity to independently work on my project, include my own ideas and ultimately publish them for the first time. They taught me a thorough way of working of which I will continue to profit long past this thesis both personally and professionally.

I also would like to thank all other members of the TMS study group (alphabetically: Neal Conway, Katharina Drummer, Sophia Fuss, Katrin Giglhuber, Theresa Hauck, Anna Kelm, Antonia Kubitscheck, Tobias Laub, Stefanie Maurer, Axel Schröder, Maximilian Schwendner, Noemie Wildschutz). The colleagueship and friendliness of this group have greatly contributed to this thesis.

Furthermore, my thanks go to the neurosurgical clinic of the Klinikum Rechts der Isar lead by Univ.-Prof Dr. med. Bernhard Meyer and all the staff working at the clinic who rendered this study possible and helped with patient acquisition.

I would further like to acknowledge the Max-Weber program of the Studienstiftung des deutschen Volkes as well as the medical graduate center of the TUM graduate school who have supported me throughout my studies and during this project.

Moreover, I could not have pursued my studies as well as this project without the constant support of my friends and my family. Thanks to them I always had someone to turn to backing and council.

Finally, I wish to close this part by wholeheartedly thanking my wife Daniela. Her deep understanding and loving support through all ups and downs of this study have helped me in a way words can hardly express.

13. PUBLICATIONS

Original paper

Sollmann, N., Goblirsch-Kolb, M. F., Ille, S., Butenschoen, V. M., Boeckh-Behrens, T., Meyer, B.,, Krieg, S. M. (2016).

Comparison between electric-field-navigated and line-navigated TMS for cortical motor mapping in patients with brain tumors.

Acta neurochirurgica. doi:10.1007/s00701-016-2970-6